Probabilistic Resource Modeling of Vein Deposits

by

Dhaniel Antunes de Carvalho

A thesis submitted in partial fulfillment of the requirements for the degree of

Master of Science

in

Mining Engineering

Department of Civil and Environmental Engineering

University of Alberta

Abstract

Tabular vein deposits represent important projects and mining operations worldwide. Mining cost are high and are impacted by uncertainty in the geometry of the vein. Uncertainty can influence mine planning and operation. For this thesis, simple tabular vein structures with single or multiple stacked layers with gentle folds and disturbances are considered. There are many types of deposits that can be included in to this definition with different metals and commodities. Current techniques do not provide an assessment of the uncertainty in these types of deposits.

Traditional and current workflows for mineral resource evaluation can be divided in the definition of the stationary domains, and the estimation or simulation of grades and properties. The estimation domains for tabular vein deposits are usually defined by explicit modeling, implicit modeling, or surface interpolation. These are deterministic methodologies that do not capture the geometry uncertainty as they generate a single vein solid.

This thesis proposes a framework that captures geometric and other uncertainties, implements post-processing and sensitivity analysis to quantify vein resources uncertainty. The geometric uncertainty considers a local coordinates system, position and thickness uncertainty. The local coordinates system matches the vein geometry, grade and thickness modeling conform to the vein geometry, and anisotropy is modeled correctly. Position and thickness uncertainty from drill holes with shallow angle intersections are dealt with by imputing the geometric position perpendicular to the plane of continuity. Position and thickness distributions are calculated, merged, and sampled. Footwall and hangingwall

surfaces are simulated using position and thickness values from imputation. Each realization has a different vein geometry. Other uncertainties are external boundaries and holes, grades, and parameter uncertainty. Fixing a single boundary for the vein is not realistic; multiple boundaries should be modeled. A different boundary is selected for each realization. Grades are usually modeled in regular grids that do not adapt to local variations in the vein geometry. An unstructured tetrahedron grid is used for grade simulation. The tetrahedron grid fits exactly the facet-based geometric model of the vein. Grades are simulated using different distributions realizations as input. Results from vein geometry and grade simulation can be summarized with post-processing and sensitivity analysis.

Many aspects of mine planning, operation, resources reporting, and classification can be supported by these results. The major geostatistical concepts and techniques are reviewed. The proposed framework is explained with implementation details. Two case studies are presented: a single mineralized structure of gold vein deposit; a multiple layer silver vein. Results and discussion are presented.

Acknowledgments

I would like to thank my wife Ana for coming with me on board of this challenge. Life is much more delightful and easier when you can rely on such an intelligent and kind-hearted person. Her support is essential to all my personal and professional achievements. Secondly, I would like to thank my supervisor Dr. Clayton Deutsch. His passion for teaching inspired me to chase this title. Clayton's mastery and ownership in geostatistics are fascinating and encourage his students to be the spearhead of the field. I also thank the Centre for Computational Geostatistics (CCG) and industry sponsors for all support throughout my research.

I would also like to thank all my friends at CCG. Geostatistics and coding seemed much easier with all your help. Thank you all my friends in Edmonton for all the travels, camping, climbing, snowboarding, partying and unforgettable experiences we had in these two years. Your friendship made all this effort worth it. For those in Brazil, the distance will only strengthen our connection and friendship. Hope to see you soon. A special thank you to my late friend Jorge (Fofão): your bright spirit, generosity and incredible knowledge in geostatistics have blessed all of us that were lucky enough to have had you in our lives during your (so brief) passage through Earth. Thank you, my dear friend, colleague and mentor.

Finally, I would like to thank my family for supporting all my dreams. You are my foundation and I owe you the world.

Table of Contents

List of Figures

List of Abbreviations

DF	distance function
DHS	drill hole spacing
FW	footwall
HW	hangingwall
kOz	kilo ounces
MSE	mean squared error
Mt	million tons
NI 51-101	National Instrument 51-101
PLC.	piecewise linear complex
PGE	platinum group elements
PPMT	projection pursuit multivariate transformation
QP	qualified person
QA/QC	quality control
RBF	radial basis function
SEDEX	sedimentary-exhalative
SGS	sequential gaussian simulation
SB	spatial bootstrap
SSE	sum of squared errors
TLS	total least squares
VI	vein indicators

Chapter 1. Introduction

Tabular vein deposits represent important mining operations worldwide. The geometry and resource uncertainty of hydrothermal veins and other tabular deposits is addressed. Mine planning and operation require accurate and reliable resources and reserves. There are several established techniques used in industry and academia for resource assessment. Understanding the resource uncertainty would support technical decisions including drilling, exploration, and mine planning. Current techniques do not provide a full understanding of the variability and uncertainty in these deposits. A new workflow is proposed to evaluate the uncertainty in tabular vein resources.

1.1. Definition of Veins and Tabular Deposits

This section reviews veins and tabular deposits. For the purpose of this thesis, the term veins or tabular deposits refers to simple vein structures with single or multiple stacked layers with gentle folds and disturbances. Complex veins with anastomosing, bifurcating, interlacing, and multiple faulting is not the focus of this work. Figure 1.1 gives a schematic illustration of this.

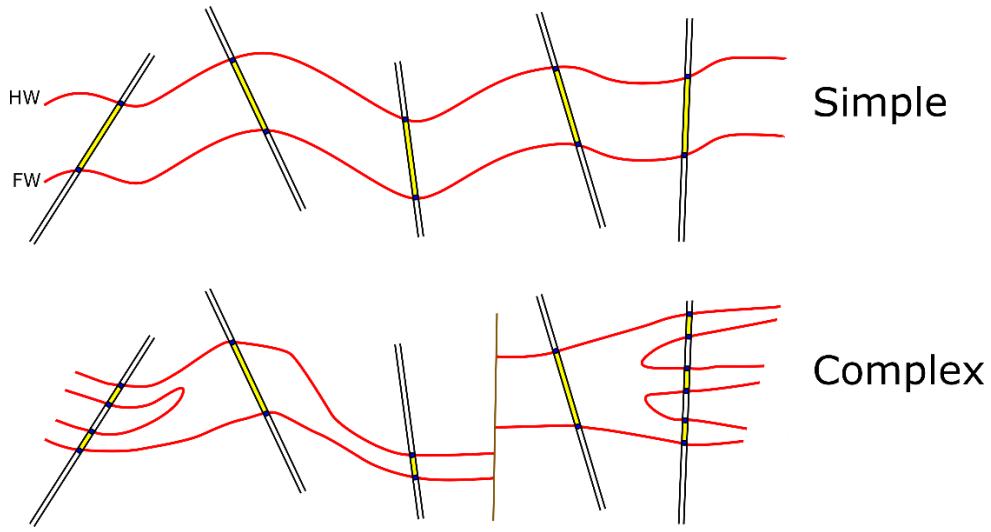

Figure 1.1: Schematic cross section examples of simple and complex tabular vein structures. There is no specific scale, but the horizontal extent is tens to hundreds of meters and the vertical extent is 1 to 10 meters. HW is the hangingwall or top of the vein. FW is the footwall or bottom of the vein. The vein intersections are highlighted in yellow and interpreted by the red lines.

1.1.1. Hydrothermal Vein Deposits

As explained by Edwards and Atkinson (1986), hydrothermal mineral deposits have a genesis associated with hot aqueous fluids. Metals and minerals are deposited by precipitation and association with the host rock and hydrothermal fluids. These fluids can have different origins and form many types and shapes of mineral deposits. In the context of this work, only hydrothermal deposits contained within veins will be discussed. Vein deposits are historically important for ancient miners and are still responsible for a significant metal production in the world. Usually associated with high mining and operation costs, the principal commodities that are mined from veins are gold, silver, zinc, lead, tungsten, uranium, cobalt, tin, and platinum group elements (PGE). Gold vein mining is responsible for a large of the United States production, and with high prices and demand, many projects are becoming economically feasible. For some metals like tungsten, more than half of the global production is resulting from wolframite-bearing quartz vein mining. Typical uranium vein-type deposits represent up to 20% of the total world resources (IAEA, 2009). An example of a hydrothermal vein section can be seen on Figure 1.2.

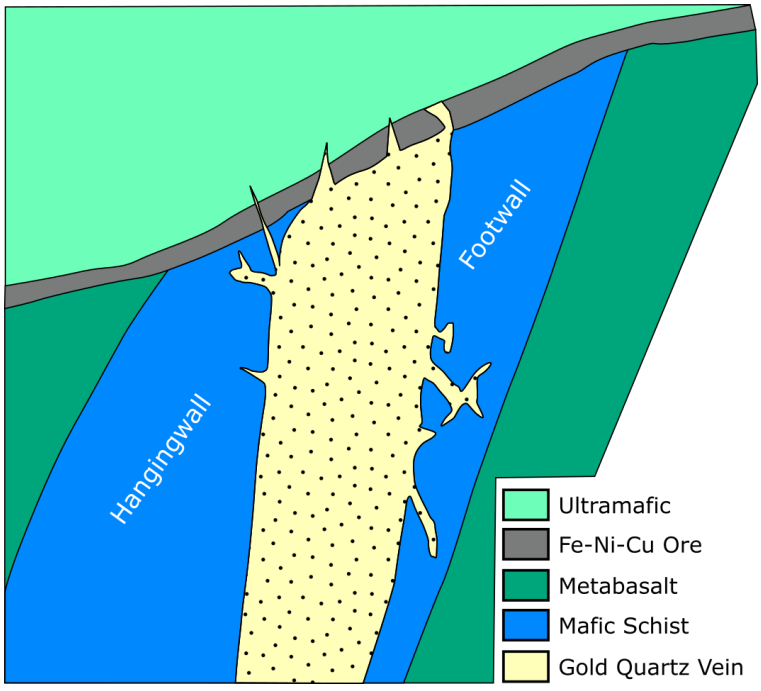

Figure 1.2: Schematic diagram of an auriferous quartz vein (modified from Edwards and Atkinson (1986)). Thickness vary from 1 to 2 meters.

Hydrothermal vein deposits can be classified based on the nature of the ore fluid, temperature and pressure conditions, and geological setting. The ore fluids are saline aqueous solutions that can be subdivided in four types: (i) surface water, (ii) deeply penetrating groundwater, (iii) metamorphic water, and (iv) magmatic water. The understanding of the origin of the mineralization fluid is essential to develop better metallogenetic models of a deposit. Isotopic signatures can help determine the nature of the hydrothermal fluids in addition to the tectonic setting, mineral association, and geochemistry. Regarding temperature and pressure conditions, hydrothermal veins deposits can be classified as epithermal, mesothermal, and hypothermal (Lindgren, 1922). Epithermal deposits are usually formed at shallow depths (shallower than 1500 meters) and fairly low temperatures (50-200°C). They form as vein fillings, irregular branching fissures, stockworks, mineralization is not uniform along strike, and there can be vertical zoning. Mesothermal deposits are formed at moderate temperatures (200-300°C) and pressures (around 1 to 5km deep). There could be associated with copper porphyry deposits extensive alteration zones with ribbon structures parallel to vein walls and can be associated with ultramafic rocks. Hypothermal deposits are usually formed at great depths (several kilometers) and high temperatures (300 to 500°C). On geological setting, it is clear there is a strong relation between ore deposits and associated rocks, and so, vein deposits can be closely connected to distinct geological context.

1.1.2. Other Tabular Deposits

In addition to hydrothermal vein deposits described above, there are a large number of tabular and layered deposits that are crucial for world ore production. Some examples include: tabular magmatic deposits, stratiform sediment-hosted copper-lead-zinc deposits, weathered ore formations, coal seams, and uranium with sedimentary affiliation.

Tabular magmatic deposits are formed by segregation of ore minerals during the crystallization process of the magma. The principal elements produced in these ore formations are platinum group elements (PGE), nickel, copper, chromium, vanadium, and titanium, with secondary production of cobalt and gold. These deposits are generally associated with mafic and ultramafic intrusive rocks with ore mineral as pentlandite, pyrite, pyrrhotite, chalcopyrite, chromite, and vanadiferous magnetite. The igneous intrusions can

be separated in two types: The Bushveld Complex and Great Dyke. They are usually sills and layered lithologies subdivided into lower ultramafic and upper mafic zones tilted or slightly deformed by subsequent tectonism. The layers can range from centimeters to more than 1m of thickness.

Sedimentary-exhalative (SEDEX) lead-zinc deposits are a temporal and geographical restricted mineralization. They have been formed by release of mineralized hydrothermal fluids in a water reservoir. The ore minerals are usually galena and sphalerite and with silver associations. Pyrite and pyrrhotite are common as well. There are large deposits in Australia, USA, and Canada. It can be found in many different geometries, but usually stratiform and stratabound. Weathered ore deposits form by alteration by physical and chemical process. The weathered minerals are more stable than the original ones. The physical weathering breaks the rocks and create larger surfaces that increase the activity of chemical weathering. A large diversity of deposits can be formed by weathering including bauxite (aluminium), nickel laterites, kaolin, supergene sulphide and manganese. Bauxite is the main aluminium ore and it is composed by aluminium hydroxides, gibbsite, and diaspore, resulting from the weathering of a variety of silicate rocks as granite, gneiss, and syenite. There are large deposits in Guiana, Venezuela, Brazil, Colombia, Jamaica, USA, China, Russia, and others. An example of a layered bauxite deposit section can be seen on Figure 1.3.

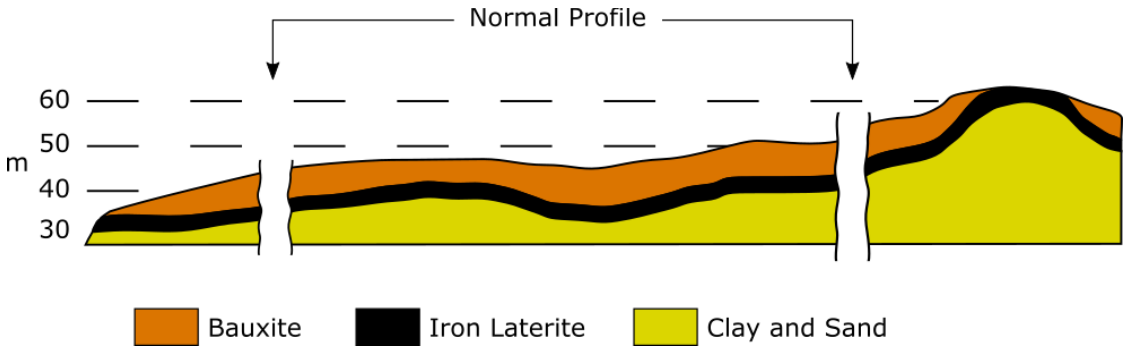

Figure 1.3: Profile of bauxite deposit and its layers (modified from Lillehagen, 1979).

Nickel laterite deposits are formed by the leaching of nickel from olivine, serpentine or nickeliferous magnetite, silicates, and garnierite. This type of deposit accounts for most of the available resources for this commodity. There are large deposits in New Caledonia, Australia, Indonesia, and Philippines. Smaller deposits can be found in Brazil, Colombia, and USA. A layered nickel profile can be seen on Figure 1.4.

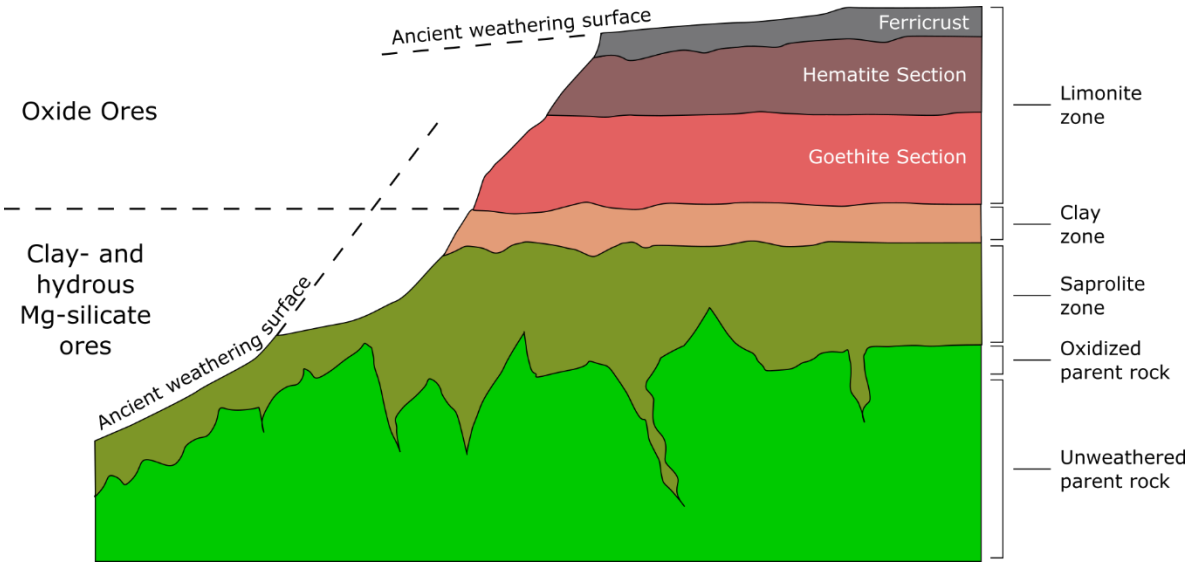

Figure 1.4: Profile of nickel laterite deposit and its layers (modified from Marsh & Anderson (2011)). Profiles can be a few to tens of meters thick.

Coal deposits are another type of tabular deposits that results from the accumulation of plant matter and debris within a specific depositional context that controls the geometry of the seams and beds. Even though the majority of uranium deposits related to sandstones and unconformities, there are some classical vein deposits that form tabular structures.

1.2. Traditional Modeling and Resource Estimation

Methods and workflows applied by industry will be reviewed. The mineral resource evaluation process can be divided in two main steps. The first is the definition of estimation domains, that are defined as volumes of rock with similar mineralization controls and consistent statistical characteristics (Rossi & Deutsch, 2014) and geological meaning. This

domaining is also known as the decision of stationarity (Isaaks & Srivastava,1989). The second step is the estimation or simulation of the grades within the interpreted stationary domains. In addition to inverse distance techniques, there are several well-established kriging estimators and simulation techniques referenced by many authors including Journel and Huijbregts (1978); Isaaks and Srivastava (1989); Deutsch and Journel (1998); and Chilès and Delfiner (2011). Such estimation does not produce results with uncertainty quantification, while non-linear kriging estimators may generate local probabilistic resources. Simulation methods could be applied to grade within the fixed ore body geometry. Fixing a single geometry for the mineralization domain will not capture the full variability of the deposit. Some common methodologies used to generate the geometry and grade estimation are reviewed.

1.2.1. Explicit Modeling

Explicit modeling is a traditional deterministic method for geological modeling that relies on manual digitization and interpretation. This technique requires 2D interpretation and digitisation of the mineralization in cross, longitudinal and plan sections. After outlining the ore body in 2D it is necessary to tie these polylines together to generate a 3D wireframe. The strong advantage of this explicit modeling approach is the close attention given to the data and deposit and the ability to incorporate geological interpretive information. An example of a vein modeled with explicit methodology can be seen on Figure 1.5.

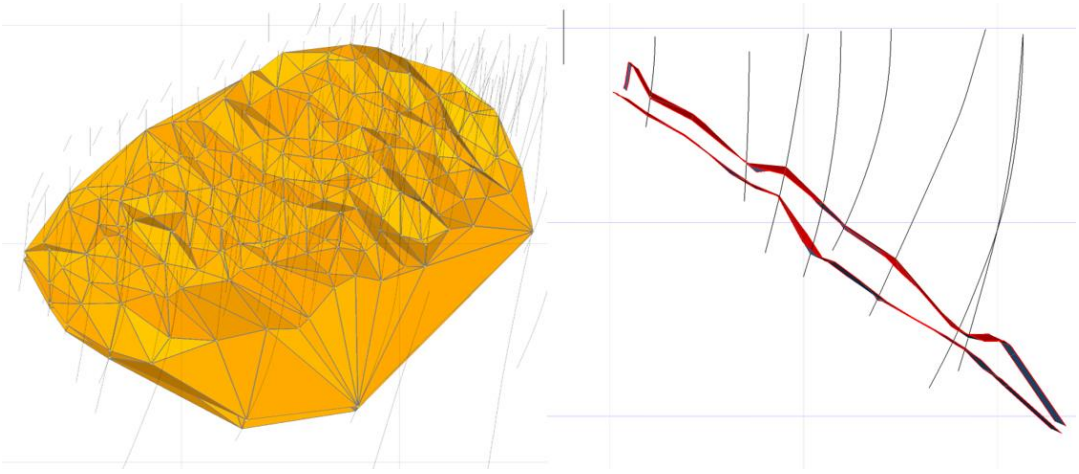

Figure 1.5: Example of a auriferous tabular vein modeled with explicit methodology. Average thickness is around 4 meters. Cross section on NW-SE direction.

However, as pointed by Cowan et al. 2003, this task is time consuming, cannot be automatically updated with new data information, editing involves complex manipulation, and the model is not easily replicated by other modelers as it is dependent on personal interpretation. In addition to these points, explicit modeling does not provide uncertainty measurement, as it generates a single wireframe of the ore body geometry.

1.2.2. Implicit Modeling and Surface Interpolation

Implicit modeling is another deterministic method referenced by many authors including Cowan et al. 2003, Chilès et al. 2004, Silva & Deutsch (2012), Martin & Boisvert (2017), and others. It is much faster than the explicit methodology and repeatable with consistent parameters. The idea is to automatically model wireframes using distance or volume functions based on data configuration, categories, and anisotropy. The established model is to fit a radial basis function (RBF) interpolator to the signed distance function values at a set of drill holes (Martin & Boisvert, 2017). An example of a vein modeled with implicit methodology can be seen on Figure 1.6.

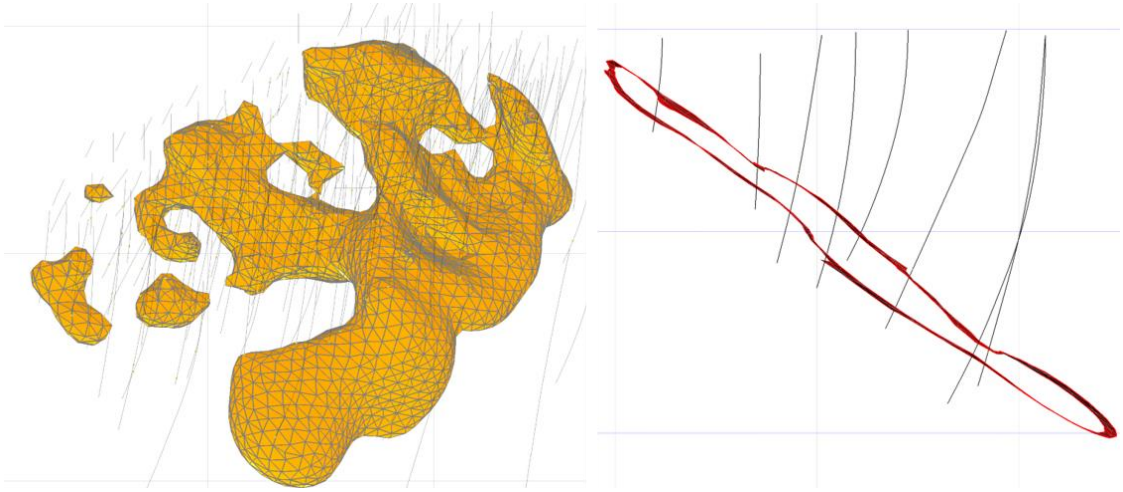

Figure 1.6: Example of the previous vein (Figure 1.5) modeled with implict methodology.

This methodology is driven by indicator data, contacts, foliation measurements, structural data, and interpretation. The goal is to generate wireframes representing the contact

between different lithological, structural, and grade zones. The main advantages if compared over explicit modeling are not having to manually draw interpretation on sections, much shorter processing time, and model update flexibility (Bertossi et al. 2013). Even though there are several advantages, it is difficult to reproduce the strong 2D anisotropy of vein deposits, particularly in narrow veins. Besides, the product of this approach is a single wireframe vein, where there is no geometric or volumetric uncertainty assessment.

Vein wireframes are also modeled with surface interpolation. The general idea is similar to the indicator coding of positive and negative intercepts and interpolate footwall and hangingwall positions as a surface. After that, thickness is associated to this surface. Most of the times, global kriging or RBF is used for the interpolation. Boundaries and pinch-outs are dealt with distance buffers, manual clipping, and inversion of footwall and hangingwall positions with negative intercepts. Similar to previous approaches, this methodology produces a single wireframe, which does not capture the geometric uncertainty of the modeled vein. An example of a vein modeled with surface interpolation can be seen on Figure 1.7.

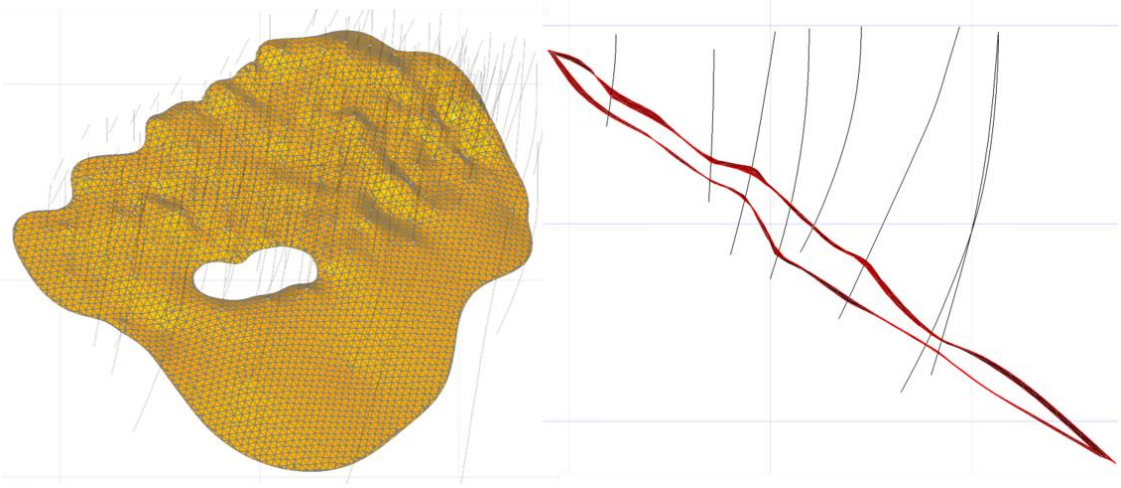

Figure 1.7: Example of the previous vein (Figure 1.5) modeled with surface interpolation.

1.2.3. Grade and Properties

After generating the vein geometry and wireframes, grades and properties must be assigned to a block model to predict tonnage and grade. Some classical methodologies are worth mentioning. The polygonal method is based on assigning areas of influence around drill hole data. Each polygon represents the area closer to a particular drill hole compared to all others. It is based on the intuitive idea that each sample grade has an influence proportional to its area of influence. Currently, it is mostly used for calculating declustering weights for samples. The nearest-neighbor method is similar to the polygonal method, but instead of drawing polygons, the grades are assigned directly to a block model. The blocks are assigned the grade of the closest drill hole data without any averaging between multiple samples. There is no smoothing and grades can change abruptly from one block to another. This method produces larger errors than others and it is mostly used for calculating declustering weights and as a checking tool. The inverse distance method is based on a linear weighted estimator. The grades assigned to the blocks are a smoothed version of the samples grades. The weight of each sample is based on the distance between data and the block of interest. Inverse distance was widely used in the industry, but its applications is steadily decreasing due to geostatistical methods.

The most widely used geostatistical methodology is kriging. Kriging is associated with the acronym B.L.U.E, which stands for "best linear unbiased estimator" (Isaaks & Srivastava,1989). It is linear as its estimates are a weighted linear combination of the available nearby drill hole data; unbiased as it tries to have the mean of the estimates equal to the true mean; and best as it minimizes the variance of the error. Kriging is presented by several authors as Journel and Huijbregts (1978), Isaaks and Srivastava (1989), Deutsch and Journel (1998), and Chilès and Delfiner (2011). As listed by Rossi & Deutsch (2014), the most common types of kriging are simple kriging, ordinary kriging, and universal kriging. The kriging equations account for redundancy of the data, closeness, and variance (Pyrcz & Deutsch, 2014). Kriging calculates a single prediction of the grades. There is no joint or multilocation uncertainty evaluation with the estimation result.

Simulation is required to understand joint uncertainty of the grades at multiple locations. Geostatistical conditional simulations have been used for several mining applications. The goal is to reproduce the histogram and spatial continuity from the original conditioning

data. The result of a conditional simulation is large number of equiprobable realizations for each node. Usually, simulation is carried out on a high-resolution grid and the averaged to a SMU or other mining scale. Many simulation algorithms are used for conditional simulations including Sequential Gaussian Simulation (SGS) (Isaaks, 1990). The SGS algorithm is related to multigaussian kriging algorithm. All conditional distributions are Gaussian and simple kriging produces the mean and variance.

1.3. Problem Statement

There are several aspects of mineral resource evaluation for vein deposits. The representation of these thin tabular deposits is critical for accurate exploration drilling, mine planning, resources and reserves calculation, and mine operation. Current practices for vein modeling are limited in terms of the structure of the models and uncertainty evaluation. As described above, explicit modeling with manual digitisation requires a high level of attention to data and geological interpretation. This methodology is inflexible and does not provide any uncertainty assessment. Implicit modeling is faster and easier to create models, but results in a single solid of the vein with poor anisotropy modeling. Surface interpolation accounts for the strong anisotropy but also generates a unique geometry of the modeled vein. The use of kriging is common practice for vein resources estimation, but there is no joint uncertainty quantification. Simulation methods could be applied to grade within the fixed ore body geometry. Fixing a single geometry for the mineralization domain will not capture the full variability of the deposit.

There is a need to develop a flexible modeling workflow that quantifies overall uncertainty for tabular vein deposits. It is essential that the workflow accounts for many sources of uncertainty including coordinates, position of the surfaces, thickness values, boundaries, holes, grades, and data uncertainty. A workflow is proposed for uncertainty assessment in tabular vein deposits.

1.4. Thesis Outline

Chapter 2 briefly introduces the proposed framework for modeling tabular vein deposits. It explains the importance and how to capture the geometric uncertainty and other types of

uncertainty on tabular vein deposits. It also describes the available grid topologies used in natural resources evaluation. Traditional Cartesian and regular block models are reviewed. Unstructured tetrahedron grids are also presented. It reviews the method to understand uncertainty and setup simulations for the task. Chapter 3 describes geometry uncertainty evaluation derived from the proposed framework. It explains the importance and the procedure to create a local coordinates system, how to capture the uncertainty on the position of surfaces (footwall and hangingwall) and thickness values, and how to use this uncertainty to generate multiple realizations of the vein geometry. Chapter 4 explains how to capture other sources of variability in vein resources as external boundaries and pinch-outs, grades, parameter and data uncertainty. Chapter 5 clarifies methods to implement and process the results of this workflow using post-processing, sensitivity analysis, mine planning optimization, and mineral resource classification and reporting. Chapter 6 demonstrates the application of the workflow on two case studies: a single layer Au deposit, and multiple layers Au-Ag deposit. Chapter 7 reviews conclusions and possible future work.

Chapter 2. Framework for Tabular Deposits Modeling

Current practices do not permit uncertainty quantification in tabular deposit modeling. Traditional methodologies such as explicit, implicit, and surface modeling generate a single model. There is no joint uncertainty evaluation with kriging. Simulating grades with a fixed ore body geometry will not capture the variability and uncertainty of the deposit.
A novel modeling workflow is proposed. The workflow quantifies uncertainty for tabular vein deposits accounting for many sources of uncertainty including position of the bounding hangingwall and footwall surfaces, thickness values, boundaries, holes and grades uncertainty.

2.1. Proposed Framework

The following subsections explain the proposed workflow for modeling tabular vein deposits. The proposed workflow is based on capturing the uncertainty and using the results for a better understanding of the variability in the geometry and grades. The general idea is to generate multiple realizations of the vein geometry and boundaries with unstructured grids that matches the shape of the vein. There are three main parts: geometric uncertainty, other sources of uncertainty, and implementation. Geometric uncertainty is related to local coordinates systems, positions of surfaces and thickness, and surface simulation. Other sources of uncertainty are linked to external boundaries and holes, grades and properties, and parameter uncertainty. The implementation reflects on how to use the results in post-processing, sensitivity analysis, mine planning optimization, classification, and reporting. More details of each step will be given in the following chapters.

2.1.1. Geometric Uncertainty

Most of the time, the original Cartesian coordinate system used in exploration and mining are not aligned with the vein geometry and grade anisotropy. If resources are modeled, estimated, or simulated in this original system, the estimated grades might be unrealistic by not following the vein shape. Thickness is not always easily calculated due to inclined

drill holes, that are typical in vein deposits. To avoid these problems, it is recommended to use local coordinates that match the vein geometry and anisotropy. As mentioned, the focus of this thesis is on simpler tabular vein deposits with gentle folds or disturbances. For these types of mineralization, rotating, translating, and fitting a plane improves resource evaluation and modeling. Usually, the goal is to align the new local axes (u, v, w) to the dip, strike, and thickness, respectively. An automatic fitting approach for defining the local coordinates system is recommended. The method, Total Least Squares (TLS) (or Orthogonal Regression Modeling), consists in a linear regression modeling by fitting the plane that minimizes the error between drill holes intercepts and the vein plane (Ostenberg & Deutsch, 2017). TLS is calculated based on each intercept midpoint. The local coordinates are obtained by the product of original coordinates and the transformation matrix. In this new local coordinate system, geometry and thickness modeling are easier and more geologically realistic.

Position and thickness uncertainty are captured with imputation of geometry data. It is required due to inclined drill holes, and for a more realistic uncertainty assessment of footwall and hangingwall intercepts. Imputation is the process of inferring missing values at locations with partial information. The geometry data of veins and tabular deposits consists of thickness and elevation, which will be a function of the (u, v) position. Most of the time, drill holes are not perfectly perpendicular to the vein plane making it difficult to calculate and define thickness values. Thickness and elevation could be estimated at these data locations, but estimation would produce a single value for missing data. For a more realistic assessment, data imputation is proposed. Imputation amounts to simulating elevation and thickness at missing data locations first; it is essential to account for both thickness and position distributions for a better positioning of the intercept, while preserving uncertainty. There will be imputed data files generated for each surface simulation. Imputation will be performed by simulating the opposite surface to the reference surface. After simulating these locations, the locations of the intercepts of the base surface are also simulated. With simulated elevation and thickness distributions, it is necessary to merge these distributions and sample values to better define the position of the intercept, as there are two different distributions.

After generating the imputation files, surface and solid modeling can proceed. Surface simulation is performed to quantify position and tonnage uncertainty. To preserve the uncertainty from imputation, each surface realization should use a single and different imputation file. The position and thickness values are kept as pairs to prevent crossing in individual realizations. External limits and holes are considered later, therefore only internal samples and intercepts are used in surface simulation. In this workflow, the base surface will be simulated using elevation values, and the opposite surface using thickness values. As an example, considering the footwall as the reference surface: the footwall surface will be simulated using w elevation, while the hangingwall is established with thickness simulation. These thickness values are then added to the simulated footwall to find the final hangingwall position. After surface simulation, there will be many different vein solids.

2.1.2. Other Sources of Uncertainty

The external limits and holes are an important source of uncertainty. Vein external boundaries and holes can be modeled using a distance function (DF) (Hosseini & Deutsch, 2007) methodology. This technique delineates the boundary location and assesses uncertainty from drill holes coded with the Euclidean distance from the nearest geological contact defined. The distance is positive if outside the vein, and negative if inside the vein, where the isosurface with zero distance is the boundary of the vein. The uncertainty bandwidth can be calibrated and used to generate many different boundaries. For this workflow, drill holes are coded as intersecting the vein or not. Distance is calculated for the set of data interpolated using global kriging. Each geometry realization, from surface simulation, will be clipped by a different boundary.

Grade and property modeling will be carried out within each simulated vein in an appropriate grid. Grids can be regular parallelepipeds or unstructured tetrahedra, depending on user's choice. A regular grid in original coordinates will not match the detailed vein coordinates and structure as blocks do not follow the anisotropy and vein geometry. Moreover, only a small percentage of grid blocks in the full 3D grid network fall inside the vein. Even in local coordinates, as explained above, regular grid blocks are not optimal. To fill the vein geometry properly, the grid resolution should be very high, with small block

size, creating millions or even billions of cells. Also, in a high-resolution model, blocks near vein surfaces will have outside/void portions, that are difficult to manage. Alternatively, sub-cells could be used, which would also increase the number of created cells. A proposed solution is to use an unstructured grid of tetrahedrons, which would efficiently fill and fit the vein geometry. A tetrahedron grid fits perfectly in the vein geometry solid with fewer cells. The barycenter and volume of each tetrahedron cell can be calculated based on the node positions, as well as discretization. As there are hundreds of surface realizations and wireframe solids, a separate tetrahedron grid is generated for each vein geometry realization. Each tetrahedron will have its relative position calculated based on grades anisotropy, either proportional or surface conforming. Grades and properties are simulated for each realization grid.

Simulated realizations that use fixed input parameters can underestimate the global uncertainty (Deutsch, 2004). This underestimation can be very significant in cases where the domain is much larger than the range of the variogram. Each realization will reproduce nearly the same input histogram from data. To account for the uncertainty in the histogram it is required to establish the distribution of uncertainty and generate geostatistical realization with different histograms and other input parameters. The spatial bootstrap is recommended for the task (Deutsch, 2004). The methodology uses simulation to resample the input data while preserving the spatial correlation.

2.1.3. Implementation

Another important aspect is how to manage all realizations and final results. Post processing is required to evaluate tonnage and metal uncertainty of the vein/tabular deposit. Many results can be extracted from simulated surfaces, grades, and grids. The expected surfaces (e-type) and solid model can be extracted, as well probability models. Probability volumes could be calculated, for both geometry and grade. Probabilities on geometry could be used for stope optimization (Manchuk, 2007). Results can also be used to determine global uncertainty on reserves and total metal content.

Sensitivity analysis can be applied to understand the contribution of uncertainty of each input variable. It is important to characterize the system by exploring relationships between variables, assess the quality of the existing model, simplify complex models, and prioritize

research objectives (Saltelli et al, 2008). Thickness, grades, distance function thresholds, area and other variables can be ranked and compared to understand the impact of each factor on the final metal content and available resources.

Mine planning and optimization can also be supported by this uncertainty workflow. Stope designing and sequencing is normally executed within a single vein geometry and grades estimation. Analyzing multiple geometry and grade realization can lead to optimization of costs and revenue. Dilution and ore loss can be balanced and understood depending on the position of footwall and hangingwall.

Another aspect of mineral resource evaluation supported by this workflow is classification and reporting. Geometry and grade uncertainty can be employed to assist the resources and reserves competent person to establish a classification criterion. Production volumes or periods can be analyzed to understand uncertainty for measured, indicated, and inferred classes. If the differences between classes are not suitable, then classification criteria should be reviewed. The expected resources could be reported in the final resources report and table. Uncertainty could be reported using tonnage and grades percentiles, probabilities, and confidence intervals.

2.2. Grid Topology

Developing and populating grids with grades and physical properties is an essential step in resources modeling. Most estimates rely on regular Cartesian gridding due to geostatistical assumptions, simplicity, and performance. Unstructured grids can be an alternative as a natural gridding methodology for geological phenomena. Aspects of both gridding methodologies are presented.

2.2.1. Cartesian Grid

The majority of resource estimates are carried out on regular block models or Cartesian grids. These block models describe the 3D volume of geological and mineralization domains with small parallelepipeds (Figure 2.1). Grids are essential elements for mineral resource and reserve estimation, stope, and pit optimization, mine planning and scheduling. The geometry of the grid is dependant on the deposit type, geology, ore geometry, mine

characteristics, and equipment size. For some sedimentary or stratigraphic deposits with low thickness values, two-dimensional grids are suitable as there is no vertical zonation or resolution of grades. Stacked two-dimensional grids are also appropriate.

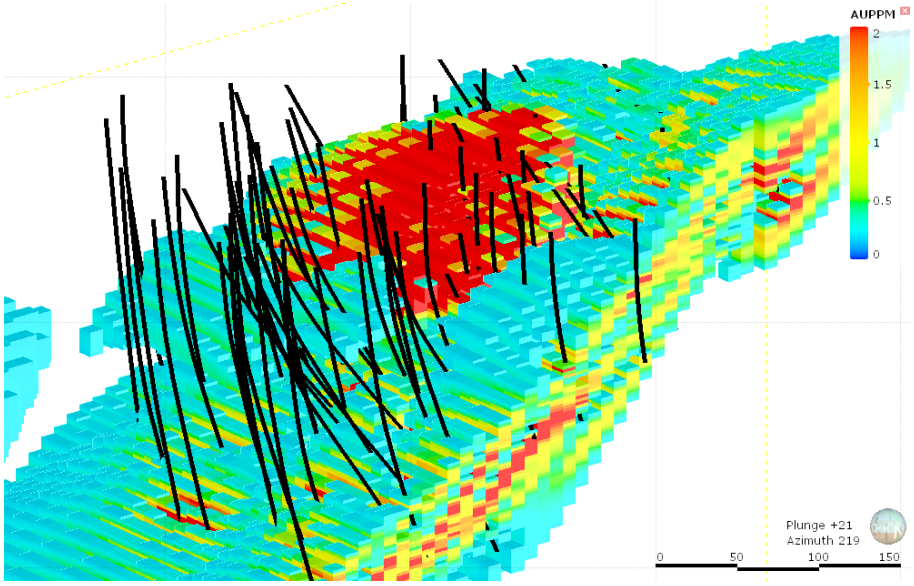

Figure 2.1: Interpolated block model of a gold deposit. Average thickness is around 7 meters. Drill hole are shown as black lines.

Usually, three-dimensional block models are employed for large deposits and thick veins. The size of each block is based on drill hole spacing, deposit geometry, and mine requirements. The size must be balanced between ease of estimation and mine planning. According to Journel & Huijbregts (1978), a good guideline for block size is to choose dimensions around 1/3 to 1/2 of the drill hole spacing. Small block sizes would result in artificial smoothing of the estimates, as adjacent block would receive almost the same estimate. Large block cells would not fully capture the resolution from drill hole spacing. It is subjective and based on other factors as mining experience, production, equipment size, and mining method. Block sizes can match bench or stopes heights. Sub-blocks can be used but with care on creating unrealistic small cells. Cartesian grids should cover all drill hole data used for modeling and wireframe extrapolation. For open pit operations, the block model should cover the final pit limits. For underground mine operations the block model should cover all mineralization. Grids can be clipped by topography. Rotated grids are recommended to match the geology and mineralization geometry. Many variables can

be stored in a block model as grade estimates, specific gravity, lithology, alteration, oxidation, mineral resource classification, mined or available ore and waste, economical factors, and many characteristics.

2.2.2. Unstructured and Tetrahedral Grids

Even though most resources are calculated using regular grids, facets and unstructured grids appear useful. Natural resources are within irregular and complicated geometric shapes and forms. An example of a discordant regular gridding can be seen on Figure 2.2. Most of the geological phenomena are derived from tectonic activity, deformation, weathering, hydrothermalism, and other natural processes. A natural gridding for complex surfaces would better describe these geological phenomena. Triangulated surfaces can be used to delineate these complex structures. A parametric implicit surface can be triangulated by a variety of methods (Hartmann, 1998). If a set of points is given, Delaunay Triangulation can be performed to generate the surface. The underlying natural three-dimensional gridding from triangulated surfaces are the tetrahedron grids. These grids are extensively used in finite element analysis (Zienkiewicz et al., 2005).

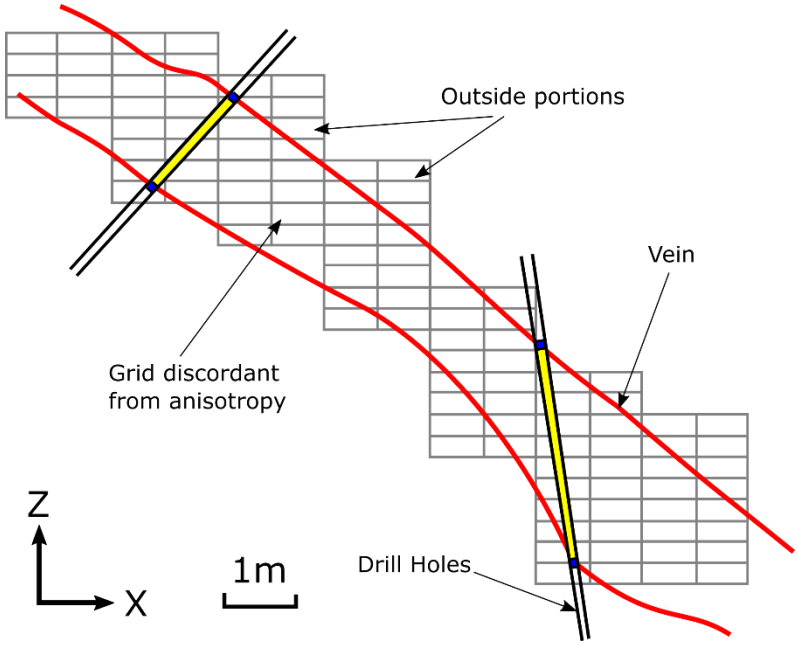

Figure 2.2: Regular blocks in original system and void portions. Tonnage calculation can be incovenient due outside/void portions. Vein and grade anisotropy is not honored.

Many authors have been using unstructured grids for modeling geological processes including Xu and Journel (1994), Mallet (2002), Caumon et al. (2005), and Manchuk (2010a). Direct sequential simulation of these grids did not further develop due difficulty in reproducing distribution models and heteroscedasticity (Pyrcz & Deutsch, 2014). Other methods implement an underlying structured grid such that geostatistical theory can be applied (Caumon et al., 2005). The underlying grid needs to be fine enough to represent the unstructured grid and produce acceptable upscaling results. Some unstructured grids are used in geostatistical modeling (Manchuk, 2010b). An example of a tetrahedral grid used in reservoir modeling can be seen on Figure 2.3.

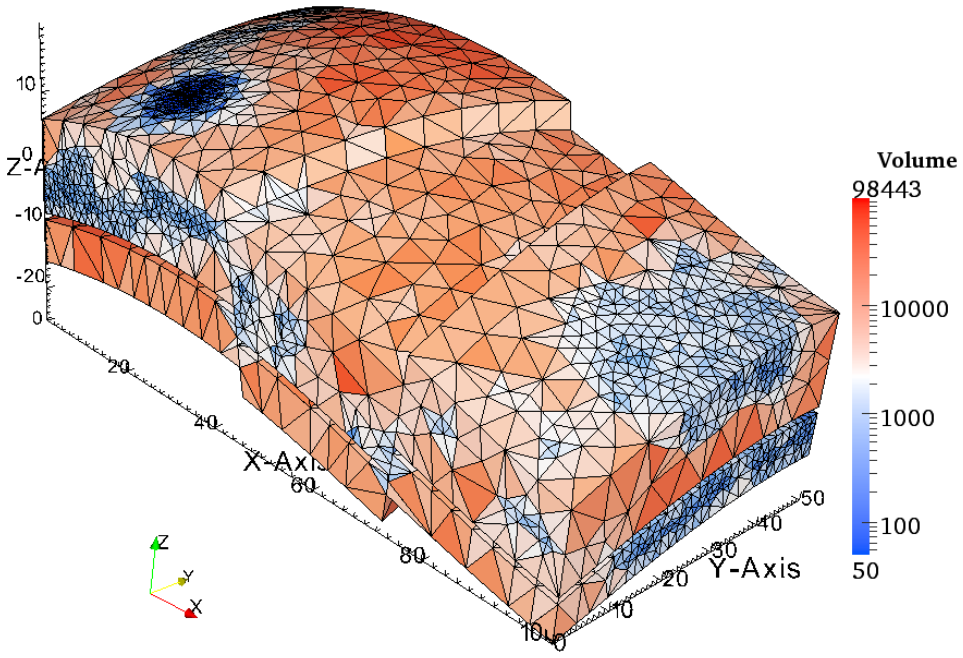

Figure 2.3: Example of a tetrahedral grid used for permeability modeling (Manchuk, 2010b). Axes in tens of meters and volumes in m^3.

2.3. Uncertainty Evaluation

Best estimates calculated by geostatistical methodologies have proven their application for many decades. Usually, the goal is to understand the variability over a large production volume or entire deposit. The setup of simulation for large scale uncertainty evaluation is more complex than a standard resource modeling workflow for local uncertainty. Deutsch

(2015) proposed a perspective to this setup of simulation for uncertainty quantification. The setup is described on Figure 2.4. A substantial number of realizations (L) is simulated without combinatorial branching of uncertainty. Each realization has its input parameters retrieved from a model of uncertainty (left yellow column), data realizations, data imputation and data with error (central green column), realizations of large scale structures, rock types and continuous variables (central blue column), summary posterior parameters calculated from the realizations (right yellow column), and response variables as resources and reserves (right pink column). Commercial software has limitations with this approach including single data, fixed boundaries, and no convenient way to compute sensitivity analysis. These limitations can be resolved with scripted workflows.

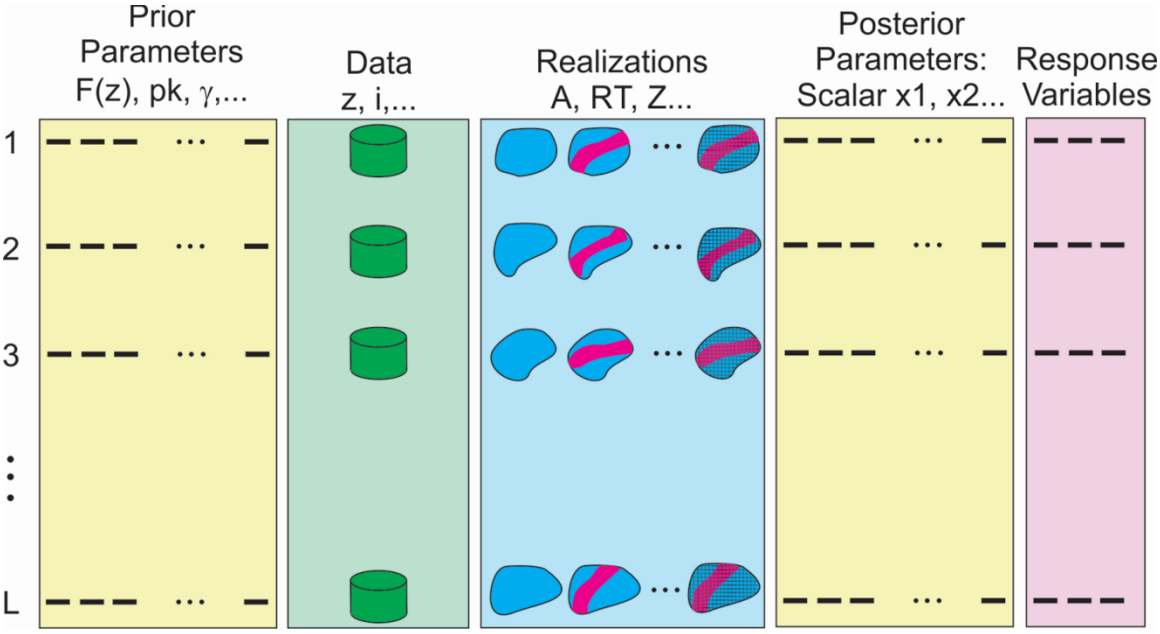

Figure 2.4: Setup of simulation for uncertainty quantification (Deutsch, 2017).

The overall workflow can go as:

1. Model Setup: This is how the geological site will be modelled. It depends on mineralization type and geology. It is necessary to specify the columns and all parameters required in the modeling workflow.
2. Parameter Uncertainty: A reasonable model of uncertainty must be assigned for critical variables. The number of data and stage of the project is critical in this

analysis. Univariate distributions and categorical proportions are usually the most important.

3. Data Uncertainty: May not be required. It depends on the number of missing data and level of uncertainty in input data. For PPMT workflows, this is step is necessary.
4. Simulation of Realizations: Mostly a computer task. Can be parallelized to avoid long processing times. Automated and manual checks are recommended.
5. Posterior Parameters: Parameters that summarize each realization are calculated after all realizations. It is required for sensitivity analysis on important parameters as volumes of different rock types, average thickness, variogram ranges, average grades, and others.
6. Transfer Function: Calculation of resources and reserves for a particular design. A distribution of uncertainty is observed. The sensitivity analysis accounts for calculated posterior parameters and response variables.

Chapter 3. Geometric Uncertainty

The geometry of a vein is of critical importance for resource estimation and mine planning. Current techniques can estimate and model the vein geometry, but with no uncertainty quantification on the position, volume, and tonnage. This chapter describes how to capture the geometric uncertainty of tabular vein deposits. Geometric uncertainty relates to uncertainty in the position of surfaces and related thickness values. It explains the importance of creating a local coordinates system. An automatic approach for fitting the new system to the plane of the vein is developed. In the local coordinates system, position and thickness must be imputed due to inclined drill holes. With a large number of imputed position and thickness values, surface simulation can be performed, and volumetric realizations can be evaluated for uncertainty quantification.

3.1. Local Coordinates

Most of the time, the original Cartesian grid system used in exploration and mining are not related to the vein geometry and grade anisotropy. If resources are modeled, estimated, or simulated in this original system, the final resources quantification can be inefficient. The estimated grades might be unrealistic by not following the vein shape and mineralization. Modeling the vein footwall and hangingwall are also negatively impacted by this decision. Thickness is difficult to calculate due to inclined drill holes, which is typical in vein deposits.

To avoid these problems, it is recommended to use local coordinates that match vein geometry and anisotropy. For tabular vein deposits, rotating, translating, or fitting a plane are enough for better resource evaluation and easier modeling. Usually, the goal is to manually align the new local axes (u, v, w) to dip, strike, and thickness, respectively, as seen on Figure 3.1.

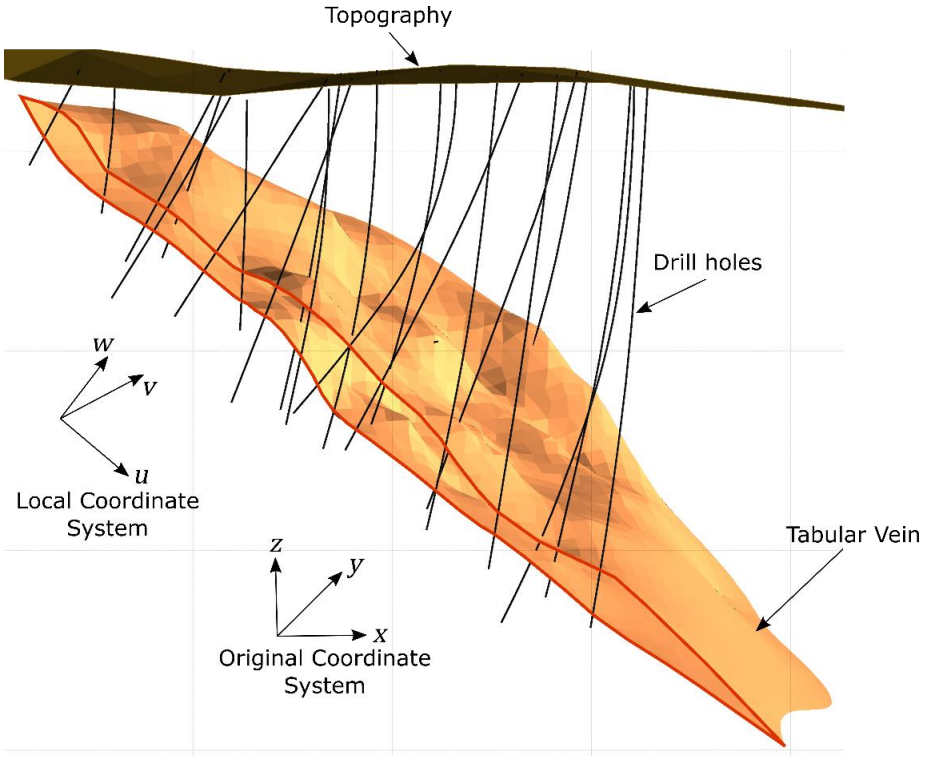

Figure 3.1: Schematic perspective view of a sliced tabular vein and coordinate systems. Thickness average is around 4 meters.

3.1.1. Total Least Squares

An automatic fitting approach for defining the local coordinates system is recommended. The method, Total Least Squares (TLS), or Orthogonal Regression Modelling, (Figure 3.2) consists in a linear regression modeling by fitting the plane that minimizes the error between drill holes intercepts and the vein plane (Ostenberg & Deutsch, 2017).

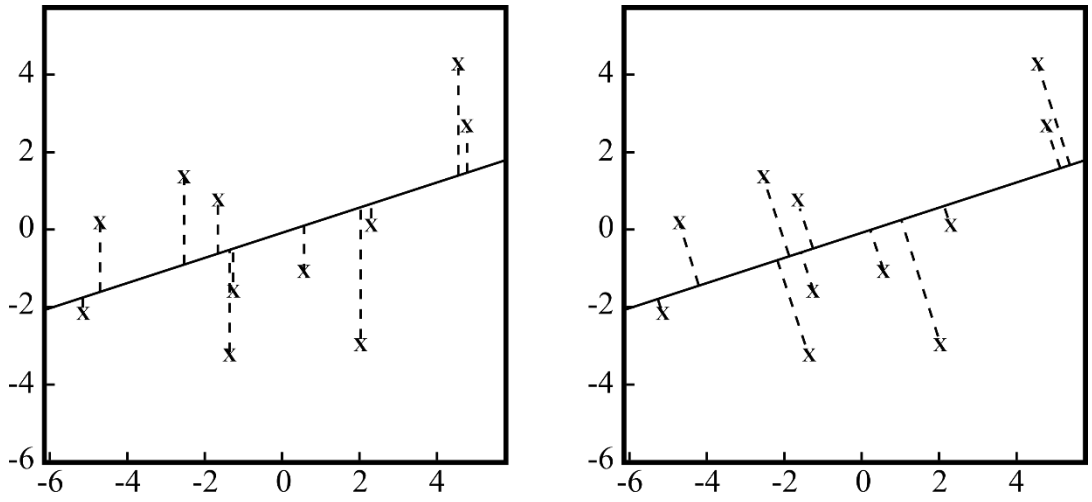

Figure 3.2: Simple linear regression (left) in which distances are measured along the y-axis, and Total Least Squares (right) in which errors are distributed over the x- and y-coordinates (Groen, 1996).

The TLS plane, π, is defined by:

$$\pi: ax + by + cz = d$$

The normal vector, that defines the orthogonal regression plane, is:

$$\vec{n} = \begin{bmatrix} a \\ b \\ c \end{bmatrix} = \begin{bmatrix} n_1 \\ n_2 \\ n_3 \end{bmatrix}$$

where $\vec{n}$ is a unit vector and a, b, c (also n_1, n_2, and n_3) are real numbers. The TLS minimizes the sum of squared errors (SSE) between the distance of samples and the orthogonal plane to the vein. TLS is calculated based on each intercept midpoint. The SSE is minimized when the all data centroid $(\bar{x}, \bar{y}, \bar{z})$ lies on the TLS plane. This normal $\vec{n}$ vector is the eigenvector represented to the minimum eigenvalue of $A^T A$, where A is an $n \times 3$ matrix of the points relative to their centroid:

$$A = \begin{bmatrix} x_1 - \bar{x} & y_1 - \bar{y} & z_1 - \bar{z} \\ x_2 - \bar{x} & y_2 - \bar{y} & z_2 - \bar{z} \\ \vdots & \vdots & \vdots \\ x_n - \bar{x} & y_n - \bar{y} & z_n - \bar{z} \end{bmatrix}$$

Using this centroid, and the normal vector obtained by TLS, it is possible to build a transformation matrix S, which combines translation matrix (T) and rotational matrix (R) to construct the local coordinate system:

$$S = T \times R$$

The translation matrix shifts the centroid of the data to the origin:

$$T = \begin{bmatrix} 1 & 0 & 0 & 0 \\ 0 & 1 & 0 & 0 \\ 0 & 0 & 1 & 0 \\ -\bar{x} & -\bar{y} & -\bar{z} & 1 \end{bmatrix}$$

The rotational matrix is created by each direction vectors. The normal vector is obtained by TLS. Strike vector $\vec{s}$ is perpendicular to $\vec{n}$ and obtained with cross product:

$$\vec{s} = \vec{z} \times \vec{n} = \begin{bmatrix} 0 \\ 0 \\ 1 \end{bmatrix} \times \begin{bmatrix} a \\ b \\ c \end{bmatrix} = \begin{bmatrix} -b \\ a \\ 0 \end{bmatrix} = \begin{bmatrix} s_1 \\ s_2 \\ s_3 \end{bmatrix}$$

Dip is perpendicular to the strike:

$$\vec{d} = \vec{s} \times \vec{n} = \begin{bmatrix} -b \\ a \\ 0 \end{bmatrix} \times \begin{bmatrix} a \\ b \\ c \end{bmatrix} = \begin{bmatrix} ac \\ bc \\ -a^2 - b^2 \end{bmatrix} = \begin{bmatrix} d_1 \\ d_2 \\ d_3 \end{bmatrix}$$

Rotational matrix rows are $\vec{d}$, $\vec{s}$, and $\vec{n}$ and it must be converted to a 4×4 matrix:

$$R = \left(\begin{bmatrix} d_1 & d_2 & d_3 & 0 \\ s_1 & s_2 & s_3 & 0 \\ n_1 & n_2 & n_3 & 0 \\ 0 & 0 & 0 & 1 \end{bmatrix} \right)^{-1}$$

The local coordinates are obtained by the product of original coordinates and the transformation matrix S:

$$[x \quad y \quad z \quad 1] \times S = [u \quad v \quad w \quad 1]$$

The back transformation, from local to original coordinates is simply obtained by the product of local coordinates and the inverse of S:

$$[u \quad v \quad w \quad 1] \times S^{-1} = [x \quad y \quad z \quad 1]$$

Given the steps, an example of the TLS calculation is shown below.

3.1.2. TLS Calculation Example

The steps below are a calculation example with data from a real tabular vein deposit. The following data consists of midpoints where drill holes intercepts vein. These midpoints are calculated based on hangingwall and footwall data:

$$\begin{array}{ccc} X & Y & Z \\ 584257 & 3319531 & 852 \\ 584241 & 3319564 & 791 \\ 584157 & 3319558 & 752 \\ 584012 & 3319483 & 733 \\ 583819 & 3319465 & 804 \\ 583893 & 3319481 & 668 \\ & \vdots & \end{array}$$

The centroid of the all data is at:

$$(584075, 3319534, 734)$$

The matrix A, which is data points regression from their centroid, starts with:

$$A = \begin{bmatrix} 182.48 & -3.67 & 117.16 \\ 166.28 & 29.34 & 56.20 \\ 82.13 & 23.5 & 17.28 \\ -62.90 & -51.35 & -1.90 \\ -182.26 & -53.60 & -66.75 \\ 277.64 & 108.63 & -5.47 \\ & \vdots & \end{bmatrix}$$

The eigenvalues (Λ) and eigenvectors (U) of $A^T A$ for all data are then obtained:

$$\Lambda = \begin{bmatrix} 463798 & 0 & 0 \\ 0 & 5181 & 0 \\ 0 & 0 & 49307 \end{bmatrix}, \qquad \mathrm{U} = \begin{bmatrix} -0.9581 & -0.2705 & 0.0937 \\ -0.2859 & 0.9214 & -0.2628 \\ 0.0152 & 0.2786 & 0.9602 \end{bmatrix}$$

The normal vector is the eigenvector corresponding to the minimum eigenvalue, 5181:

$$\vec{n} = \begin{bmatrix} -0.2705 \\ 0.9214 \\ 0.2786 \end{bmatrix}$$

The translation matrix is defined as:

$$T = \begin{bmatrix} 1 & 0 & 0 & 0 \\ 0 & 1 & 0 & 0 \\ 0 & 0 & 1 & 0 \\ -584075 & -3319534 & -734 & 1 \end{bmatrix}$$

Using cross product, the strike and dip vectors can be calculated and normalized:

$$\vec{s} = \begin{bmatrix} -0.9594 \\ -0.2817 \\ 0 \end{bmatrix}, \vec{d} = \begin{bmatrix} -0.0785 \\ 0.2673 \\ -0.9603 \end{bmatrix}$$

The rotational matrix is then:

$$R = \left(\begin{bmatrix} -0.0785 & 0.2673 & -0.9603 & 0 \\ -0.9594 & -0.2817 & 0 & 0 \\ -0.2705 & 0.9214 & 0.2786 & 0 \\ 0 & 0 & 0 & 1 \end{bmatrix} \right)^{-1} = \begin{bmatrix} -0.0785 & -0.9594 & -0.2705 & 0 \\ 0.2673 & -0.2817 & 0.9214 & 0 \\ -0.9603 & 0 & 0.2786 & 0 \\ 0 & 0 & 0 & 1 \end{bmatrix}$$

The transform matrix is then calculated:

$$S = T \times R = \begin{bmatrix} -0.0785 & -0.9594 & -0.2705 & 0 \\ 0.2673 & -0.2817 & 0.9214 & 0 \\ -0.9603 & 0 & 0.2786 & 0 \\ -840965.17 & 1495675.48 & -2901066.65 & 1 \end{bmatrix}$$

The angles of strike and dip are:

$$s_1 < 0, \qquad strike = 360 - \cos^{-1}(-0.95) = 253.6°$$

$$dip = \sin^{-1}(0.96) = 73.8°$$

Samples and intercepts are rotated and translated using matrix S. In this new local coordinate system, geometry and thickness modeling are easier to deal and more appropriate. All subsequent steps such as geometry data imputation, surface simulation,

gridding, and grade/property simulation are executed in this local coordinate system. After all modeling, drill hole data, simulated surfaces and gridded values are back rotated to the original coordinate system.

3.2. Position and Thickness

Imputation of geometry data is required due to inclined drill holes and for a better uncertainty assessment of volume and tonnage. Imputation is the process of inferring missing values at samples locations. The geometry data of veins and tabular deposits consists in position (elevation) and thickness and will be a function of the (u, v) position in the local space. As a regular estimation or simulation, values will be based on nearby samples and drill hole data. Most of the time, drill holes are not perfectly perpendicular to the vein plane making it difficult to calculate and define thickness values. In Figure 3.3, it is possible to see that the thickness at drill hole 1 is known, but at drill hole 2, the true thickness value is uncertain. Thickness and elevation could be estimated at data location, but estimation would produce a single value for missing data. For a more realistic tonnage uncertainty assessment data imputation is proposed by simulation of geometry data. After simulating elevation and thickness distributions for each intercept, merging them and sampling a value is recommended for a better positioning of the intercept, while preserving uncertainty. There will be hundreds of imputed data files generated, each one used in an individual realization for future surfaces simulation. Some steps and calculation are shown for a gold deposit with 220 drill holes, in which 182 intersect the vein.

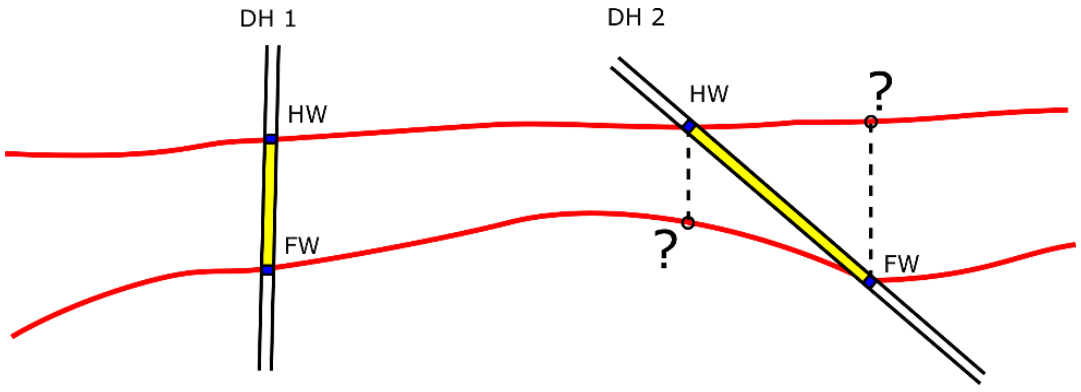

Figure 3.3: Thickness calculation and different results. In the sketch, drill hole 1 thickness is known, as it the hole is nearly vertical. For drill hole 2, the dashed lines show different possibilities of thickness values due to hole inclination.

3.2.1. Prerequisites and Data Assembly

All data must be fitted, rotated, and translated to the plane of the vein. A base surface, hangingwall or footwall, must be chosen to facilitate the workflow. Usually, the selected surface is the most well-behaved and stable. If both surfaces have similar behavior, any selection is accepted. Imputation will be performed by simulating intersections of the opposite surface. As an example, if the footwall is the base surface, the hangingwall of inclined drill holes will be projected to the footwall plane and its location simulated. This simulation will be based on elevation and thickness of nearby footwall and hangingwall intercepts.

Data used for this workflow is intercepts of the vein deposit. As elevation and thickness are modeled in areas where the vein exists, only intercepts inside the vein are required. External intercepts, which consists in boundaries, holes, and collapsed regions, are used for boundary modeling (Carvalho & Deutsch, 2017). The internal intercepts are the only information needed and at local coordinates (u, v, w).

3.2.2. Global Thickness Distribution and Local Values

Local thickness values are needed as data for imputation and global thickness distribution for further transformations. The existence of inclined drill holes makes it difficult to correctly calculate thickness values (Figure 3.3). Even so, both local values and the global distribution of thickness are normally calculated in the local coordinate system from plane fitting step. Even if these thickness values are uncertain, they will be merged with w elevation to get more accurate values. To calculate thickness for each intercept, a simple subtraction of hangingwall by footwall local elevation is executed:

$$Th = w_{HW} - w_{FW}$$

where Th is the calculated thickness for the intercept, w_{HW} is the local elevation of intercept hangingwall, and w_{FW} is the local elevation of intercept footwall. As a precaution, a maximum angle tolerance is applied to remove thicknesses where the angle between

hangingwall and footwall intercepts are too high. The first step to select the tolerance angle is to calculate this angle:

$$\theta = \cos^{-1}\left(\frac{w_{HW} - w_{FW}}{\sqrt{(u_{HW} - u_{FW})^2 + (v_{HW} - v_{FW})^2 + (w_{HW} - w_{FW})^2}}\right)$$

where θ is the angle between hangingwall and footwall intercept, u_{HW}, u_{FW}, v_{HW}, v_{FW}, w_{HW}, and w_{FW} are the u, v, and w coordinates, respectively, of hangingwall (HW) and footwall (FW). This calculates the angle in degrees for all intercepts, which 90° means horizontal drill holes (parallel to fitted plane), and 0 means vertical drill holes (perpendicular to fitted plane). Maximum angle tolerance angle can be based on calculated angle distribution. Ideally, only a small number of calculated thickness values are rejected. A cumulative distribution function of calculated angles for the data can be seen on Figure 3.4. A maximum angle of 34° seems to be a reasonable choice. Thickness values, from drill holes with angles higher than the tolerance, are rejected and assigned as missing data. During imputation, these rejected thickness will be also imputed. An example of the procedure described above, can be seen on Figure 3.5.

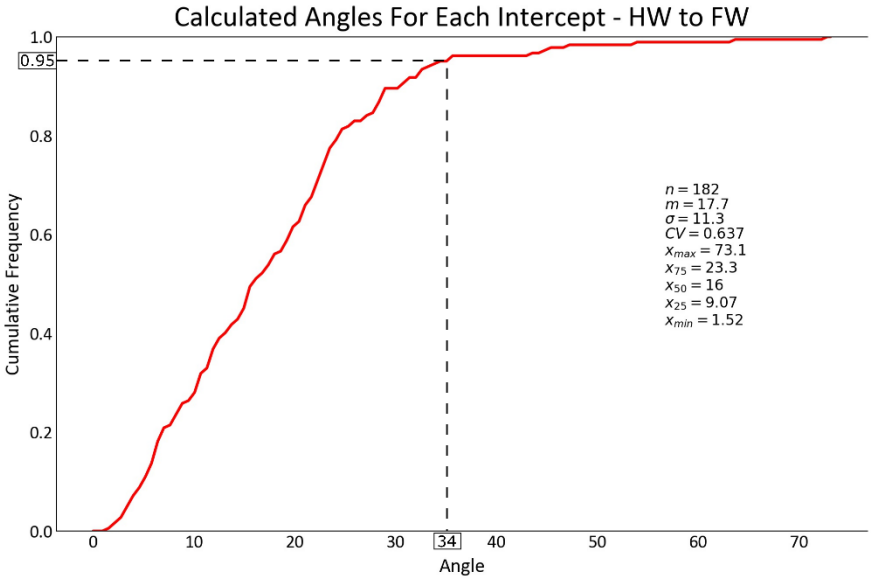

Figure 3.4: CDF of calculated angles between hangingwall and footwall, used for maximum angle tolerance evaluation. The percentile 95 is chosen as maximum angle tolerance, which represents 34° for this data.

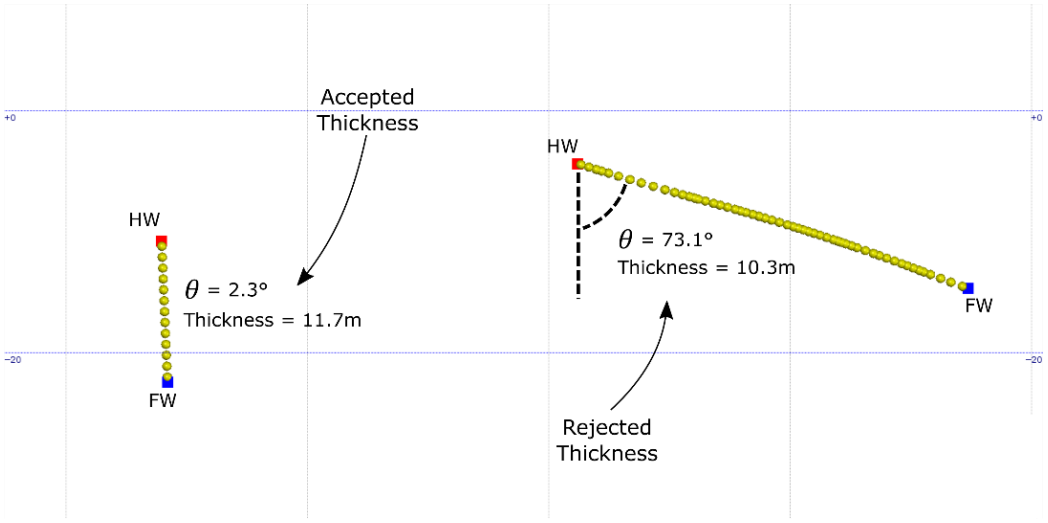

Figure 3.5: Cross section perpendicular to the fitted plane showing an example of rejected thickness values for simulation. The drill hole on right has an angle of 73.1°, which is higher than the set tolerance of 34°, and so, a missing value is assigned for this record.

3.2.3. Variograms

Variograms are required for data imputation, as elevation and thickness distributions are calculated using Sequential Gaussian Simulation (SGS). Variograms are calculated at local coordinates, in 2D projection on the vein plane. Like most well-established simulation algorithms, both variables need to be transformed to normal scores. Variograms need to be calculated and modeled for both elevation and thickness normal score data, separately. It is expected that both position and thickness variables variograms are stable and well-behaved, with considerable continuity, due to the geometry of these simple tabular vein deposits. However, depending on each mineralization and deposit, a variogram can be more stable than the other. In Figure 3.6, an example of variogram impact depending on vein geometry. Some depositional or erosional deposits can show different surfaces behaviors (case A), and so, base surface variograms are more stable than thickness variograms. The opposite happens when a vein with constant thickness is deformed proportionally (case B); thickness variograms are more stable than elevation variograms.

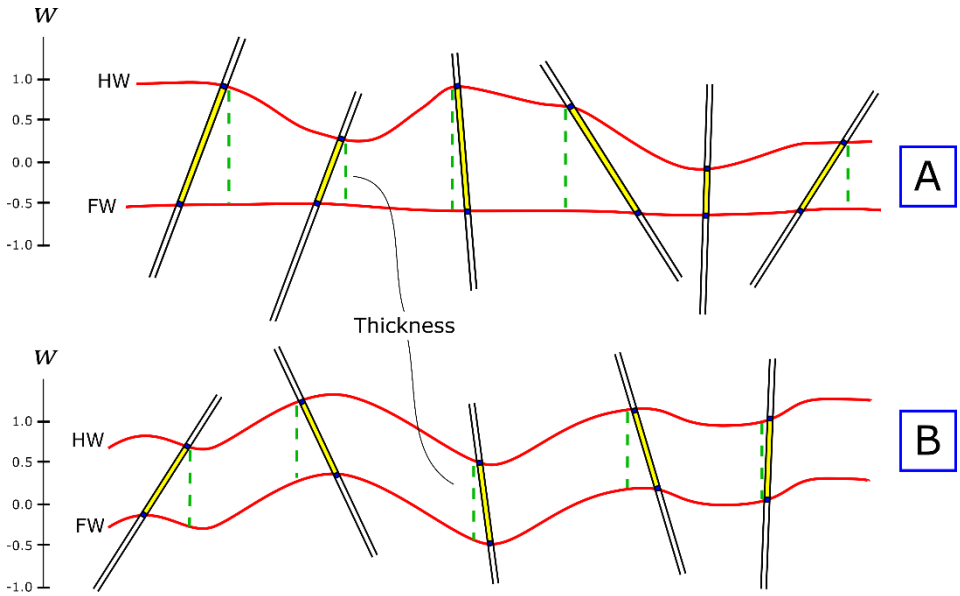

Figure 3.6: Different geometries and variograms impact. Green dashed lines show thickness. For case A, if footwall is the base surface, *w* variograms are more stable than thickness variograms. In case B, thickness variograms are more stable than *w* elevation variograms.

Even though plane fitting aligns u axis to dip, and v to strike, it does not mean that variograms will be more structured and continuous on these directions. As an example, in the data used, more structured variograms are found on azimuth 157.5° (Figure 3.7), that might be related to other geological controls influencing geometry. Another important aspect is to model using Gaussian variograms. Since geological surfaces are being modeling, the short scale variability should not be too high. Large variogram ranges are expected. The coefficient of variation and nugget effect should be low, and so, stronger conditioning is anticipated.

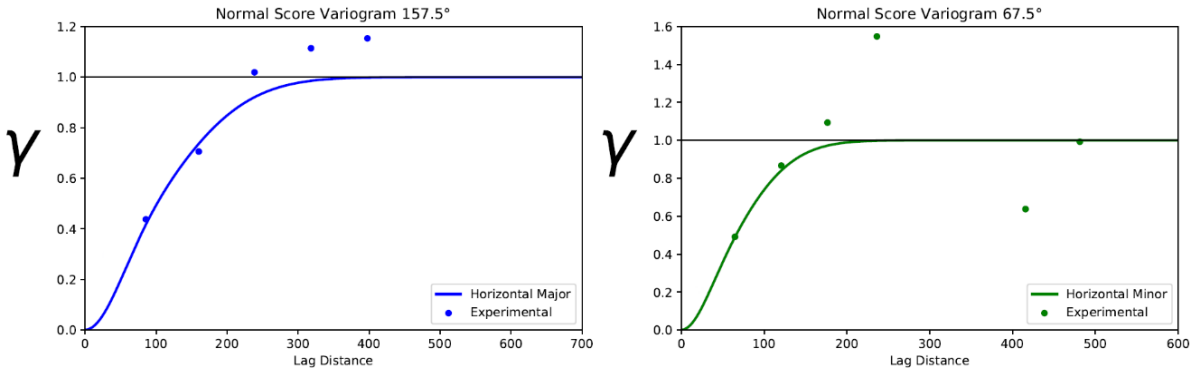

Figure 3.7: Modeled *w* elevation variograms for referred data.

3.2.4. Elevation and Thickness Distributions Simulation

The calculation of variables distributions is executed with Sequential Gaussian Simulation (SGS) by visiting each missing location. The geometry data from the vein, used in this step, are also w elevation and thickness values. Data should be normal score transformed for variogram calculation and modeling. It is important to store transformation tables for future transformation required for merging distributions. A base surface must be selected. For illustration purposes, assume the footwall is the base. This implies that hangingwall intercepts are projected at footwall and its position will be simulated based on footwall elevation values and thickness values. Afterwards, footwall intercepts are projected and their elevation and thickness distributions are simulated using data nearby. In Figure 3.8, it is easier to visualize the procedure above. Simulating elevation and thickness distributions, sequentially and for both footwall and hangingwall surfaces, at the same time for each realization guarantees that results are anchored, preventing crossing between hangingwall and footwall on imputed files and future surface simulation.

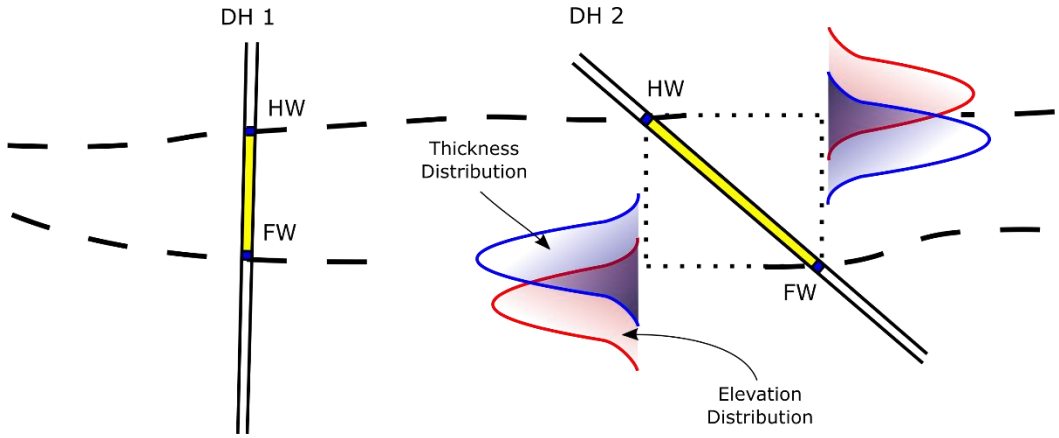

Figure 3.8: Intercepts projection and position simulated. For each intercept, there will be 2 simulated position distributions, one based on near footwall elevation values (red), and the other on calculated thickness values (thickness). Dashed lines are an interpretation of the vein surfaces. Dotted lines show the projection.

Kriging could be used for distribution calculation. Sequential Gaussian simulation is chosen for its convenience on implementation on the generation of imputed files and speed.

An important aspect of this step is that simulation will be carried at data location, and so, an appropriate algorithm for irregular grid should be used. The USGSIM software from CCG (Manchuk & Deutsch, 2015) is recommended for the implementation. The imputation option of the software will be used, and so missing values will be imputed. The input file requires all footwall and hangingwall intercepts and its projections, so the number of records will be twice the number of drill holes that pierced the vein. Required records are u, v, and w local coordinates and thickness values calculated previously. For rejected thicknesses due to high angle drill holes checking, imputation will be also performed.

The final goal of this process is to generate a number of imputation files that match the number of future surface realizations, in which each realization utilizes an individual imputation file, capturing a more realistic uncertainty of the intercepts positioning. Each file needs a complete distribution for elevation and thickness, that will be merged and sample afterwards. As an example, before merging, if hangingwall and footwall surfaces will be simulated 100 times, then 100 imputation files need to be generated, in which every file will have 100 realizations of elevation and thickness values for every imputed intercept. It is important to use a different seed number for each realization. The search volume is based on domain dimensions and variograms. The variogram parameters should be the same as calculated and modeled beforehand for each variable. With all parameters set, it is possible to run imputation of distributions for all drill holes.

3.2.5. Merging Imputed Distributions

It is necessary to merge the elevation and thickness distributions and sample a value from it. As shown on Figure 3.8, it is difficult to affirm the real position of the projected intercept at the opposite surface. Merging is required to better define the position of the intercept; the merged distribution is more precise than either one of the original calculated distributions. To preserve the uncertainty on the vein geometry, a random value from the merged distribution is sampled. Taking the average of the merged distribution would remove most of the variability and uncertainty.

Before merging, it is required for both distributions to be set to a common variable space. Thickness is chosen as the common space, and so, elevation distribution will be transformed to thickness space. The first step is to back transform w elevation normal

distribution to original values. The second step is to calculate thickness elevation from this back transformed distribution and the reference surface. The third step is to low/top cut calculated thickness values that are lower or higher than the minimum and maximum values from global thickness distribution. The fourth, and last, step is to normal score transform these calculated thickness values using the global thickness distribution as reference. With these steps, both distributions (original calculated thickness distribution and transformed w elevation) are at the same thickness space and merging can be applied (Figure 3.9). It is important to state that the thickness values from position transformation are assumed to be in Gaussian shape.

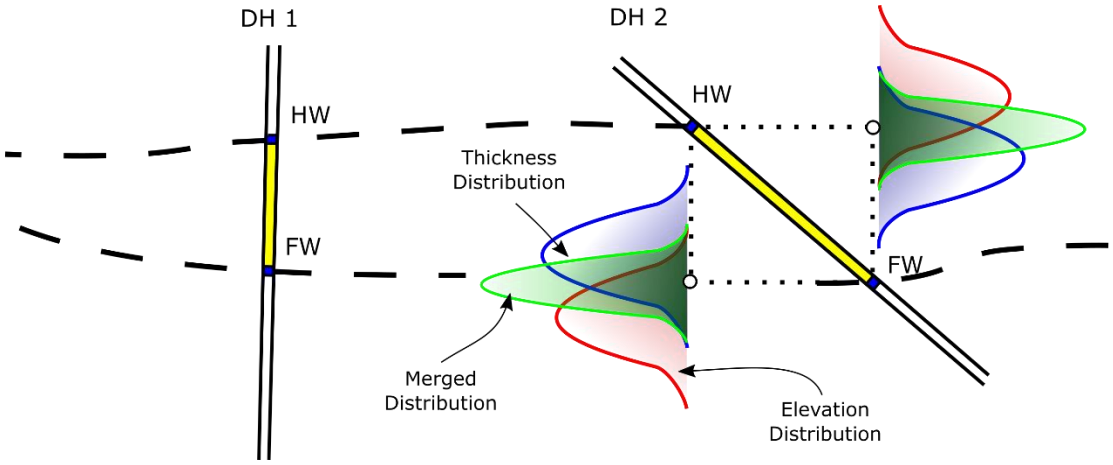

Figure 3.9: Sketch of elevation and thickness distribution merging. In this example, footwall is the base surface. Both surfaces positions are known on drill hole 1, as it is nearly vertical. For drill hole 2, footwall and hangingwall projected position are defined by merging thickness (blue) and transformed elevation (red) distributions. The merged distribution (green) is then randomly sampled and an imputation file is saved.

The methodology chosen for merging simulated distributions is the method of error ellipses with geological data (Rezvandehy & Deutsch, 2014). For merging, both distributions should be normal. Error ellipses equation, adapted for two univariate distributions, can be seen below:

$$\overline{X} = C\left(\frac{m_1}{\sigma_1^2} + \frac{m_2}{\sigma_2^2}\right), C = \left(\sigma_1^{2^{-1}} + \sigma_2^{2^{-1}}\right)^{-1}$$

where $\overline{X}$ is the vector representing the location of the weighted average, C is the resultant variance, m_n is the univariate mean, and σ_n^2 the univariate variance. Error ellipses is selected for the task as Bayesian updating requires a strong prior distribution, and error ellipses enforces the update distribution to locate between distributions (Figure 3.10).

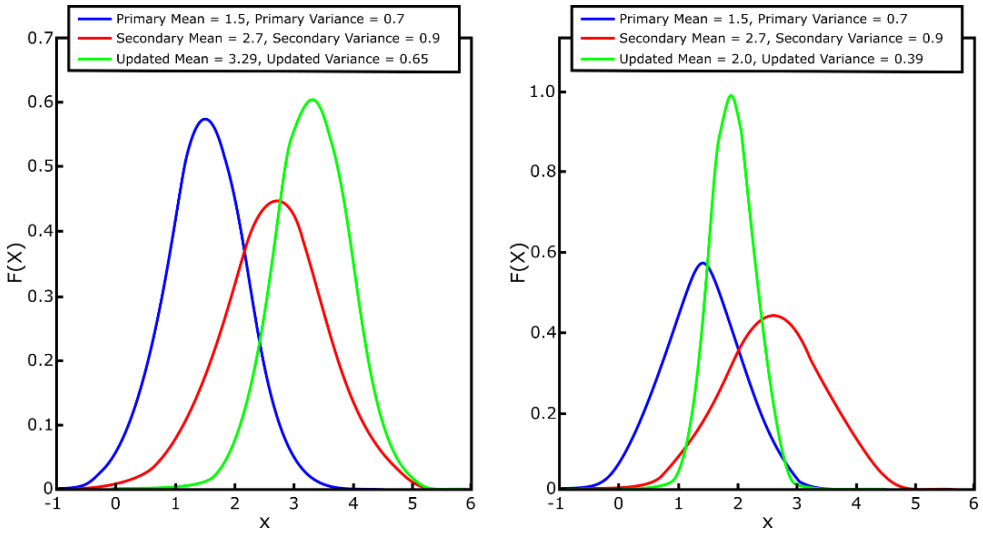

Figure 3.10: Probability density functions of combining two distributions (red and blue) with predetermined mean and variance. The result of combining is in green by Bayesian updating (left) and error ellipses (right) (Rezvandehy & Deutsch, 2014). Bayesian updating could lead to many results depending on circumstances. The method of error ellipses enforces the merged distribution to be in between original distributions.

After merging distributions, a random sample from the merged distribution is selected to preserve uncertainty. Imputation file can be saved or back transformed to original values. Each intercept receives the thickness sampled value and w elevation is calculated by subtracting or adding thickness from reference surface elevation.

Most of the vein deposits do not present many crossing drill holes. For this reason, sampled locations are not used for conditioning of sequential imputed locations. In most cases, drill holes are separated enough so there is no much influence from previous imputed position. Most of the weight comes from the same drill hole.

3.3. Surface Simulation

After generating the imputation files, surface and solid modeling can be executed. Surface simulation is performed to quantify uncertainty in volume. A sketch of simulated surfaces can be seen on Figure 3.11, where the red lines are the expect hangingwall and footwall and the gray lines are realizations. To preserve the uncertainty from imputation, each surface realization should use a single and different imputation file. The position and thickness values are kept as pairs to prevent crossing in individual realizations. To facilitate posterior triangulation and wireframe construction, a regular equilateral triangular grid is recommended. Also, triangular meshes may produce smoother surfaces that efficiently match unstructured grids of tetrahedrons. The recommended resolution, based on triangle side length, is at least one quarter of the drill hole spacing.

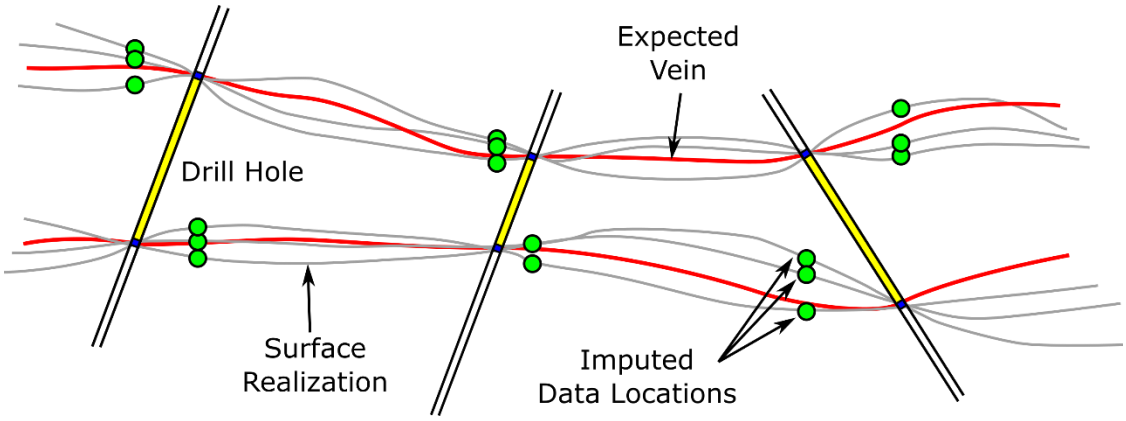

Figure 3.11: Sketch of surface simulation. Red lines are the expected (estimated) surfaces and gray are realizations. The green dots show imputed data locations.

Lower resolution grids result in apparently smoother surfaces since the values are smoothly interpolated between widely spaced nodes. The nugget effect should be exceptionally low as there is no abrupt changes in elevation and thickness values of the veins. Gaussian variograms are recommended for the modeling. Zero nugget effect values could lead to instability in the covariance matrix. Infinitesimal nugget effect values are recommended to avoid such instabilities. If correlation exists between position and thickness, a multivariate modeling is required. Projection pursuit multivariate transformation (PPMT) could be considered for the task (Barnett et al., 2014).

External limits and holes are considered later, therefore only internal samples and intercepts are used in surface simulation. In this workflow, the base surface will be simulated using elevation values, and the opposite surface using thickness values. As an example, considering the footwall as the base surface: the footwall surface will be simulated using w elevation, while hangingwall established with thickness simulation. These thickness values are then added to the simulated w_{FW} to find the final w_{HW} position in the triangular grid. Grid limits should not have high extrapolation from drill hole data. It is recommended to use a maximum of twice the average drill hole spacing (DHS). Average DHS can be calculated using Silva & Boisvert (2014) software. Vein boundaries and holes can be modeled using a distance function (DF) (Hosseini & Deutsch, 2007) methodology, and will be detailed in the next chapter. To honor drill holes intercepts and collected data, it is recommended to add the hangingwall and footwall intercepts as nodes in the respective simulated triangular grids. An example of a triangulated surface is seen in Figure 3.12.

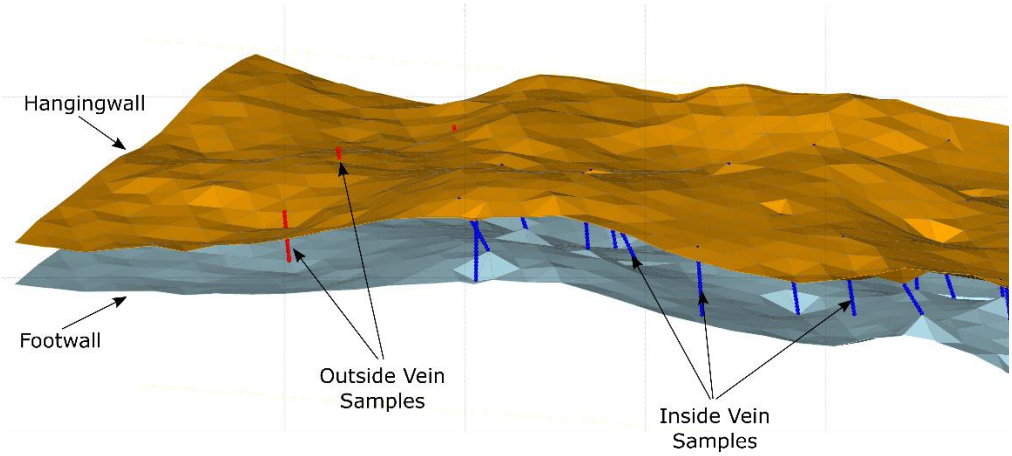

Figure 3.12: Example of a triangulated expected surface, using triangular grid and snapping samples, before distance function boundary modeling.

At the end of surface simulation, many vein solids are generated, and geometric uncertainty is captured. Each realization solid is stored for later gridding and grade modeling.

Chapter 4. Other Sources of Uncertainty

In addition to geometric uncertainty, there are other important sources of uncertainty when modeling tabular deposits resources. These include external boundaries and holes modeling, grades and properties simulation, and parameter uncertainty. Boundaries are important for tonnage and volumetric assessment. Extrapolation must be reasonable defined. Grades and properties are to be simulated within an unstructured tetrahedron grid with the correct anisotropy modeling. Parameter uncertainty modeling accounts for histogram uncertainty. Fixing a single input histogram does not capture the uncertainty in grade modeling. Data and survey quality may also be important aspects to be considered. Small deviations in position can transform to large errors in the intercepts of the deposit.

4.1. External Boundaries and Holes

The uncertainty in position and thickness is evaluated early in the workflow with geometric data imputation and surface simulation. Data imputation accounts for input data with multiple data realizations in the position and thickness values. Imputed data are used for surface simulation and multiple vein geometries are generated. These steps, however, do not account for the external boundaries and the presence of holes in the veins (Figure 4.1). External boundaries and holes should also be modeled with uncertainty in the resource estimation workflow. A different boundary realization will be considered for each surface realization of the vein. Boundaries will be modeled as areal limits using the distance function methodology and simulation (Hosseini & Deutsch, 2007). The distance function (DF) is used to interpolate and map the vein boundary based on vein indicators (VI). The indicators are $VI = 0$ when outside the vein, and $VI = 1$ inside the vein. The DF is calculated by the Euclidean distance between each sample and the nearest sample with a different indicator, inside and outside the vein. The distance values are given a sign depending to the value of the vein indicator. Distances inside the vein are considered negative, while distances outside the vein are considered positive. The calculated Euclidean distance can be modified to account for anisotropy as:

$$df = \sqrt{\left(\frac{dx}{ax}\right)^2 + \left(\frac{dy}{ay}\right)^2 + \left(\frac{dz}{az}\right)^2}$$

Where d is the distance between samples of different indicators in x, y, and z axis and a is the geometric anisotropy defined for x, y, and z. The df should be the minimum contact distance between all samples. For the workflow, the axes will be u, v, and w from the local coordinates system fitted with Total Least Squares. The idea is to interpolate the DF values and clip the external boundaries and holes where values are positive. The distance will be calculated in 2-D plane of the vein between the midpoint of each positive and negative intercept. Global kriging is recommended for interpolation of the distance function values to avoid artifacts (Neufeld & Wilde, 2005) that arise due to restricted search neighbourhoods. The solution then is to use all samples without any search. The grid used for global kriging the DF values should match the same triangular grid from surface simulation. The jackknife option in conventional kriging programs could be used for estimating unstructured grid locations.

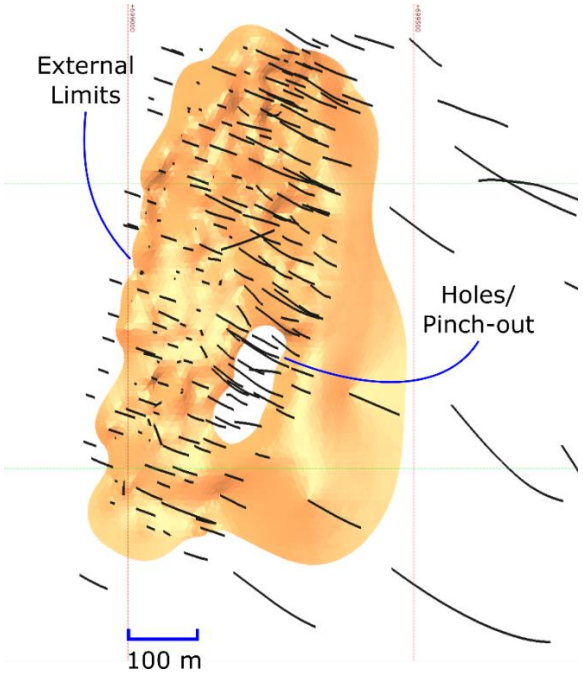

Figure 4.1: Plan view of an auriferous vein showing external boundaries and holes, typical structures present on vein deposits.

The uncertainty bandwidth is based on the C parameter, which is an additive constant applied the modified Euclidean distance:

$$DF = \begin{bmatrix} (d + C) & \forall\, VI = 0 \\ (d + C).-1 & \forall\, VI = 1 \end{bmatrix}$$

Where d is the modified Euclidean distance and C is the constant parameter. The C parameter controls the uncertainty width by adding or subtracting to the Euclidean distance. The distance between $-C$ to $+C$ is the bandwidth space between vein and non-vein areas. Calibration of the C should be performed (Munroe & Deutsch, 2008). Each realization requires a different C parameter resulting in a different boundary for the vein geometry. A random value could be selected between $-C$ to $+C$. For a reasonable uncertainty bandwidth, the random number should be sampled from a uniform distribution. The β parameter controls the location of the bandwidth defined by C and must be chosen carefully. The calculation of the modified distance function goes as:

$$DF = \begin{bmatrix} d/\beta & \forall\, VI = 0 \\ d.\beta & \forall\, VI = 1 \end{bmatrix}$$

The beta value is determined so that there is no bias in the final estimated tonnes, that is, the limits are not too restrictive or too large. It is important to carefully control the extrapolation of boundaries. Ideally, there should exist enough drill hole data around the vein boundaries to delineate the mineralization limits. If data is not available, pseudo-data could be added to control boundary extrapolation. The pseudo-data position should be based on the average drill hole spacing and geological knowledge.

4.2. Grades and Properties

Metal grades uncertainty is critical for vein deposits evaluation as it impacts the estimated metal content. Volumetric uncertainty is assessed with data imputation, surface simulation, and boundary modeling. Following the probabilistic resource estimation workflow, simulation is required for the grades. Geostatistical simulation considers the histogram and spatial continuity of the original data. Many well-established algorithms are available

including turning bands (Matheron, 1973; Journel, 1974), sequential Gaussian simulation (Isaaks, 1990), LU Decomposition (Luster, 1985; Alabert, 1987), and others. This thesis recommends the use of an unstructured tetrahedron grid, which is a natural gridding alternative for geological structures. The tetrahedron grid matches the vein geometry. Most simulation algorithms are developed for regular grids and block models. For simulation in an unstructured grid, there is need for modifications. The ultimate sequential Gaussian simulation algorithm (USGSIM, Manchuk & Deutsch, 2015) is recommended for the task. The algorithm uses its imputation capability to simulate unstructured grids. Anytime the data is heterotopic, the algorithm executes the imputation before running simulation. The input data is the unstructured grid and an imaginary (nonexistent) and uncorrelated variable is created. Where the imaginary variable is defined, all other variables are simulated by USGSIM imputation. As the imaginary variable is uncorrelated with other variables, there is no influence on the results.

Simulation is executed on a high-resolution grid, at data scale, enough to provide a sufficient number of nodes within the grid volumes of interest. The block size of interest should meet mining specifications, drill hole spacing, and geometry of the ore body. The TetGen algorithm (Si, 2015) can be used for grid generation. For tetrahedralization, a watertight solid is required. This solid is also referred to as a piecewise linear complex (PLC). The PLC cannot have intersections that do not form a cell and cannot have open edges (Figure 4.2).

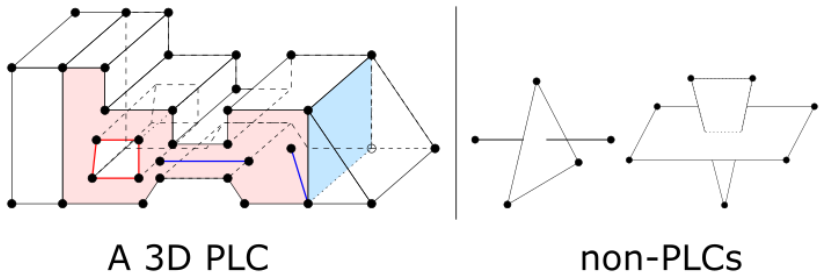

Figure 4.2: Examples of a 3D PLC and non-PLCs. The left example shows a non-convex facet is and has a hole in it (red line). It has also edges and vertices foating in it. The right shaded area shows an interior facet separating two sub-domains. The right example shows non-PLCs (Si, 2015).

The fine resolution grid must comply with a reasonable discretization design for each tetrahedron. The discretization design must be flexible as tetrahedron sizes are variable depending on vein geometry adaptation. Areas with lower thickness values presents smaller tetrahedrons, whereas thicker areas present larger tetrahedrons (Figure 4.3).

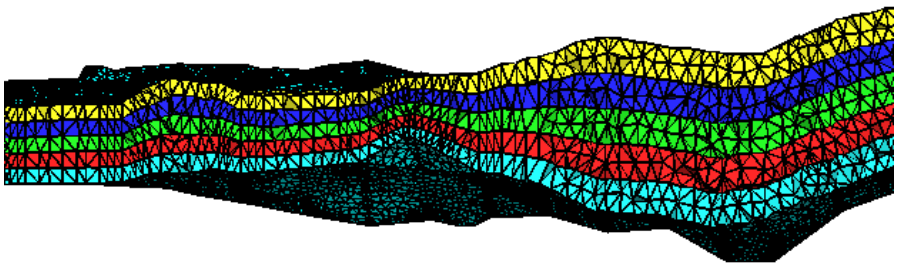

Figure 4.3: Section of a tetrahedralized vein showing tetrahedron adaptation for distinct thicknesseses areas. Colors denotes different internal layers created to account for anisotropy modeling. Average thickness is 8 meters.

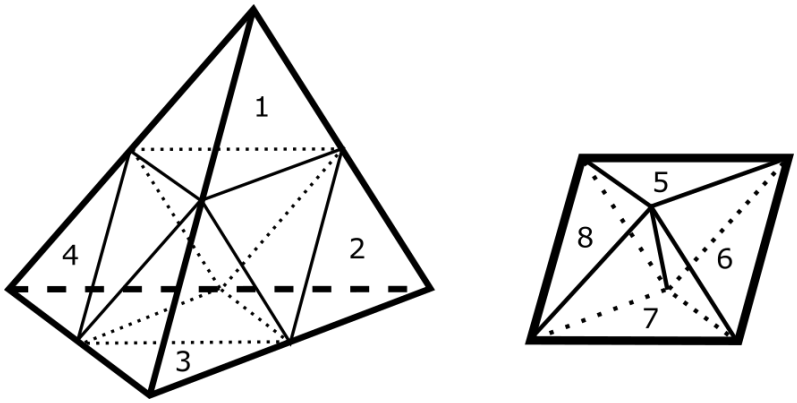

Figure 4.4: Regular refinement of the faces (Bey, 1995) and resulting sub-tetrahedra. The original tetrahedron on the left is subdvided in 8 sub-tetrahedra. Four congruents sub-tetrahedra are shown on left. Internal octahedron are then subdivided again.

The recommended tetrahedron (T) discretization design follows a regular refinement presented by Bey (1995). The objective is to subdivide each T tetrahedron in 8 sub-tetrahedra, $T_1, \ldots, T_8$, of equal volume, in such a way that each corner of a son T_i coincides with either a corner or a, edge midpoint of T (Figure 4.4). Discretization points that represent equal volumes inside the tetrahedron is reasonable.

To describe the regular refinement algorithm, it is assumed T to be given by an ordered sequence of its vertices: $T = [x_0, x_1, x_2, x_3]$. For $0 \leq i, j \leq 3,\ i \neq j$, it is denoted by $x_{ij} = (x_i + x_j)/2$ the edge midpoint x_i and x_j. The algorithm can be formulated as follows:

$$divide\ T = [x_0, x_1, x_2, x_3]\ into\ the\ subtetrahedra\ T_i, 1 \leq i \leq 8\ , given\ by$$

$$\begin{aligned} T_1 &= [x_0, x_{01}, x_{02}, x_{03}] & T_5 &= [x_{01}, x_{02}, x_{03}, x_{13}] \\ T_2 &= [x_{01}, x_1, x_{12}, x_{13}] & T_6 &= [x_{01}, x_{02}, x_{12}, x_{13}] \\ T_3 &= [x_{02}, x_{12}, x_2, x_{23}] & T_7 &= [x_{02}, x_{03}, x_{13}, x_{23}] \\ T_4 &= [x_{03}, x_{13}, x_{23}, x_3] & T_8 &= [x_{02}, x_{12}, x_{13}, x_{23}] \end{aligned}$$

The regular grid refinement is adapted, and 5 different discretization designs are tested in terms of mean squared error (MSE). The designs go with 1, 8, 27, 64, 216, and 512 discretization points within each tetrahedron. All of them are developed maintaining the regular refinement property of equal volume sub-tetrahedra. A single discretization point corresponds to the barycenter of the tetrahedron. The design with 8 points is obtained with one regular refinement. The 64-points design is obtained in two sequential refinements. Likewise, the 512 design is obtained with a third refinement. The 27-points discretization design is generated by first subdividing the original tetrahedron in 3 levels of equal height Each level is then refined by the described algorithm, generating sub-tetrahedra of equal volume. The first level on top is a single congruent sub-tetrahedron; the second level has 7 sub-tetrahedra, being 3 bordering congruent sub-tetrahedrons, and 4 sub-tetrahedrons in the centre, formed from the central octahedron; the third level has 19 sub-tetrahedra, being 6 bordering congruent sub-tetrahedrons, 12 sub-tetrahedrons from octahedrons and 1 sub-tetrahedron in the centre. Figure 4.5 illustrates this design. The 216 design is generated by refining the 27 sub-tetrahedra. It is noteworthy to state that all designs result in equal-volume sub-tetrahedra (Bey, 1995).

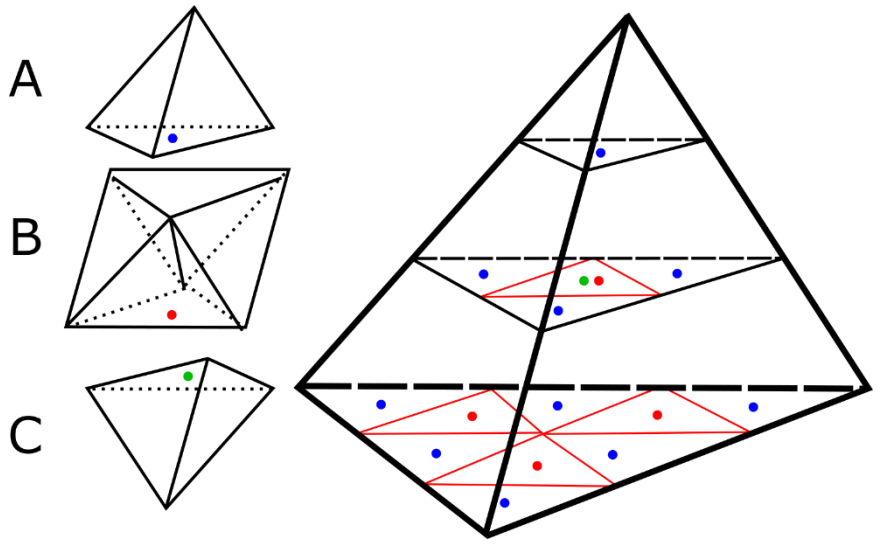

Figure 4.5: Modified refinement design to generate 27 and 216 equal-volume tetrahedrons. The original tetrahedron (right) is subdivided in 27 subtetrahedra. The subtetrahedra is shown on the left. Each color represents a type of subdomain. There are 10 tetrahedrons of type A, 4 octahedrons of type B (that is formed by 4 tetrahedrons), and 1 tetrahedron of type C.

A fine resolution grid is created within a tetrahedron and the truth is simulated. A lognormal distribution is chosen as base test. The discretization designs are simulated 200 times and MSE is calculated based on the truth. Results can be seen on Figure 4.6. The selected design is with 27 discretization points. The MSE difference between a single point and 27 points is around 0.146, which is substantial drop. The MSE difference between 27 points and 64 points is around 0.015, which is about ten times less; therefore, 27 discretization points seems reasonable.

Metal grades and properties follow vein structures and surfaces. This anisotropy is due to the hydrothermal flow, orientation of deposition, and structural controls during the mineralization genesis and development. Common types of vein anisotropies are: proportional and surface conforming. For proportional anisotropy, the greatest continuity of grades follows a plane that maintain its position relatively to the thickness of the vein (hydrothermal fluids). In the case of a conforming surface, hangingwall or footwall, grades follow a plane parallel to the conforming surface (depositional or erosional deposits). These types of anisotropies are illustrated on Figure 4.7.

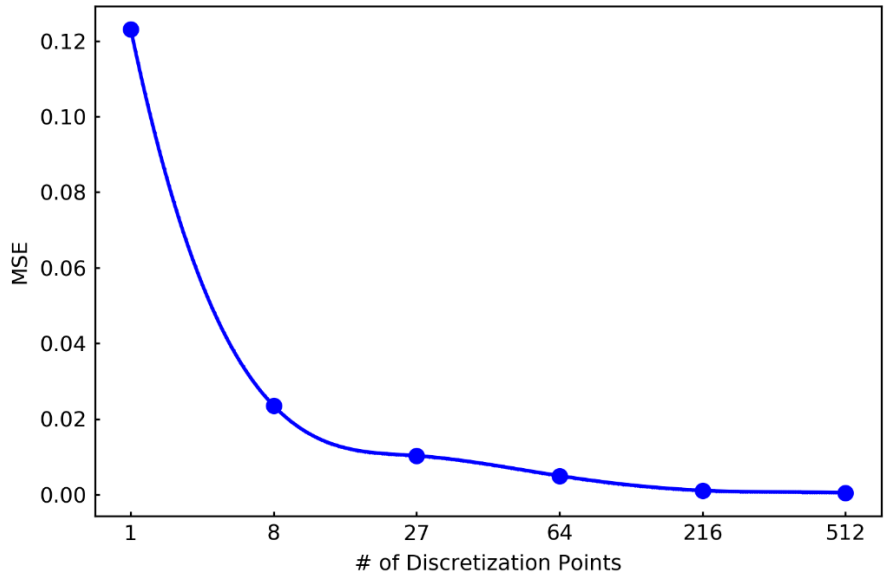

Figure 4.6: Mean squared error for 6 discretization designs, all with equal-volume sub-tetrahedra.

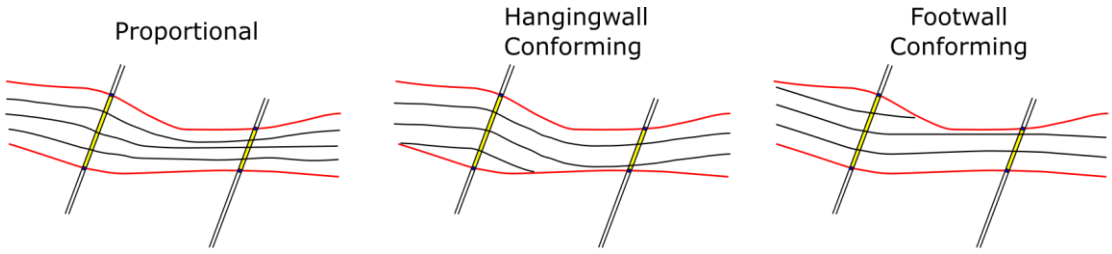

Figure 4.7: Types of grade anisotropy on a tabular vein deposit (Deutsch, 2005).

For surface conforming, the anisotropy surfaces are at a fixed offset from a reference surface. For proportional anisotropy, the surfaces are modeled as a proportion of the thickness value at that location. For a point p_i, (u_i, v_i, w_i), w_{RS} is the w coordinate of the reference surface, interpolated at the same location, (u_i, v_i). For surface conforming, the w' coordinate is then:

$$w' = w - w_{RS}$$

If proportional anisotropy is being modelled, the w' coordinate is the data point's position in the vein as a proportion of the thickness at that point. w_{FW} and w_{HW} are the interpolated location of the footwall and highwall surfaces at the same location, (u_i, v_i). The w' coordinate is then:

$$w' = \frac{w - w_{FW}}{w_{HW} - w_{FW}}$$

With these new coordinates, models will naturally follow vein geometry and anisotropy, in agreement with geological factors. If many variables are being modeled within the vein, a multivariate modeling is required. Projection pursuit multivariate transformation (PPMT) is one modern approach for the task (Barnett et al., 2014), particularly for simulation.

4.3. Parameter Uncertainty

Parameter uncertainty is an important aspect of vein resources uncertainty evaluation. There is uncertainty in global statistical parameters for grade modeling. Simulating with fixed input parameters can substantially underestimate the global uncertainty. Underestimation of uncertainty can be higher for large domains relative to the variogram ranges. Uncertainty in the histogram should be accounted by establishing different distributions and generating each geostatistical realization with a different distribution. The Spatial Bootstrap (SB) is recommended for uncertainty in the histogram (Deutsch, 2004). The original bootstrap is an application of the Monte Carlo simulation methodology formulated by Efron (1982). It consists in a statistical resampling technique that quantifies the uncertainty by resampling the original data. The following procedure illustrates the bootstrap procedure to calculate the uncertainty of the experimental mean m_Z from n data of a single variable $(z_i, i = 1, \dots, n)$: (1) Construct the representative distribution of the Z random variable using declustering and debiasing techniques: $F_Z(z)$. The equal weighted histogram of the data could be also used; (2) Draw n values from the assembled distribution, by generating n uniformly distributed random number $p_i, i = 1, \dots, n$ and record their respective quantiles: $z_{s,i} = {F_Z}^{-1}(p_i), i = 1, \dots, n$. The number of data drawn is equal to the number of data available. Simulated distributions are not equal to original

as there is replacement; (3) Calculate the experimental mean m_Z; (4) Return to step 2 and repeat a desired number of times; (5) Assemble the distribution of uncertainty with the calculated statistics.

The bootstrap assumes independence between data. For highly correlated samples and closely spaced drill holes this assumption is unrealistic. To account for spatial correlation between samples, a geostatistical simulation technique is used. LU decomposition is recommended (Deutsch, 2004) for its efficiency and simplicity. A three-dimensional variogram is required for the task and multivariate Gaussianity and stationarity are assumed, as in any other geostatistical technique. Many different statistics can be calculated including mean, variance, cutoffs, mean above/below cutoff, and others, which can be used for later modeling. Correlation in the samples result in greater uncertainty than no independence between data.

For vein resources uncertainty quantification there are some important variables to evaluate in terms of histogram uncertainty. The variables are position of the base surface, thickness values, and metal grades. For position and thickness, it is recommended to perform spatial bootstrap before the imputation process. Geometry imputation will generate a number of imputation files based on position and thickness simulated and sampled distributions. The use of a single histogram for position and thickness underestimates the resource uncertainty. Grade histograms are closely reproduced by simulation. The average grade between each geostatistical realization is very similar. The spatial bootstrap is recommended before grade simulation, and each realization should use a different parameter.

Variogram uncertainty could be also applied to the workflow (Rezvandehy & Deutsch, 2017). For this work, variogram uncertainty is not performed. Variograms controls the spatial continuity of position, thickness, and grades but have little impact on final resources. Grade and geometry are expected to be fairly consistent, and so, variogram uncertainty impact on global resources would be minimal.

Chapter 5. Implementation

Geometric uncertainty is quantified by creating a local coordinates system, imputing position of surfaces and thickness with simulation, and simulating vein geometry using all position and thickness values. Multiple boundaries are also simulated. Each surface realization has a different boundary. The spatial bootstrap is employed to account for uncertainty in the input data histogram. Grades are simulated inside the unstructured tetrahedron grid. All these steps produce a large number of vein geometry wireframes and grade realizations. Managing all realizations and presenting simulation outcomes is necessary to understand and quantify uncertainty. Post-processing and sensitivity analysis are used for this assessment and quantification. Mine planning optimization, resource classification, and reporting are equally supported by the results of the workflow. These methodologies are reviewed and examples are presented.

5.1. Post-Processing

The probabilistic resources estimation workflow generates multiple realizations of the vein geometry, boundaries, and grades using conditional simulation. All resulting realizations are considered equiprobable and have the correct histogram and variogram within statistical fluctuations. Simulation does not have the smoothing of kriging and does not have any conditional bias. Simulation provides joint uncertainty assessment, point scale uncertainty, change of support, uncertainty on stopes, benches, mining plans, and schedules. Simulation allows for understanding of information effect, selectivity, dilution, and ore loss by simulation of grade control process. Forecasting metal recovery is also attainable. Each block can be assessed, for each realization, and a transfer function applied to predict metallurgical process and recoveries. Geometallurgical uncertainty models are then obtained.

Managing multiple realizations is a challenging task and perhaps underestimated by resources estimation practitioners. It represents, at each location, a range of possible values. There are different ways to summarize and visualize the results of simulated realizations including:

- Average of all simulations: The e-type mean is the point-by-point average of all realizations and it is the expected value at each location. This e-type model is very similar to the kriged model.
- Probability and mean above threshold: Given a cutoff grade or value of interest, the probability and mean to be above the cutoff can be calculated for each block. It is important to evaluate which blocks have high probability of being ore, waste, and other classifications.
- Probability maps: For each location, is possible to calculate the local distribution of the block. Specific quantiles of interest can be analyzed, such as 10, 50 and 90%. Any areas with high grades on p10 are surely high-grade regions. Areas wit low grades on p90 are surely low-grade regions. These maps can assist the qualified person to classify resources and reserves (e.g., if yearly volumes are within 15% the predicted average 90% of the times, then this resource is measured)
- Global uncertainty: A summary table can be organized to understand uncertainty on global grades, tonnages, and metal content. The calculations are performed on each realization and global distributions are calculated for each variable.

For vein resources uncertainty assessment, most post-processing described above is applicable. With multiple realizations of geometry and boundary, probability maps to be in the vein can be calculated. An example of probability maps for veins can be seen on Figure 5.1. The map on the left shows the probability of nodes to be inside the vein, calculated by the multiple boundary models. This is an important tool to evaluate stope placement. In areas with low probability of the vein being present, stopes should be reconsidered, and additional drilling executed. The map on the right shows the probability map of thickness to be higher than 10m. This is also important for mine planning, where geotechnical and mining constraints may influence on stope designing. Probability surfaces can be generated given important predefined quantiles. An example of probability surfaces can be seen on Figure 5.2. Stopes could be optimized given the probabilities of presence of the vein. There is higher certainty of presence of the vein in its inner areas. There is lower certainty of presence of the vein in its outer areas.

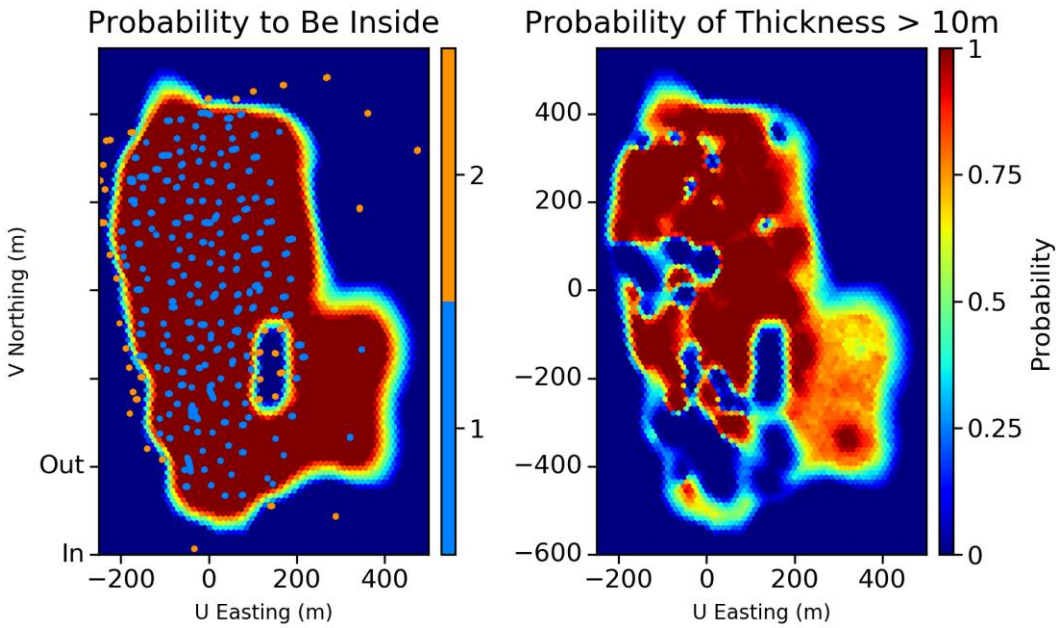

Figure 5.1: Auriferous vein probability maps. Probability map to be inside the vein (left) and to thickness be greater than 10m (right). Samples inside (blue dots) and outside (orange dots) are showed on left map.

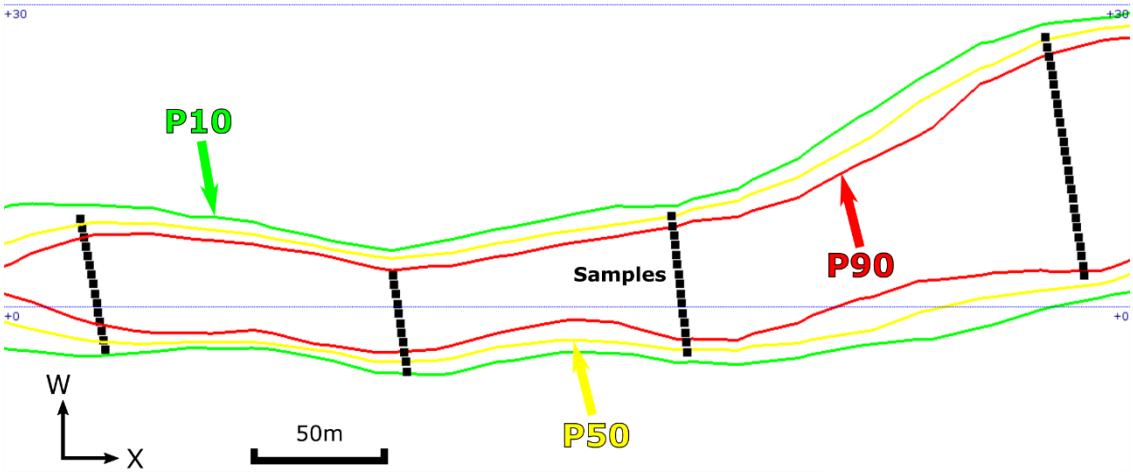

Figure 5.2: Cross-section of an auriferous vein probability surfaces. Surfaces are generated for p10, p50, and p90 quantiles. There is a higher probability of existence of the vein on inner parts of the mineralization. The farther from the core of the vein, lower are the probabilities of its existence.

5.2. Sensitivity Analysis

Sensitivity analysis is a step in the study of complex engineering systems. It investigates the relationship between the input parameters and response variables. Model responses are related somehow to model parameters, and sensitivity analysis supports understanding the relationships with mathematical modeling. The intrinsic relationship between variables and the model may be known by the modeler, but the relative importance of each variable, and their rankings, might not be understood. It is crucial to understand which variables impact most on the response model and its uncertainty. Variables with high impact need more attention and investigation.

The goal of the sensitivity analysis is to detect and quantify changes in values of the model caused by changes in the input variables (Saltelli et al., 2008), ranking the variables by importance or impact. It not only characterizes the relationship between input parameters and response variables, but also the interaction between input parameters. The quality of the model can be evaluated, and complexes models may be simplified. Variables with higher impact can be prioritized and uncertainty evaluation can be complemented by sensitivity analysis results. Sensitivity analysis has been used to evaluate models of uncertainty in natural resources (Deutsch et al., 2002; Zagayevskiy & Deutsch, 2011). Sensitivity coefficients are defined as the partial derivative of a model of response with respect to input variables. The partial derivative is replaced with the ratio of response change to change of the input variable that caused this variation, fixing values from other variables. An alternative approach for the calculation is regression analysis (Zagayevskiy & Deutsch, 2011). Linear and quadratic regressions are used to calculate first and second order sensitivity coefficients. Graphical representation of the results of sensitivity analysis is recommended. A tornado chart is widely used to present local and global sensitivity analysis. First and second order sensitivity coefficients can be plotted with original units or standardized. An example of a tornado chart with standardized sensitivity coefficients can be seen on Figure 5.3.

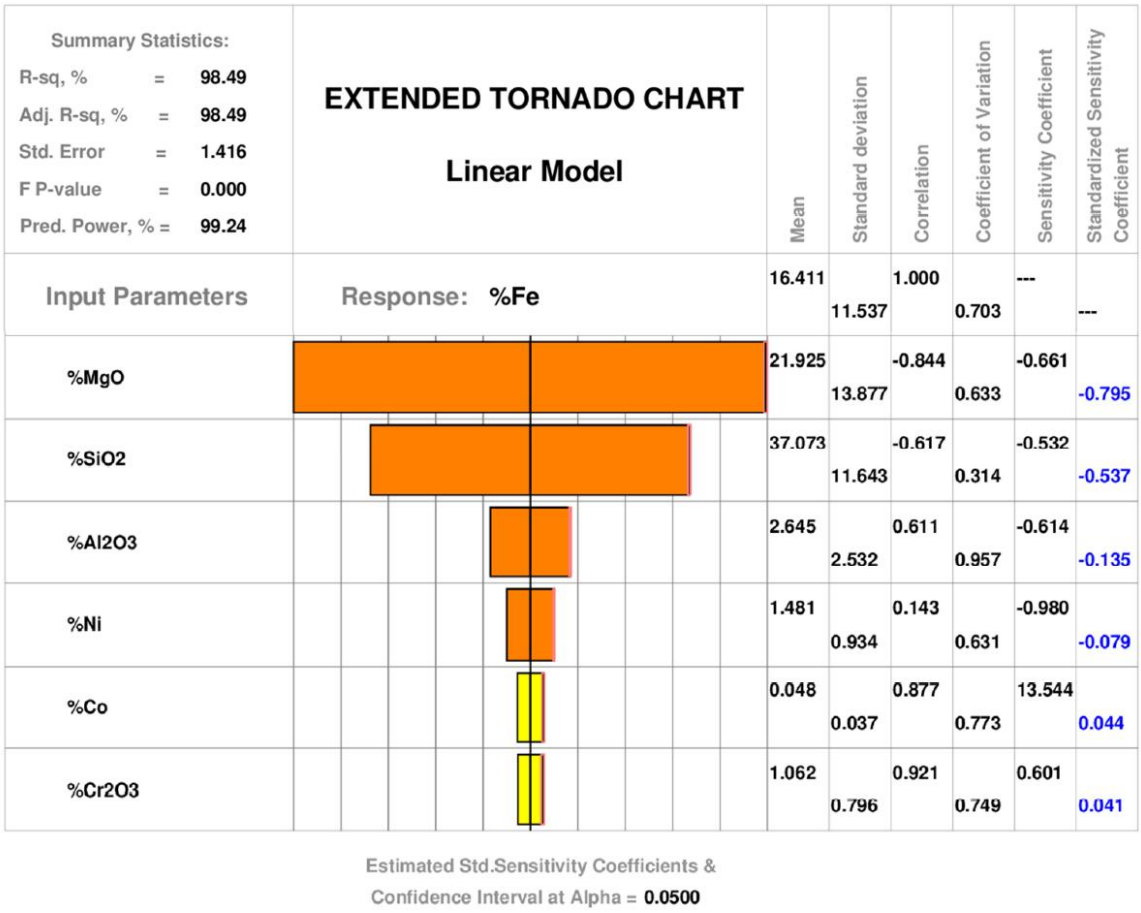

Figure 5.3: Tornado chart for a multivariate study (Zagayevskiy & Deutsch, 2011). The chart shows the impact of input variables on the response variable (Fe). It can be interpreted that MgO, SiO_2 and Al_2O_3 have most impact on Fe prediction. Other variables have little impact on the response.

Sensitivity analysis is recommended for in the proposed probabilistic workflow for vein resources. The evaluation could be applied both local and globally. Similar to Deutsch (2015) perspective for uncertainty simulation, a summary table is calculated and processed. Stopes or nominal production volumes could be used for local analysis. Global resources are also evaluated within the entire deposit. For vein resources, input variables should contain simulated grades, the 2D area of the vein, the C parameter, simulated surface position, and simulated thickness values. Response variables are mainly related to volume or tonnage and metal content. Input and response variables should be calculated for each realization. The sensitivity analysis can highlight the input variables that impact most the

calculated tonnages and metal content. It is expected that geometry variables have more influence on volume and tonnage, while grades impact metal content.

5.3. Mine Planning Optimization

Mine planning is a crucial step in the development of mining operations. Feasibility evaluation and improvement of the economic potential of the deposit is a central objective of geologists and mine engineers. Most current techniques have been developed for open pit operations. Underground mines are increasing in number due to advances in mining technology and lower environmental impacts. Costs are still higher than open pit mines. Stope geometry design is an important factor for maximizing profits and minimizing costs. It depends on geological, geotechnical, and grade model information. Each mine has it own constraints, site specific considerations, geology, and structural properties intrinsic to the deposit. The variety of underground mining methods makes stope design a laborious task. In most cases, stope designing is performed using a single estimated block model.

The current challenge for mine planning is to develop methodologies that account for uncertainty in reserves, which is optimized using multiple simulated realizations of vein grades and geometry. The goal is to increase the value of a particular stope by modifying and optimizing an existing design. It is unfeasible to execute this type of stope optimization by hand due geological complexity and uncertainty, which is quantified by simulation and multiple model realizations. A framework for steeply dipping ore bodies is presented by Manchuk (2007). Prerequisites are a consistent parametrization of the stope geometry, pre-specified mining constraints, and consistent methodology for changing the pre-existent stope design. The stope is defined as a closed triangulated entity. Constraints are imposed by the methods and procedures used for the mining as geological, geotechnical, hydrological, and mining characteristics. Multiple block models are evaluated and then clipped based on information of the block model. The position of the surfaces can be optimized based on profit of the stope. It is expected that larger stopes result in higher dilution, whereas narrower stopes result in ore loss, and so, expected profit can be optimized (Figure 5.4).

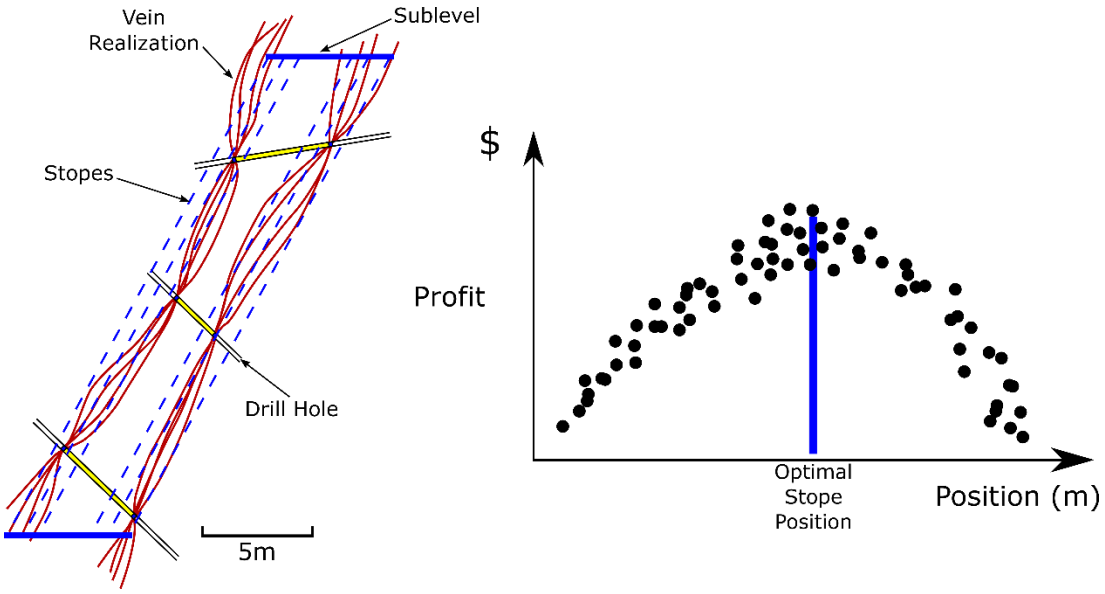

Figure 5.4: Cross section (left) showing stope geometry optimization. Stope limits (blue dashed lines) placement, on different vein realizations (red lines) change the expected profit. Maximum return can be found comparing all scenarios.

5.4. Mineral Resource Classification and Reporting

Results from the probabilistic resource estimation workflow should be used in mineral resource classification and reporting. Classification is necessary to provide a confidence assessment for the deposit's stakeholders. There are many systems used by international agencies and governments for resource and reserve classification, which all share characteristics. Current practice is typically based on geological knowledge and geometric criteria such as the number of drill holes and samples around each block, kriging variance, multiple search radii to estimate blocks, nominal grid spacing, minimum thickness, and others. Geostatistical simulation can be used to support the qualified person (QP) decision on measured, indicated, and inferred resources. Resources could be compared to a nominal production volume, and uncertainty should be below a reasonable quantity. As an example, measured resources could be defined as those predicted be ± 15% on 90% of the time for a volume of 3 months of production. For vein resources, stopes and panels are evaluated in terms of production volume and predicted grades and metal. Measured, indicated, and inferred classes criteria could be reviewed based on simulation and production results. If

measured and indicated classes present high uncertainty in predicted grades and metal, then they could be downgraded.

Resources are reported under different international codes. Guidelines have been developed as a response to the necessity of transparency in disclosure of mineral resources. This transparency is needed due investment risks and notable frauds in the past. In mining, reports are often based on a single estimated block model. Resource tables are reported from a kriged block model classified as measured, indicated, and inferred considering a cut-off grade and other mining factors including thickness, recovery, resources above the final pit or resources within stopes. With multiple realizations of geometry, boundaries, and grades it is necessary to adapt the established but constrained reporting guidelines. Uncertainty should be accounted for in the final resources table. Grades, tonnages, and metal could be reported with the expected value for each but with a summary of uncertainty below the expected value. In mining, retaining the 0.1, 0.5 and 0.9 quantiles of the variables distribution are considered reasonable. There are no current international guidelines that recommend the use of uncertainty measures for reporting in mining although it is common in the petroleum industry, as defined in the National Instrument 51-101 (NI 51-101). Nevertheless, the use of geostatistical simulation within resource evaluation and reporting, it is expected that codes and guidelines will be adapted accordingly, and techniques may be developed in time.

Chapter 6. Case Study I: Single Layer Vein

A case study illustrates the use of the developed techniques and methodologies for tabular vein resources uncertainty evaluation. The data consists of a tabular gold vein. The single vein is bounded by footwall and hangingwall surfaces. A local coordinates system is generated with TLS. Imputation files are generated for inclined drill holes. Surfaces are simulated and clipped with a different boundary for each realization. Tetrahedralization is executed for each watertight solid realization. Gold grades are simulated within unstructured grids. Results on tonnage and metal content are presented. Sensitivity analysis is carried out with input and response variables. Probability maps are shown.

6.1. Deposit and Data Description

The deposit is located in the central eastern part of Brazil. The mineralization is a classic orogenic gold type in a sheared and deformed Archean to Proterozoic greenstone belt sequence consisting of metamorphosed volcanic-sedimentary rock units intruded by younger post-tectonic igneous bodies. The gold mineralization occurs as stacked tabular horizons that are mostly concordant with the principal rock foliation. These tabular vein zones are typically 1 to 20m thick (Figure 6.1).

Grades are consistent with gold mineralization along 2000m on the strike and intercepted drillings with 1000m down dip. Strike is usually N20-30° with dips of 35 to 45° East. The database consists in 497 drill holes with more than 40 km of drilling. The average drill depth is 81m, ranging from 30 to 400m deep. The data provided by the company is for one vein. There are 220 drill holes, in which 182 intercepted the vein. Some views of the raw data can be seen on Figure 6.2. Note that most of the drilling is concentrated on the Western area of the vein, which coincides with an old open pit. Exploration drilling was executed along the dip to evaluate the continuity at depth.

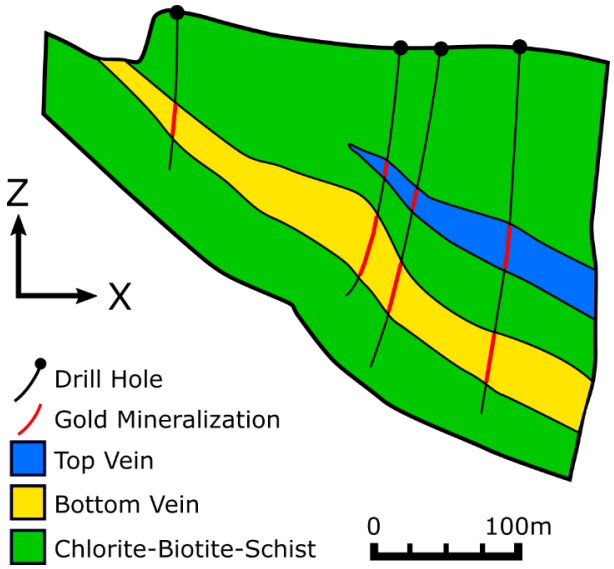

Figure 6.1: Typical geological cross-section of the studied deposit. The gold mineralization is contained by two parallel tabular veins.

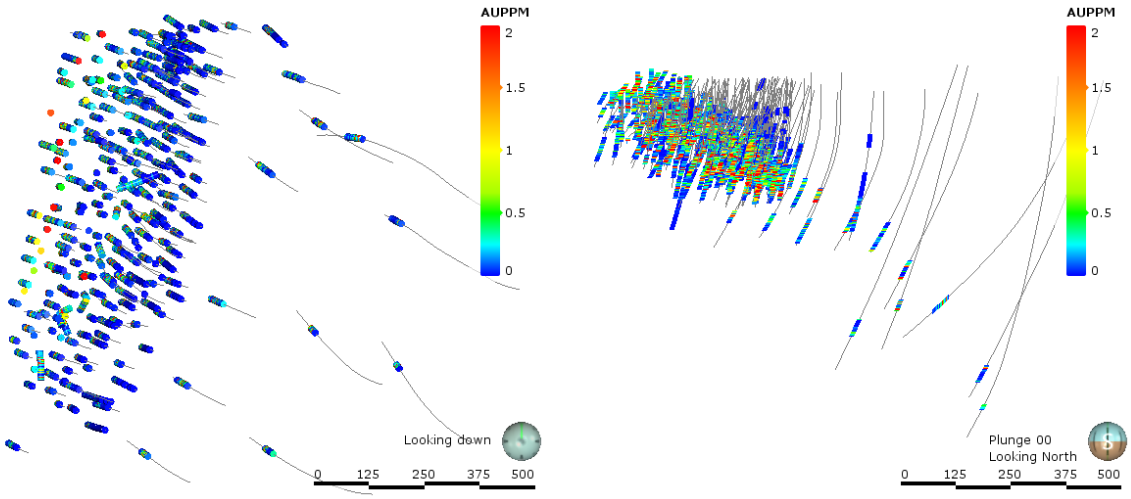

Figure 6.2: Plan view (left) and North view (right) showing drill holes configuration from data provided. Gold grades are shown in ppm.

6.2. Local Coordinates

The local coordinates system is generated using the Total Least Squares (TLS) methodology, explained previously. The data used are the midpoints from positive

intercepts of the vein. Negative intercepts are set aside for TLS calculation but are rotated afterwards. Midpoints are calculated based on hangingwall and footwall records:

X	Y	Z
699198.54	8223446	747.98
699219.04	8223503	733.80
699189.39	8223638	768.08
699049.36	8223277	795.39
699068.35	8223219	772.08
699153.65	8223639	817.68
⋮	⋮	⋮

The centroid of the all data is at:

$$(699153.78\ ,\ 8223350.09\ ,\ 740.66)$$

The matrix A, which is the difference of data points from their centroid, starts with:

$$A = \begin{bmatrix} 44.75 & 95.68 & 7.31 \\ 65.25 & 153.32 & -6.86 \\ 35.60 & 287.90 & 27.41 \\ -104.42 & -72.99 & 54.72 \\ -85.42 & -131.30 & 31.42 \\ -12.93 & 288.68 & 77.01 \\ \vdots & \vdots & \vdots \end{bmatrix}$$

The eigenvalues and eigenvectors of $A^T A$ for all data are then obtained:

$$\Lambda = \begin{bmatrix} 10060325.84 & 0 & 0 \\ 0 & 1913802.14 & 0 \\ 0 & 0 & 16367.94 \end{bmatrix},$$

$$\mathrm{U} = \begin{bmatrix} -0.2411 & -0.7966 & 0.5542 \\ -0.9691 & 0.1673 & -0.1811 \\ -0.0515 & 0.5808 & 0.8123 \end{bmatrix}$$

The normal vector is the eigenvector corresponding to the minimum eigenvalue, 16367.94:

$$\vec{n} = \begin{bmatrix} 0.5542 \\ -0.1811 \\ 0.8123 \end{bmatrix}$$

The translation matrix is defined as:

$$T = \begin{bmatrix} 1 & 0 & 0 & 0 \\ 0 & 1 & 0 & 0 \\ 0 & 0 & 1 & 0 \\ 699153.78 & 8223350.09 & 740.66 & 1 \end{bmatrix}$$

Using cross product, the strike and dip vectors can be calculated and normalized:

$$\vec{s} = \begin{bmatrix} 0.3106 \\ 0.9505 \\ 0 \end{bmatrix}, \vec{d} = \begin{bmatrix} 0.7721 \\ -0.2523 \\ -0.5831 \end{bmatrix}$$

The rotational matrix is then:

$$R = \begin{bmatrix} 0.7721 & 0.3106 & 0.5542 & 0 \\ -0.2523 & 0.9505 & -0.1811 & 0 \\ -0.5831 & 0 & 0.8123 & 0 \\ 0 & 0 & 0 & 1 \end{bmatrix}$$

The transform matrix is then calculated:

$$S = T \times R = \begin{bmatrix} 0.7721 & 0.3106 & 0.5542 & 0 \\ -0.2523 & 0.9505 & -0.1811 & 0 \\ -0.5831 & 0 & 0.8123 & 0 \\ 1535668.01 & -8033736.96 & 1101407.02 & 1 \end{bmatrix}$$

The angles of strike and dip are:

$$s_1 \geq 0, \qquad strike = \cos^{-1}(0.9505) = 18.09°$$
$$dip = \sin^{-1}(0.5831) = 35.67°$$

Samples and intercepts are rotated and translated using matrix S. Transformation results can be seen on Figure 6.3. In the first row of figures it is possible to see vein samples (red) and outside samples (black) in their original coordinate system. The second row shows transformed samples using TLS method. The transformation matrix is calculated using only samples inside the vein. Thickness modeling is more straightforward in this new local coordinate system. All subsequent steps including geometry data imputation, surface simulation, gridding, and grade/property simulation are executed in this local coordinate system. After modeling, drill hole data, simulated surfaces and gridded properties are back rotated to original coordinate system.

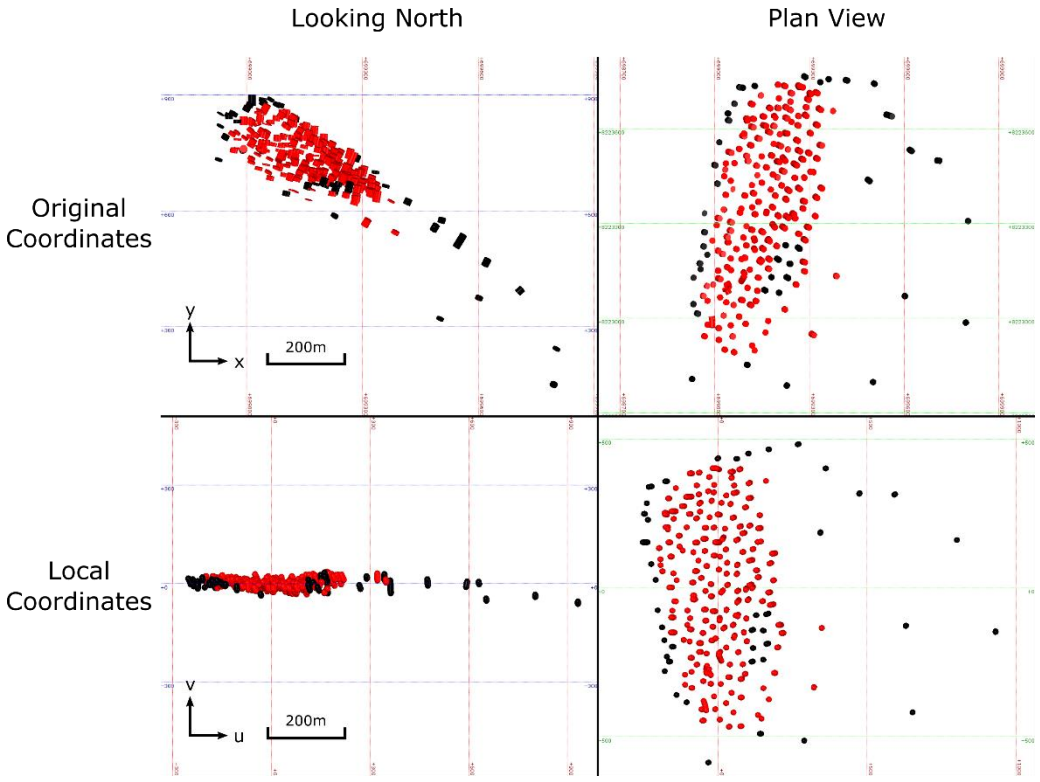

Figure 6.3: Inside (red) and outside (black) vein samples at original and local coordinates system after TLS transformation.

6.3. Geometric Uncertainty Evaluation

Geometric uncertainty relates to the uncertainty of the position of surfaces. A local coordinate system is created based on midpoints of drill hole intercepts of the vein. The dip

and azimuth are calculated as above. Imputation is executed for both footwall and hangingwall surfaces. The footwall is chosen as the reference surface. Distributions of position and thickness are calculated, merged, sampled, and imputation files are generated. Each surface realization is executed using a different imputation file. Surfaces are post-processed to generate vein solids, required for tetrahedralization and grade simulation.

6.3.1. Geometric Data Imputation

Imputation of data locations is executed in the local coordinate system. Data used for the imputation are u, v, and w positions of the footwall and hangingwall vein intercepts and thickness values. Visual inspection and geologist's information confirms that there is no substantial difference between footwall and hangingwall surfaces in terms of stability and geometry. Therefore, either surface could be selected as reference. The footwall is the selected as the reference surface. For each inclined drill hole, two distributions will be calculated to describe the footwall and hangingwall position on the opposite surface. Both distributions are then merged, and a value from the merged distribution is sampled. This sampled value characterizes a realization of the surface position. The footwall and hangingwall position data are calculated from TLS plane fitting. Thickness values are calculated for each drill hole by subtracting footwall w position from hangingwall w position. As a precaution, a maximum angle tolerance is applied to remove thickness values from the distribution when the angle between hangingwall and footwall is too high. A maximum angle of 34° seems to be a reasonable choice. The tolerance angle is selected by inspection of the distribution of angles (Figure 3.4). A total of 10 drill hole thickness values are rejected from the imputation process. For these drill holes, a missing thickness values is assigned, and imputation is executed at them. The declustered global thickness values histogram can be seen on Figure 6.4.

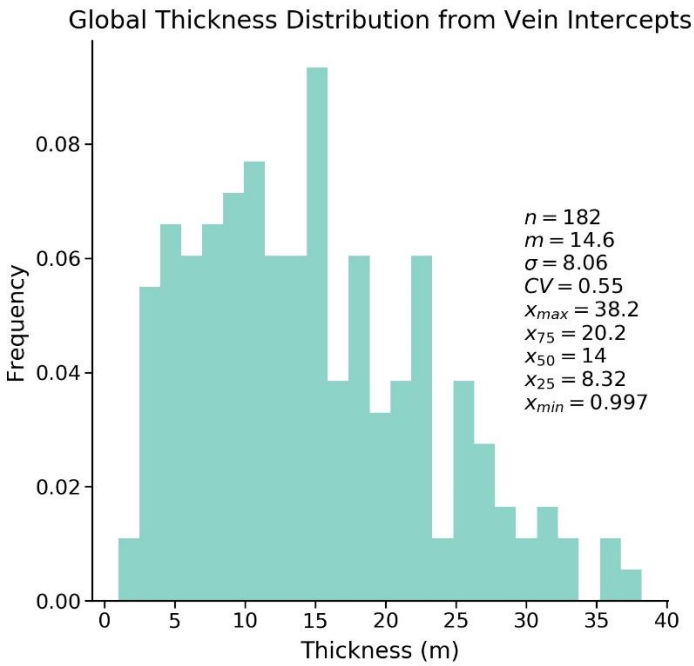

Figure 6.4: Declustered thickness values calculated from drill holes .

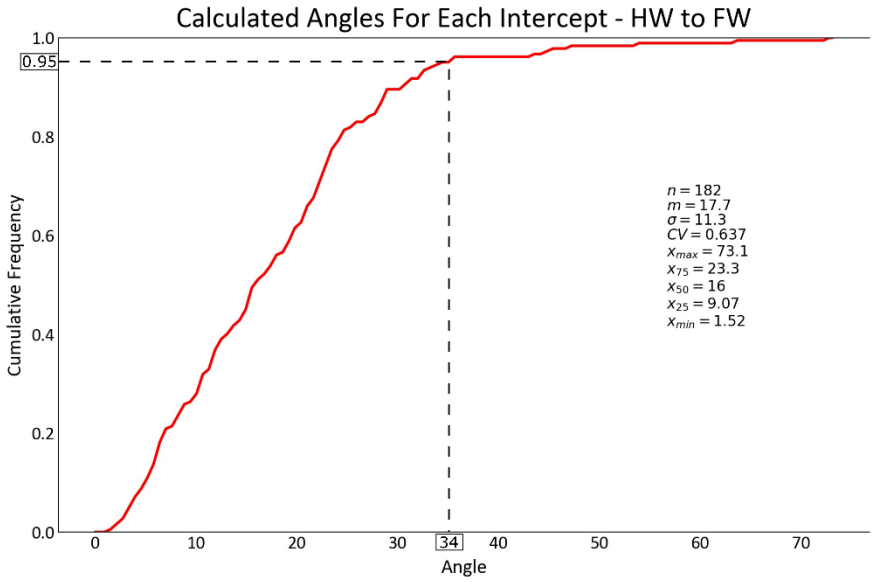

Figure 6.5: CDF of calculated angles between hangingwall and footwall, used for maximum angle tolerance evaluation. A maximum angle tolerance of 34° is chosen for this data.

Position and thickness values are normal score transformed for variogram calculation and subsequent sequential Gaussian simulation. Transformation tables are stored for later back

transformation. Variograms are calculated for both footwall and hangingwall position, and thickness values (Figure 6.6). Variograms show good structures and long ranges.

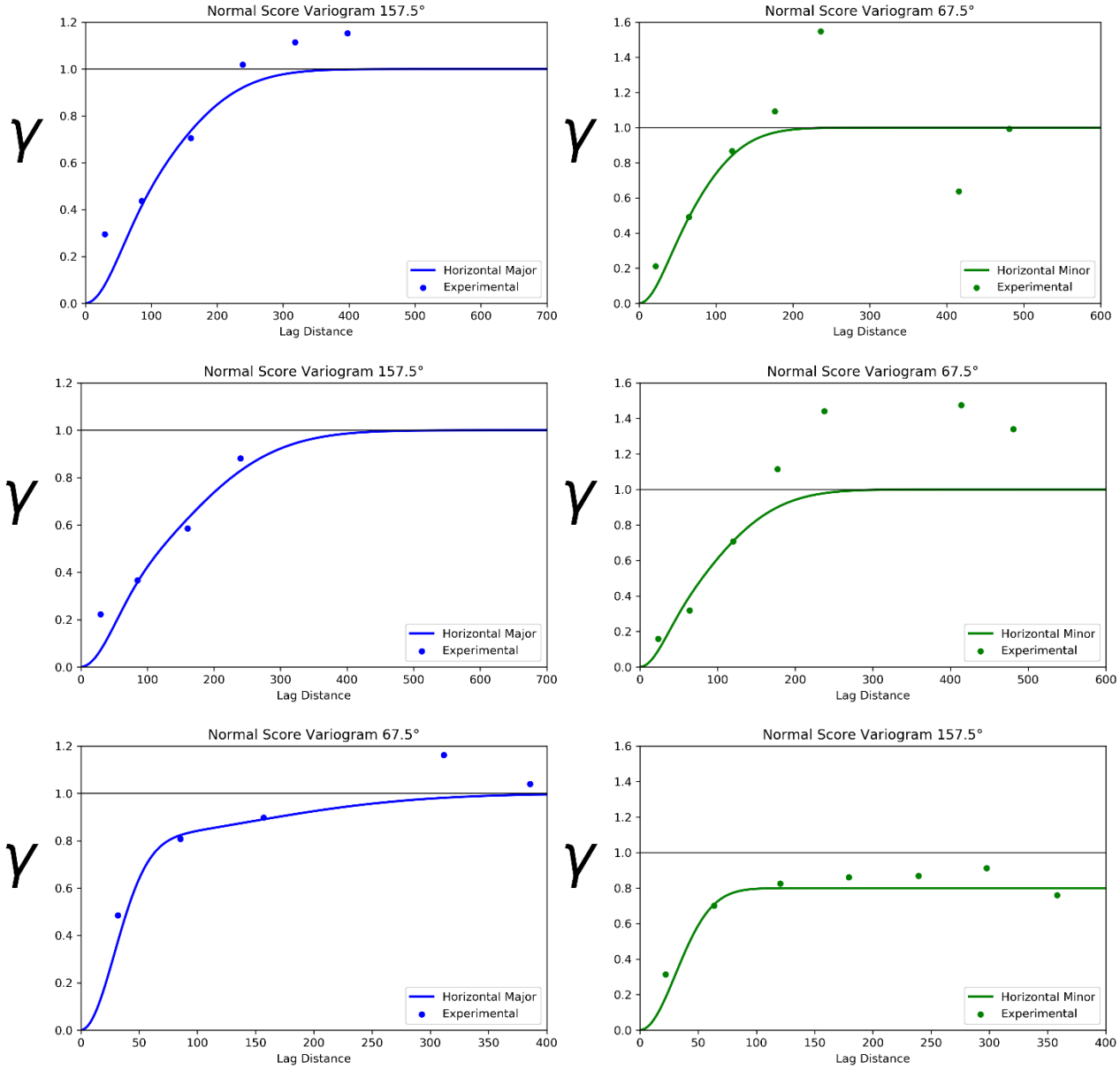

Figure 6.6: Variogram for footwall (top), hangingwall (centre) *w* position and thickness values (bottom).

The number of realizations chosen for data imputation, surface, boundary, and grade simulation is 100. The software USGSIM (Manchuk & Deutsch, 2015) is used to calculate position and thickness distributions. After distribution calculation, position distribution is back transformed to original units and thickness is calculated from the hangingwall intercept. This calculated thickness from the position is then normal score transformed

using the global thickness distribution. This transformed thickness is assumed to be Gaussian. The two thickness distributions are then merged by the error ellipses methodology and sampled. The sampled value is assigned to the intercept. Footwall imputation is executed first as it is considered the reference surface. Afterwards, hangingwall position is imputed. There are 100 imputation files generated as input data for surface simulation. An example can be seen on Figure 6.7. In this figure, there are two drill holes with the expected surfaces and four different imputed positions for both footwall and hangingwall. Each realization with a different position of footwall and hangingwall location. As expected, high-angle intercepts show higher uncertainty than low-angle intercepts (Figure 6.8). Histograms on the left show imputation results for a drill hole with an inclination 5.91°, while the right one show results for a 73.1° inclined drill hole. Histograms of average and all realizations thickness can be seen on Figure 6.9.

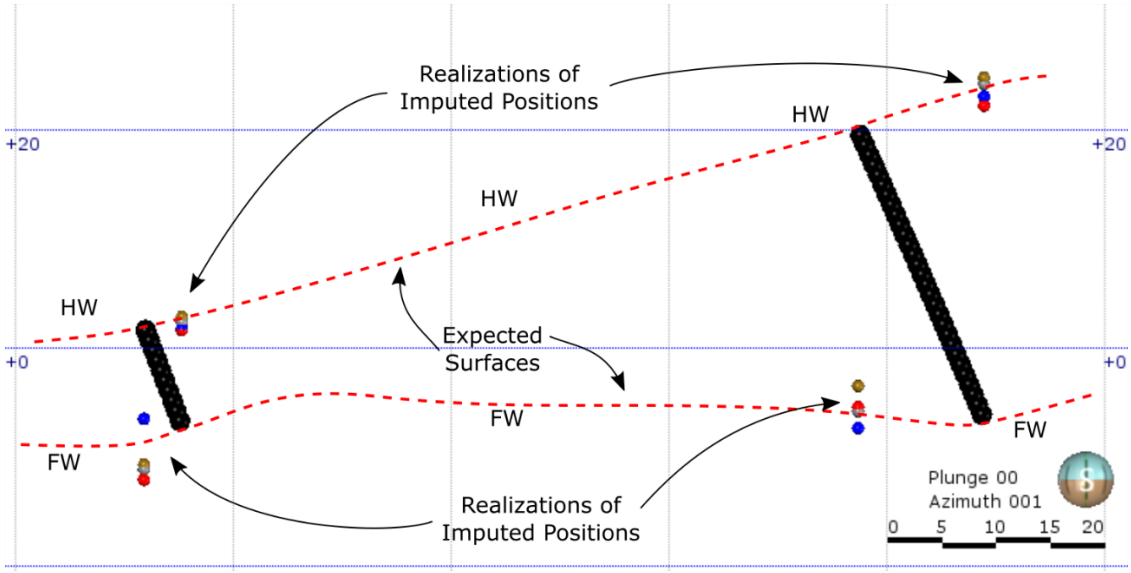

Figure 6.7: Section in drill holes (black) showing imputed positions for footwall and hangingwall. The colored circles are different position realizations.

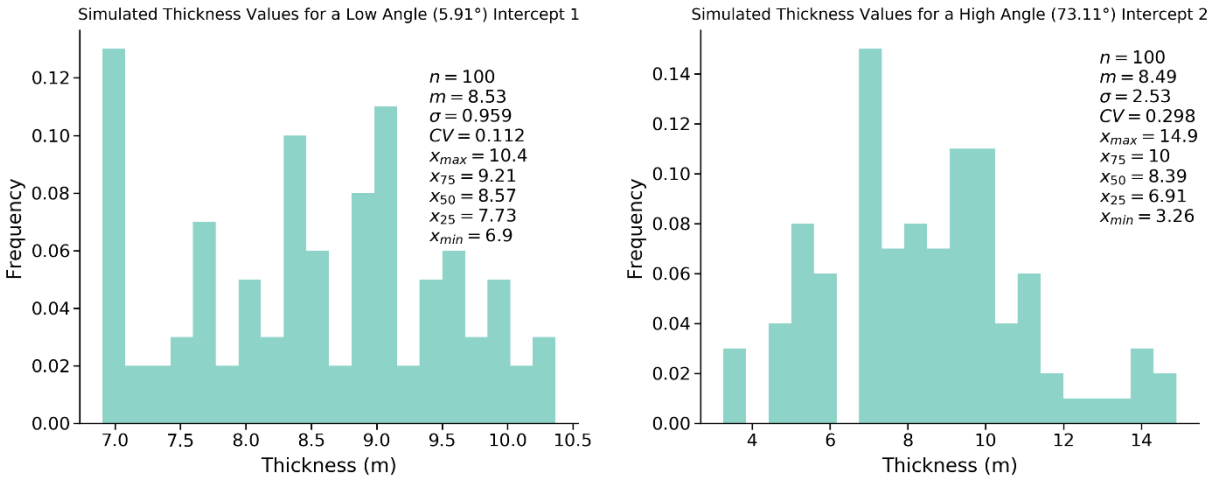

Figure 6.8: Histograms of imputed thickness data for two intercepts. The first column shows the lower uncertainty on a low-angle intercept, while second column shows high uncertainty on a high-angle intercept.

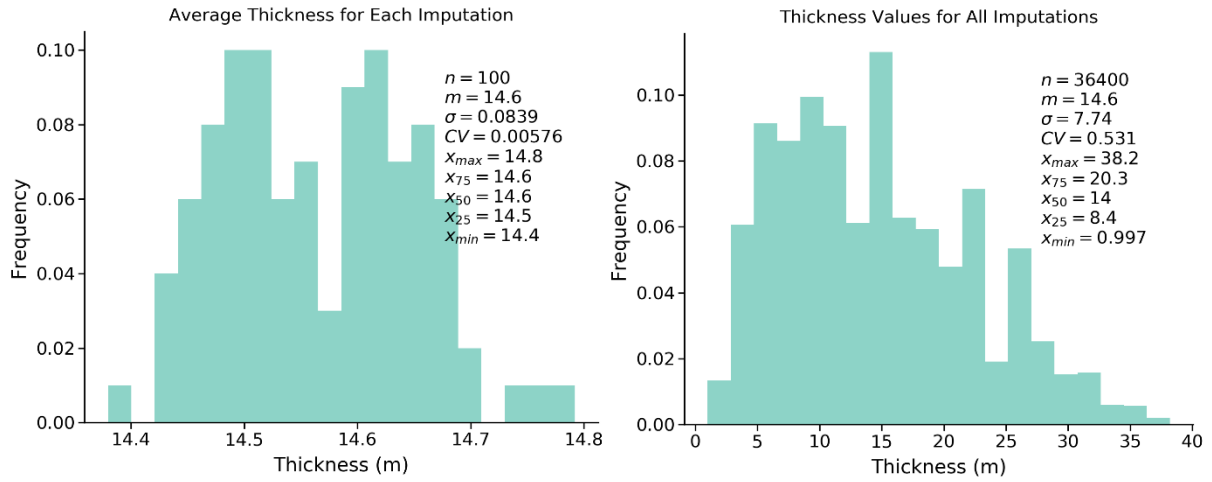

Figure 6.9: Average thickness (left) for each imputation file and all realizations thickness distribution.

6.3.2. Surface Simulation

Surfaces are simulated using drill hole data and imputed position data. To preserve uncertainty from imputation, each surface realization uses a different imputation file. Position and thickness are kept as pairs to prevent crossing between footwall and hangingwall. An equilateral triangular grid with 12m on a side is created. The size is approximately a quarter of the drill hole spacing and seems a reasonable resolution. An extrapolation border of 200m is expanded around external drill holes, which represents twice the widely spaced samples. The triangular grid is a natural gridding for the geological

structures. Original drill hole footwall and hangingwall intercepts are merged with imputed locations to execute the USGSIM software. Data is normal score transformed for simulation. The reference footwall surface is simulated using drill hole intercepts and imputed w footwall position data. The hangingwall is simulated using thickness. Both results are back transformed to original units. Simulated thickness values are then added to simulated positions from footwall to calculate the hangingwall position. Surfaces are triangulated using 2D Delaunay triangulation. A surface realization can be seen on Figure 6.10. Drill hole data intercepts are added to the triangulated surface by replacing closest nodes (Figure 6.11) with the input data.

As in all geostatistical modeling, checking is necessary to validate the results. In many cases, cross validation is used for the task. This methodology creates data sets and compare predicted values and true values by removing some data in each set. Checking one location at a time might not be enough to validate. Checking the fraction of true values might show some features of the model. Accuracy plots can be calculated to test the thickness values modeled. (Figure 6.12)

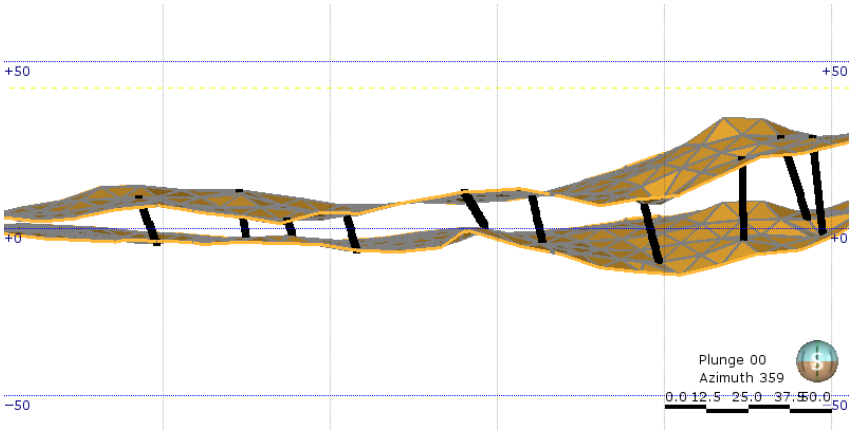

Figure 6.10: Cross section of a footwall and hangingwall surface realization. Drill hole traces are in black.

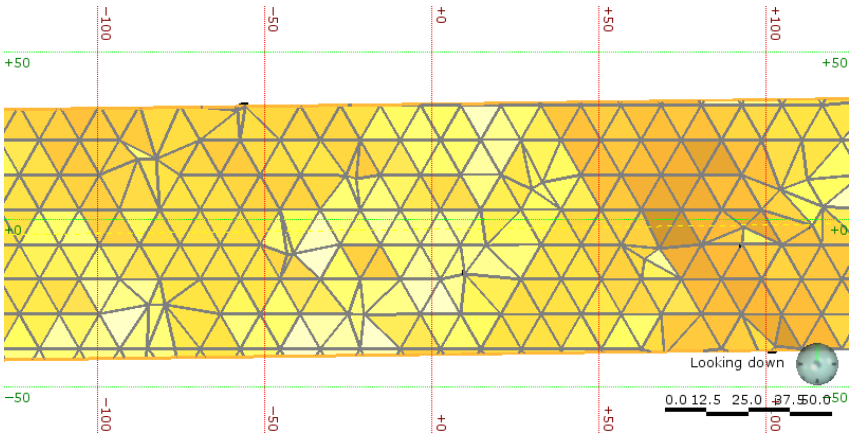

Figure 6.11: Plan view of surface realization. Irregular edges are the result of snapping the triangulation to the drill hole intercepts, honouring data information.

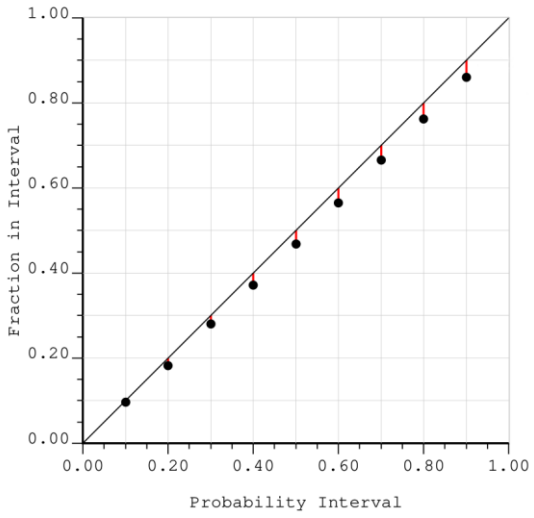

Figure 6.12: Accuracy plot for the modeled thickness values.

6.4. Other Uncertainties

In addition to geometric uncertainty, some other sources of uncertainty are evaluated. These are external boundaries and holes, grade simulation, and parameter uncertainty. The C parameter is calibrated and selected accordingly. Each surface realization is clipped by a different C parameter, and therefore, a different boundary is set. Spatial bootstrap is executed to generate multiple input data with different gold grades distribution. Tetrahedralization is executed for each watertight solid realization. Tetrahedrons are discretized and gold grades are simulated.

6.4.1. Boundary Modeling

External boundaries and holes also need to follow a probabilistic resource estimation workflow. Consequentially, different boundaries must be modeled for each surface realization. Boundaries are modeled as areal limits using the distance function methodology (Hosseini & Deutsch, 2007). The distance function is interpolated on the triangular grid. The vein indicator is defined for each drill hole intercept (Figure 6.13). From the indicator coding on the intercepts, it is possible to visualize that positive intercepts are concentrated on the left area of the drill holes. There are negative drill holes bounding the vein and also a hole in the bottom right zone. It is recommended that global kriging be used for interpolation of the distance function values. Global kriging is fast and minimizes artifacts (Figure 6.14).

The C parameter must be calibrated before boundary modeling. The methodology presented by Wilde and Deutsch (2011) is used, but with the implementation from Martin and Boisvert (2016). The implementation uses Radial Basis Function (RBF) to interpolate the sets of data and calculate the misclassification rate. The graph generated for the calibration can be seen on (Figure 6.15). The chosen value for C parameter is 50 as the misclassification stabilizes at an approximate rate of 2%.

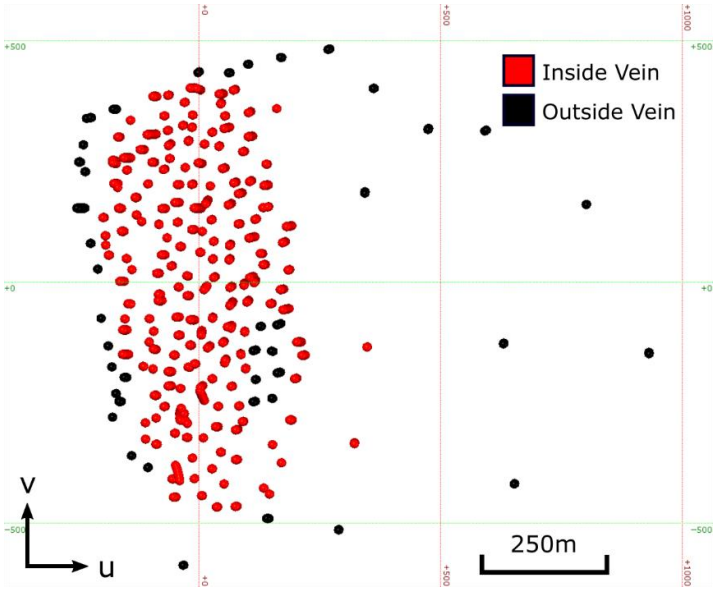

Figure 6.13: Plan view of drill holes intercepts classified with vein indicators.

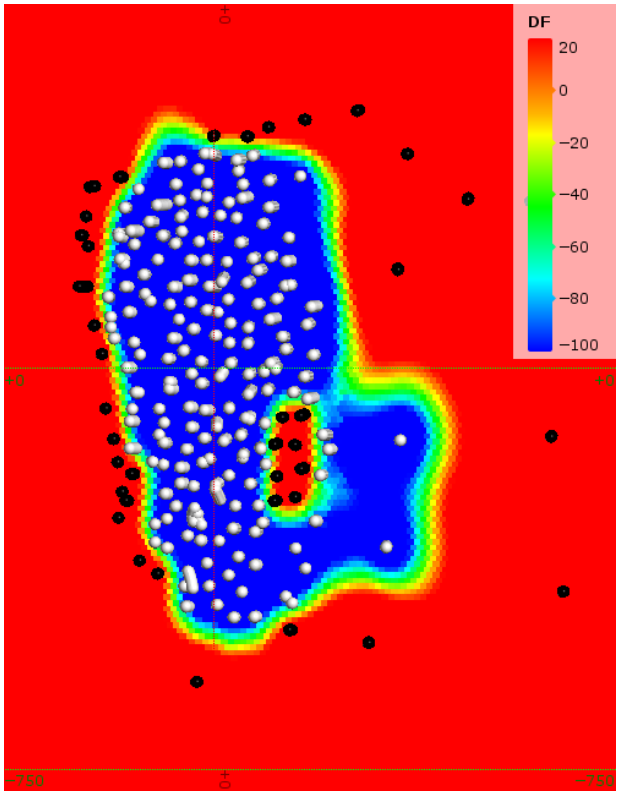

Figure 6.14: Interpolation of distance function values on the triagular grid. Inside samples are in white, outside are in black.

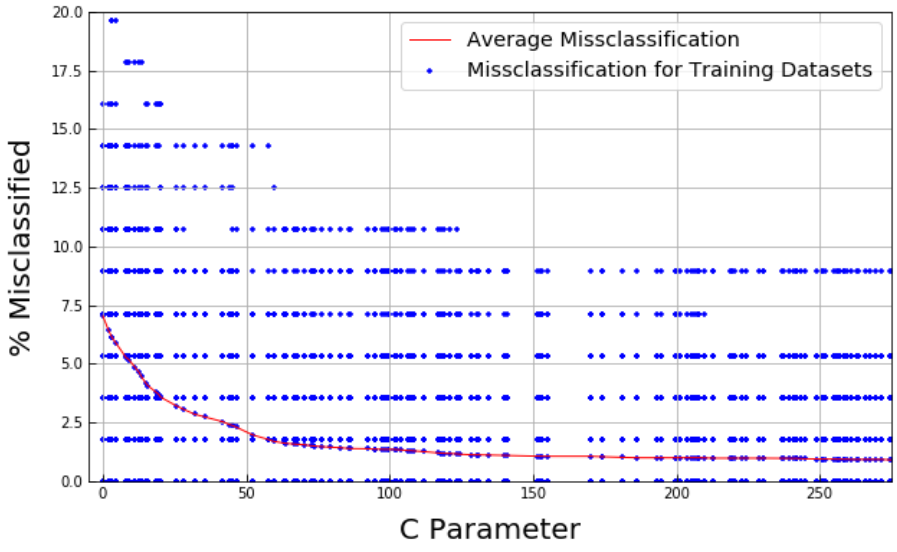

Figure 6.15: Misclassification and C parameter. The chosen value is 50 with a misclassification rate near 2%.

For each surface realization a different boundary is assigned. A uniform random value is selected between $-C$ to $+C$.

6.4.2. Surfaces and Vein Solid Processing

Before grade simulation it is necessary to process all surfaces realizations, clip boundaries and holes, and generate watertight solids. These watertight solids are necessary for the tetrahedralization with TetGen (Si, 2015).

Vein PLCs are generated by clipping surfaces realizations with distance function boundaries and vertically linking external borders and holes. The first step is to recognize the border nodes for each realization (Figure 6.16). Afterwards, each footwall border is linked vertically with its respective hangingwall border, closing the vein solid. Internal layers are also created to better control tetrahedron volumes and anisotropy modeling. An example of a final watertight solid realization can be seen on Figure 6.17.

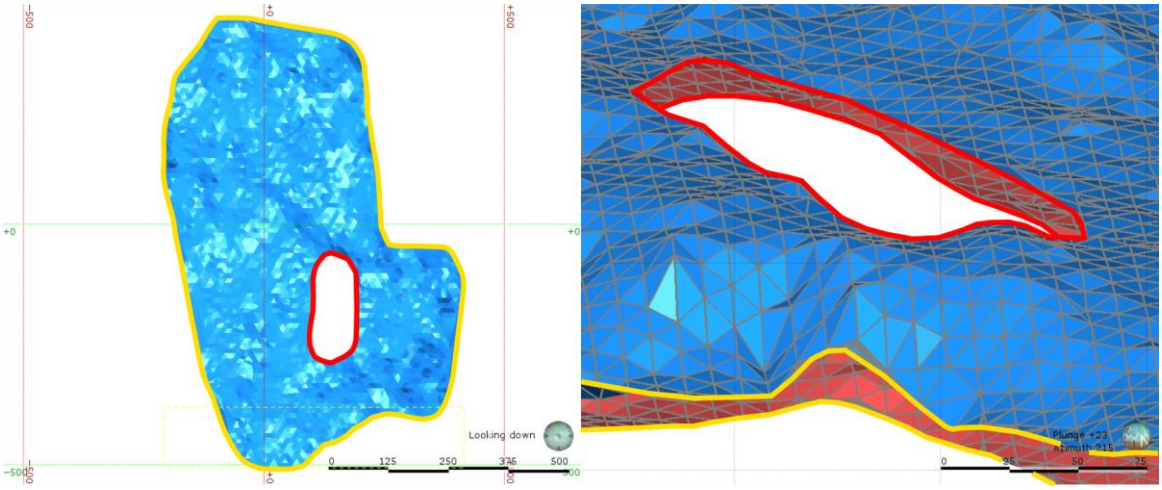

Figure 6.16: Plan (left) and perspective (right) view of surface clipped by distance function modeling. For this case, two borders are recognized. Footwall borders are then linked to hangingwall borders to generate the watertight solid.

The solid is provided to TetGen with two files. There is a file containing all u, v, and w coordinates of the nodes. The other file contains all facets from the triangulation with the nodes that form each facet. TetGen generates the tetrahedralization.

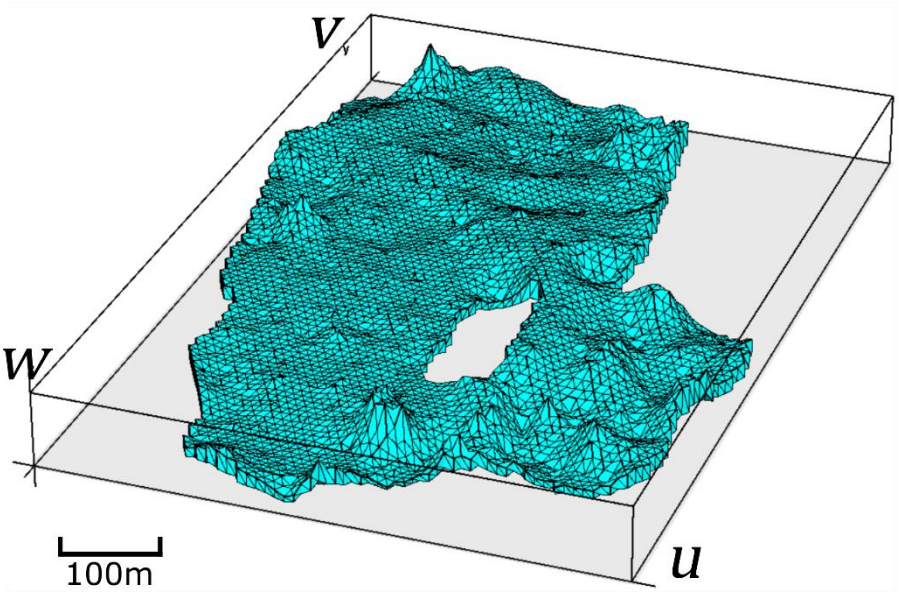

Figure 6.17: Watertight solid generated from a surface realization, boundary clipping, and border linking.

6.4.3. Grade Simulation

For this case, only gold grade is being simulated. Tetrahedralization is executed for each watertight solid realization. For global uncertainty in the gold grade distribution, the spatial bootstrap technique is implemented. Fixing a single input histogram would not preserve the uncertainty in the mean. A representative distribution of gold grades and variogram are required for spatial bootstrap (Figure 6.18 and Figure 6.19). Results from the spatial bootstrap can be seen on Figure 6.20. A proportional style of correlation between the hangingwall and footwall is assumed. No evidence of hangingwall or footwall conforming is observed in the data. Each tetrahedron barycenter and node position is calculated relative to the thickness in that section. With thickness proportion defined, the local coordinate w' is calculated. Tetrahedrons are then discretized using the 27-point design explained in Chapter 4. Gold grades variograms are calculated and sequential Gaussian simulation is executed for each vein geometry realization. An example of a gold grade realization is shown on Figure 6.21. Some results on uncertainty can be seen in the next section.

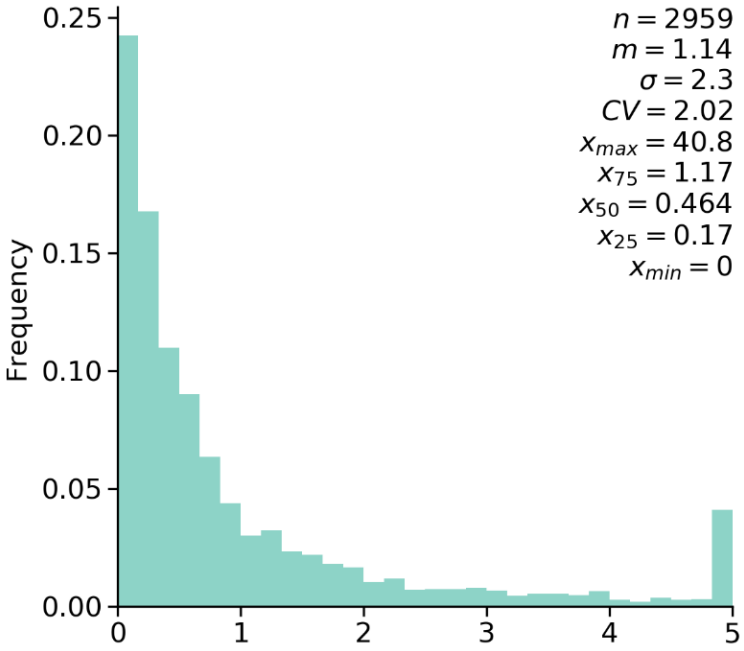

Figure 6.18: Gold grade data histogram.

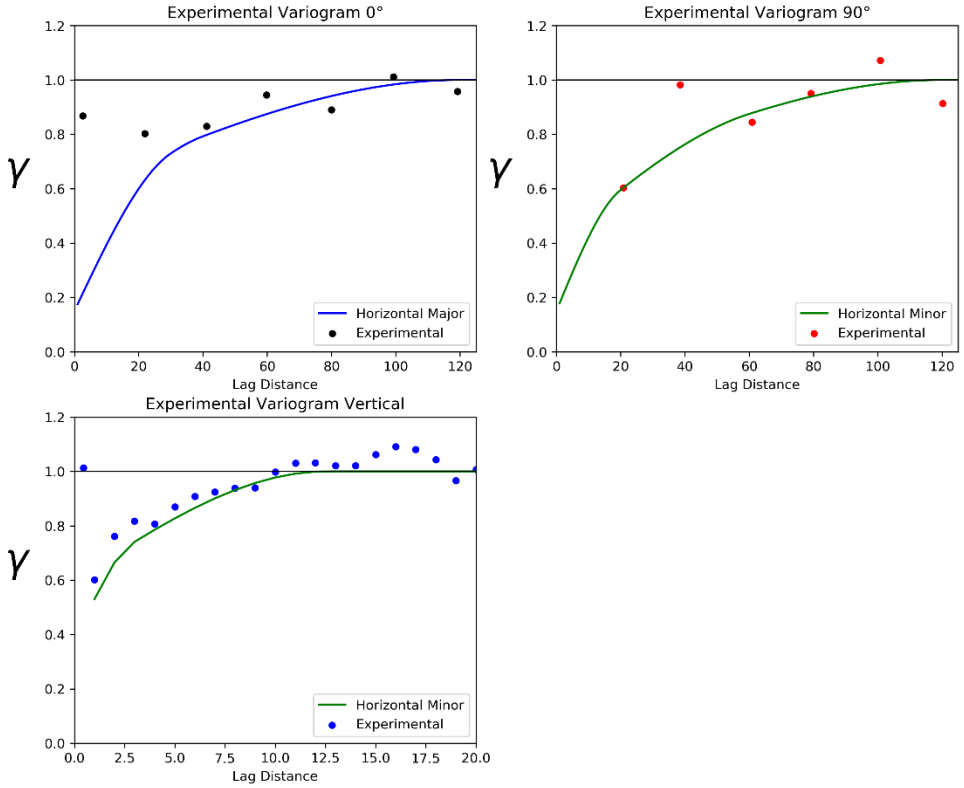

Figure 6.19: Normal score gold grade variogram.

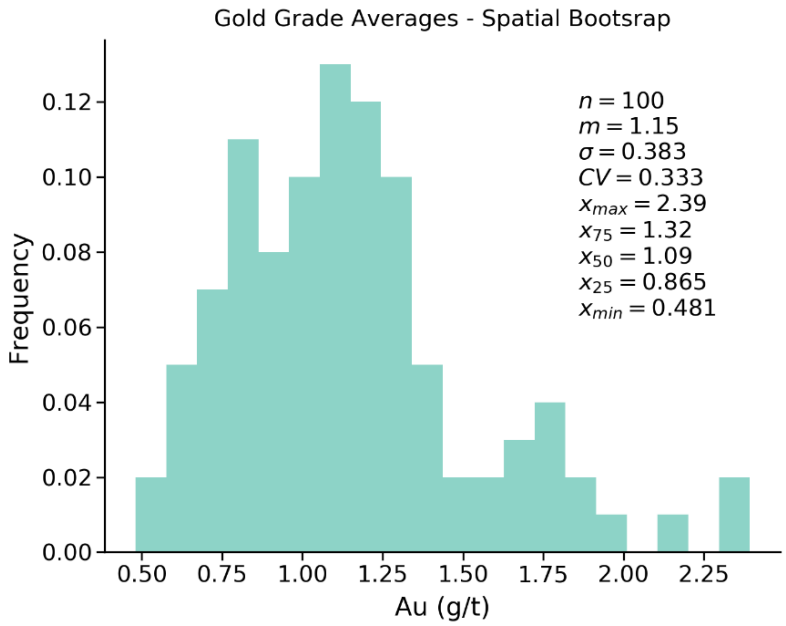

Figure 6.20: Spatial bootstrap averages for gold grade.

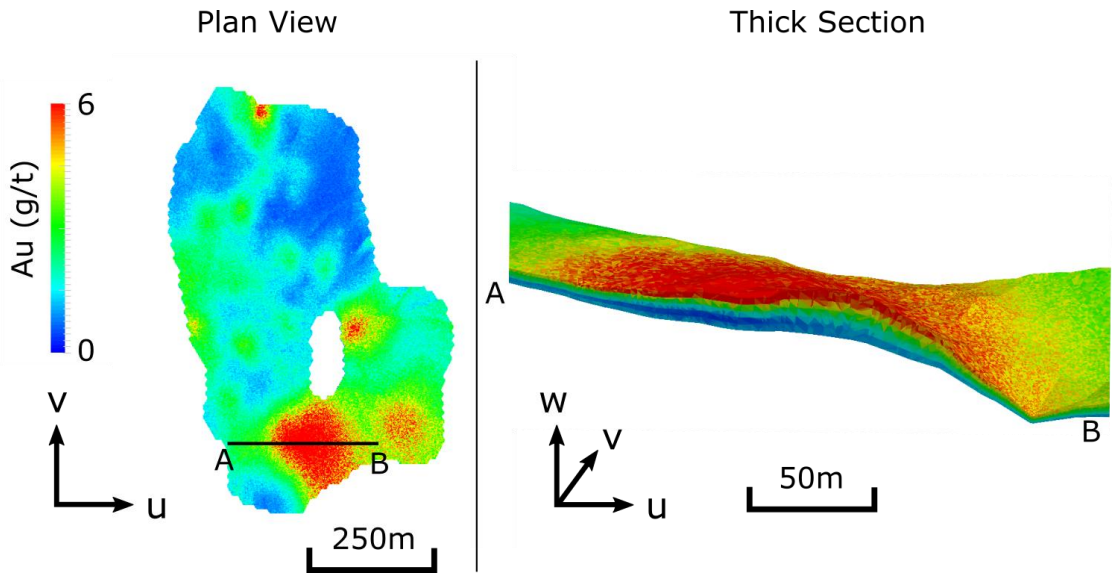

Figure 6.21: Example of a gold grade realization. A plan view (left) and a thick section (right) is shown. Proportional anisotropy is considered.

6.5. Results and Considerations

A data set from a gold hydrothermal deposit is used. The Total Least Squares (TLS) method is used to fit the plane on data and generate rotation and transformation matrices.

Calculated strike azimuth and dip angle are 18.1° and 35.7°, respectively, which match the structural data and field geologist field measurements from the ore body. Imputation of intercepts position is executed. As expected, highly inclined drill holes (comparing to fitted plane) present higher uncertainty than low-angle intercepts. Footwall and hangingwall surfaces are then simulated using different imputation files. Each realization is clipped by a different boundary and pinch-out limits by randomly selecting different C parameter. There are 100 different vein geometry wireframes, each one filled with tetrahedrons that match the exact vein shape realization. Anisotropy is considered to be proportional between the hangingwall and footwall, so both samples and tetrahedrons are flattened accordingly. Gold grade variograms are calculated and modeled. Grade simulation is executed for each unstructured grid. Global tonnage and metal are calculated for each realization and a response table is created for comparing input variables including position, thickness, C parameter and gold grades. Response variables are area, tonnage (Mt) and metal quantity (kOz) Distribution of input parameters and response variables can be analyzed on Figure 6.22.

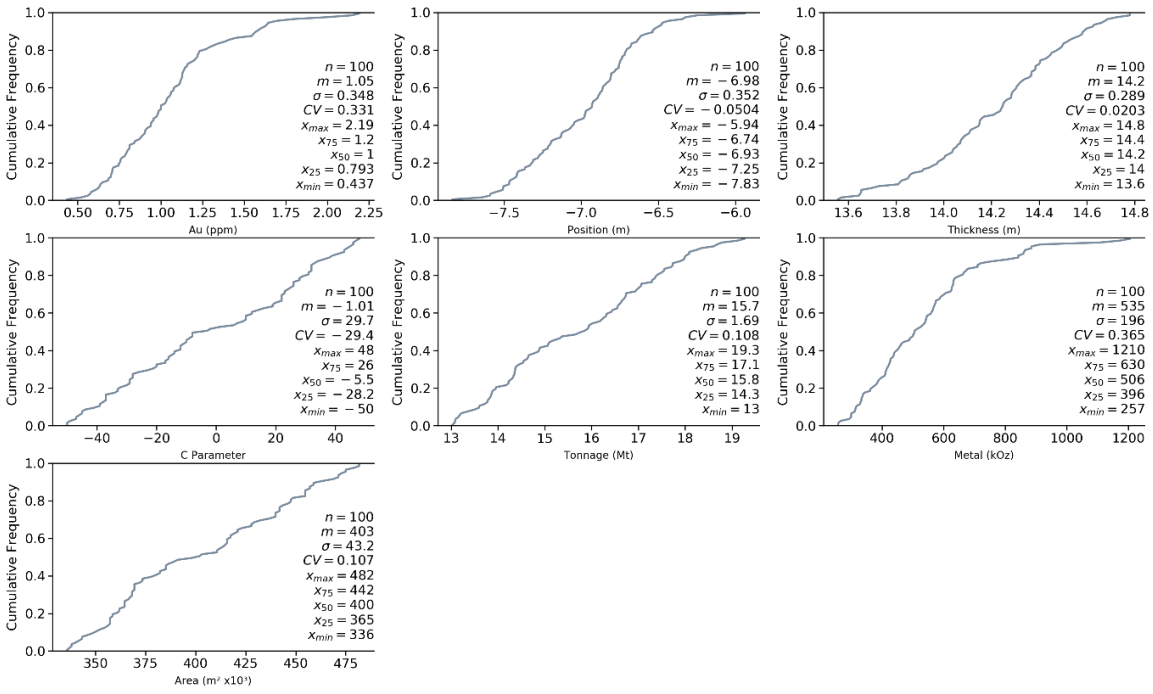

Figure 6.22: Distribution of input parameters (Au average, position, thickness, and C parameter) and response variables (area, Mt, and kOz).

The total gold content (kOz) histogram can be seen on Figure 6.23. The average metal content is 535 kOz. By comparing p80 with 651 kOz, and p20 with 368 kOz, the absolute difference is 283 kOz. For this specific interval, there is 55% of metal uncertainty on the vein resources.

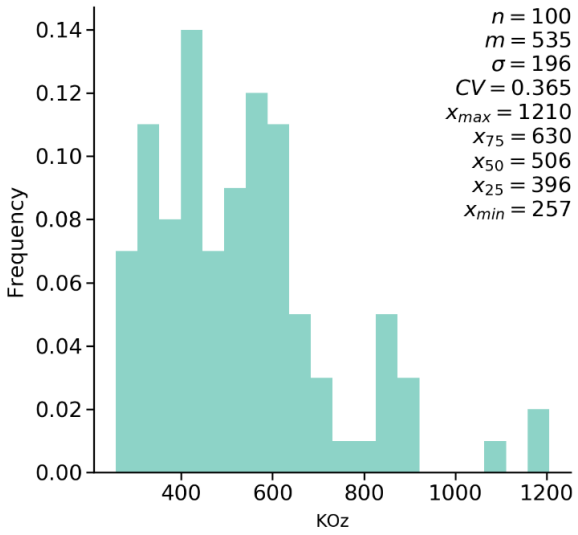

Figure 6.23: Ounces histogram for each realization.

For this case study, it is possible to state that gold grades most of the uncertainty on total gold content (Figure 6.24) while C parameter and thickness explain tonnage uncertainty (Figure 6.25). Probability maps can be seen on Figure 6.26.

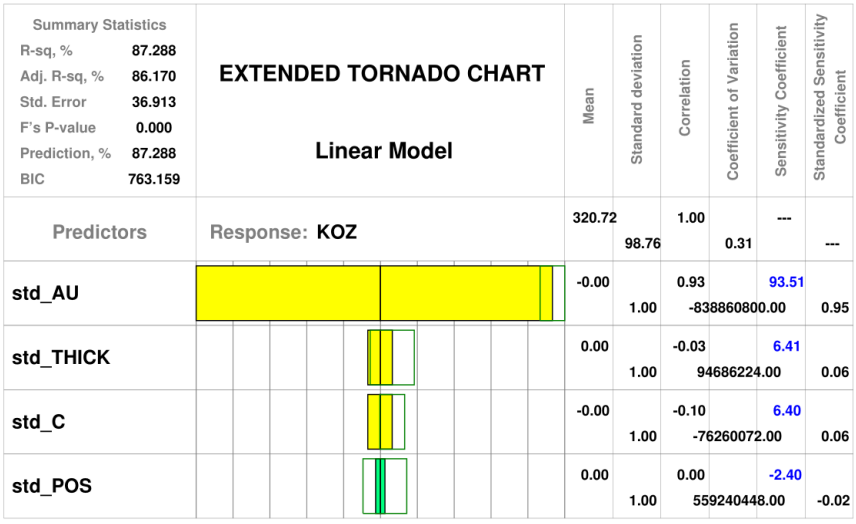

Figure 6.24: Tornado chart showing the impact of each input variable to the metal content (kOz).

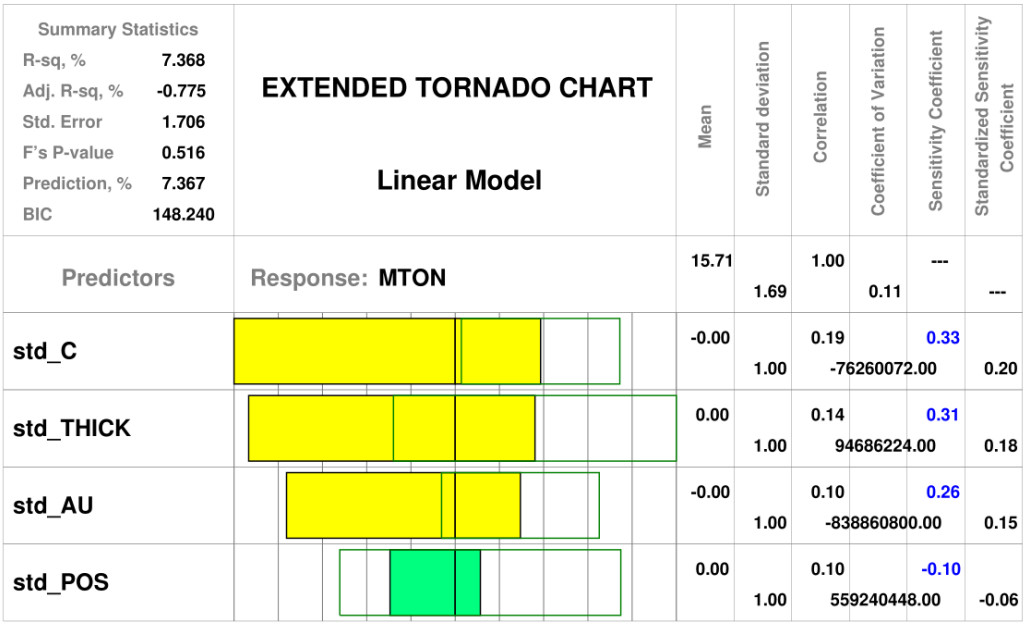

Figure 6.25: Tornado chart showing the impact of each input variable to the tonnage (Mt).

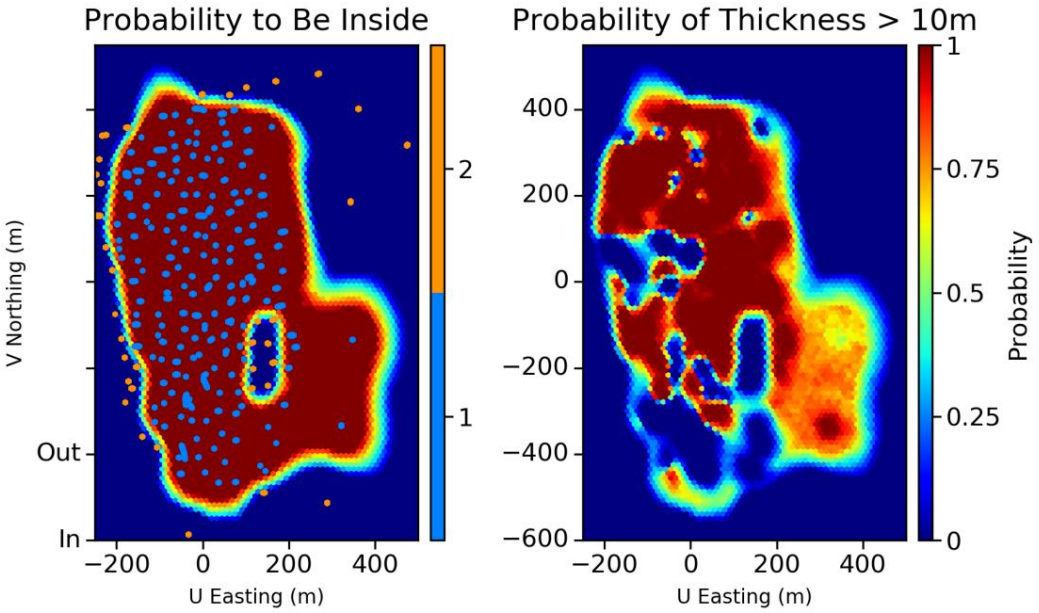

Figure 6.26: Probability map to be inside the vein (left) and to thickness be greater than 10m (right). Samples inside (blue dots) and outside (orange dots) are showed on left map.

Chapter 7. Case Study II: Multiple Layer Vein

A different case study is demonstrated. Data consists of a tabular vein type silver deposit, where the mineralization consists in three stratums. The main mineralized stratum is the inner vein, and it is bounded by a bottom and top stockwork. Uncertainty quantification procedures are similar and complimentary to the previous case study: construction of local coordinates system with TLS; geometric data imputation for inclined drill holes in each stratum; simulation of stratum surfaces and clipping each realization with a different boundary; tetrahedralization is executed for each geometry; simulation of silver grades within unstructured grid. All procedures are executed honoring strata geometry. Global and stratum results on tonnage and metal content are presented.

7.1. Deposit and Data Description

The Ag-Au mineralization is an epithermal mineralization, with sub-vertical ore bodies, capped by a clay alteration with mineralogy varying accordingly to the depth. The prospects are adularia-illite type deposits, with a vertical length typically from 100 to 400m. Silver is contained in wide vein breccia ore bodies with multiple generation of quartz-calcite-sulfide deposition. The breccia mineralization occurs as an inner vein deposition surrounded by a stockwork mineralization with lower mineralization intensity. For this case study, the mineralization is divided in three tabular stratums: bottom stockwork, inner vein, and top stockwork (Figure 7.1). Grades are higher on the inner vein stratum, while stockwork presents lower grades. The bottom stockwork average thickness is 5.8m, ranging from 1 to 14m. The inner vein average thickness is 7.6m, ranging from 2 to 15m. The top stockwork average thickness is 3.7m, ranging from 0.5 to 7m.

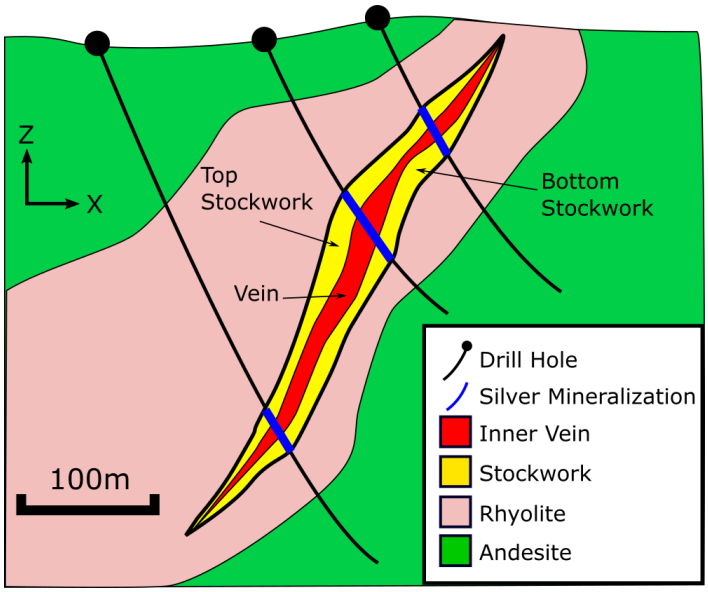

Figure 7.1: Schematic cross-section showing the mineralization. The deposit is defined by an inner vein and an outer stockwork, divided here as top and bottom stockwork.

Grades continuity is 800m along strike and 500m down dip. Strike is usually N65-75° with dips of 70° to the North. The database consists of 14 drill holes. For the study, 11 drill holes are considered. The rejected drill holes are too far from the main ore body or had incomplete assay results. Some views of the raw data can be seen on Figure 7.2. This deposit is in early exploration; boundary and geometry of the mineralization are still being investigated.

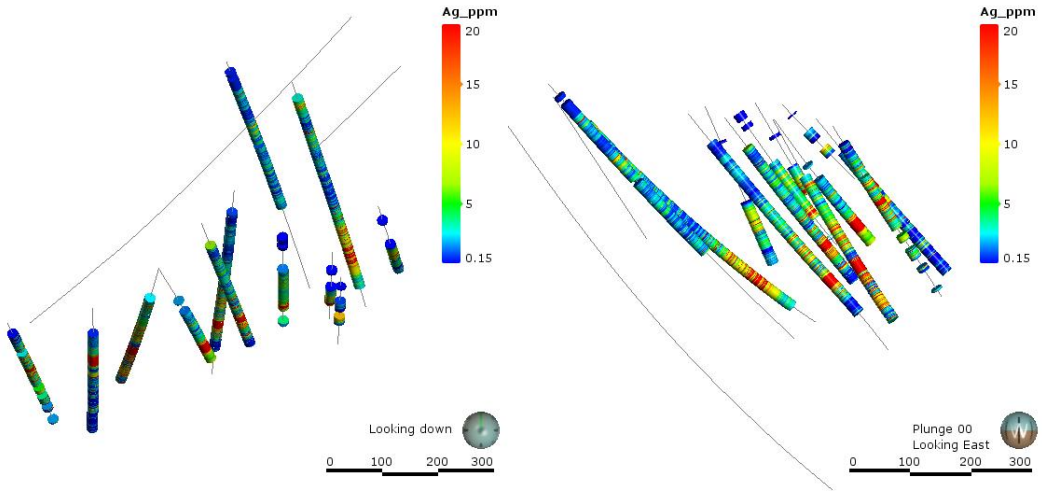

Figure 7.2: Plan view (left) and East view (right) showing drill holes. Silver grades are shown in ppm.

7.2. Local Coordinates

The local coordinates system is generated. Total Least Squares (TLS) methodology is used for the task. The data used are the 11 midpoints from positive intercepts of the entire mineralization, including outer stockworks and inner vein. Additionally, one point from a far drill hole is used to support the rotation. This point has no assay but it is described as the possible intercept of the vein. Midpoints are calculated based on hangingwall and footwall records. The matrix A, which is data points regression from their centroid, starts with:

$$A = \begin{bmatrix} 208.77 & -3.45 & 154.66 \\ 192.56 & 30.06 & 92.14 \\ 108.62 & 22.32 & 52.05 \\ -32.76 & -54.37 & 31.13 \\ -229.79 & -76.56 & 97.15 \\ -157.57 & -54.53 & -33.18 \\ \vdots & \vdots & \vdots \end{bmatrix}$$

The eigenvalues and eigenvectors of $A^T A$ for all data are then obtained:

$$\Lambda = \begin{bmatrix} 586239.32 & 0 & 0 \\ 0 & 4680.20 & 0 \\ 0 & 0 & 178802.68 \end{bmatrix},$$

$$\mathrm{U} = \begin{bmatrix} -0.9392 & -0.2740 & -0.2067 \\ -0.1962 & 0.9228 & -0.3315 \\ -0.2815 & 0.2708 & 0.9205 \end{bmatrix}$$

The normal vector is the eigenvector corresponding to the minimum eigenvalue, 4680.20:

$$\vec{n} = \begin{bmatrix} -0.2740 \\ 0.9228 \\ 0.2708 \end{bmatrix}$$

The translation matrix is defined as:

$$T = \begin{bmatrix} 1 & 0 & 0 & 0 \\ 0 & 1 & 0 & 0 \\ 0 & 0 & 1 & 0 \\ -584048.62 & -3319530.88 & -693.19 & 1 \end{bmatrix}$$

Using cross product, the strike and dip vectors can be calculated and normalized:

$$\vec{s} = \begin{bmatrix} -0.9586 \\ -0.2846 \\ 0 \end{bmatrix}, \vec{d} = \begin{bmatrix} -0.0770 \\ 0.2596 \\ -0.9626 \end{bmatrix}$$

The rotational matrix is then:

$$R = \begin{bmatrix} -0.0770 & -0.9586 & -0.2740 & 0 \\ 0.2596 & -0.2846 & 0.9228 & 0 \\ -0.9626 & 0 & 0.2708 & 0 \\ 0 & 0 & 0 & 1 \end{bmatrix}$$

The transform matrix is then calculated:

$$S = T \times R = \begin{bmatrix} -0.0770 & -0.9586 & -0.2740 & 0 \\ 0.2596 & -0.2846 & 0.9228 & 0 \\ -0.9626 & 0 & 0.2708 & 0 \\ -816216.03 & 1504762.03 & -2903425.76 & 1 \end{bmatrix}$$

The angles of strike and dip are:

$$s_1 < 0, \qquad strike = 360 - \cos^{-1}(-0.9586) = 253.46°$$
$$dip = \sin^{-1}(0.9626) = 74.28°$$

Samples from bottom and top stockwork, and inner vein are transformed using matrix S. Transformation results can be seen on Figure 7.3. The first row of figures shows vein samples in their original coordinate system. The second row shows transformed samples. All subsequent steps are executed in this local coordinate system.

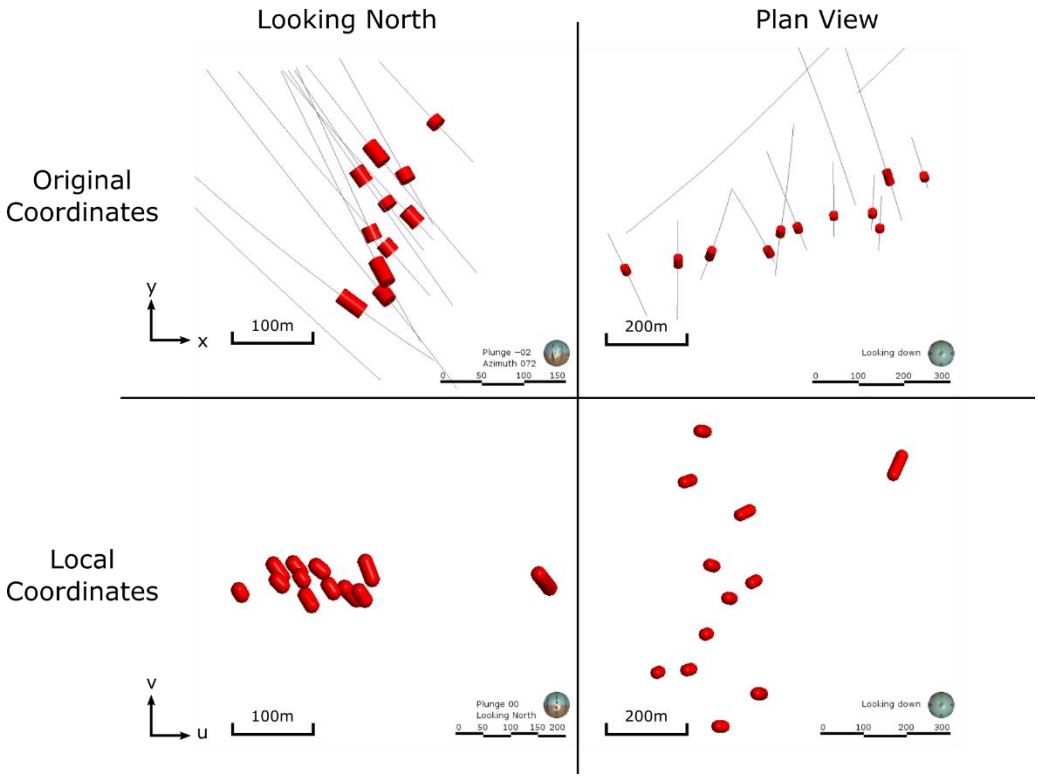

Figure 7.3: Vein samples (red) at original and local coordinates system after TLS transformation.

7.3. Geometric Uncertainty Evaluation

7.3.1. Geometric Data Imputation

Geometric data imputation is executed in this local coordinate system. The mineralization is characterized by three tabular stratums: bottom stockwork, inner vein, and top stockwork. The mineralization is also defined by four surfaces, from the bottom to the top of the structure: (1) bottom stockwork footwall, (2) contact between inner vein and bottom stockwork, (3) contact between inner vein and top stockwork, and (4) top stockwork hangingwall. Data used for the imputation are u, v, and w positions of the reference surfaces intercepts and thickness values of each tabular stratum. There is no substantial difference between surfaces in terms of stability and geometry. Therefore, for practicality, the bottom stockwork footwall is the selected as the reference surface. For each inclined drill hole, many distributions will be calculated to describe surfaces positioning (Figure

7.4). For each stratum, distributions are then merged and sampled. This sampled value characterizes a realization of the surface position. Surfaces position input data is already calculated from TLS plane fitting. Thickness values are calculated at each drill hole and for each stratum.

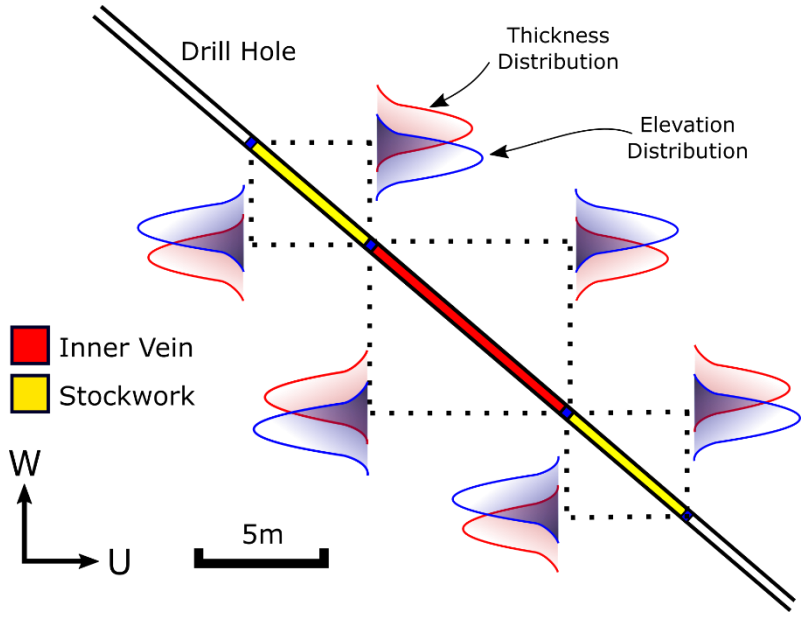

Figure 7.4: Position distributions to be calculated for each surface and drill hole intercept.

Position and thickness values are normal score transformed for sequential Gaussian simulation. Transformation tables are stored for later back transforming distributions. Reasonable variograms could not be calculated due to the low number of drill holes (11). Variograms are assumed according to vein characteristics including surfaces continuities on strike and dip directions. For imputation and surfaces simulation the following normal score variogram is assumed:

$$\gamma(\mathbf{h}) = 0 + 1.0 \cdot Gaus_{\substack{ahmax=100 \\ ahmin=70}}(\mathbf{h})$$

Being the strike the maximum continuity direction and dip the perpendicular and minimum direction. Strike and dip are azimuths 0 and 90° on local coordinates. The anisotropy is selected arbitrary by visual inspection of the data. It seems that thickness is more continuous on the strike than on dip. One hundred realizations are generated for data imputation, surface, boundary, and grade simulation. Position and thickness distributions

are calculated using USGSIM. After distribution calculation, position distribution is back transformed to original units and thickness is calculated for each stratum. Calculated thickness is normal score transformed using the global thickness distribution. These transformed thicknesses are assumed to be Gaussian. These transformed thicknesses and simulated thickness distribution are then merged by error ellipses methodology and sampled. The sampled value is assigned to the intercept as thickness and u, v, and w position.

The bottom stockwork footwall is executed first as it is considered the reference surface. Afterwards, other surfaces positions are imputed. The 100 imputation files are used as input data for surface simulation. An example can be seen on Figure 7.5. In this figure, there is one drill hole with the expected surfaces and three different imputed positions for each stratum. As expected, high-angle intercepts show higher uncertainty than low-angle intercepts (Figure 7.6). Example histograms for the bottom stockwork are shown in this figure. On the left, there are imputation results for a drill hole with an inclination of 20.6°, while the right one show results for a 49.5° inclined drill hole.

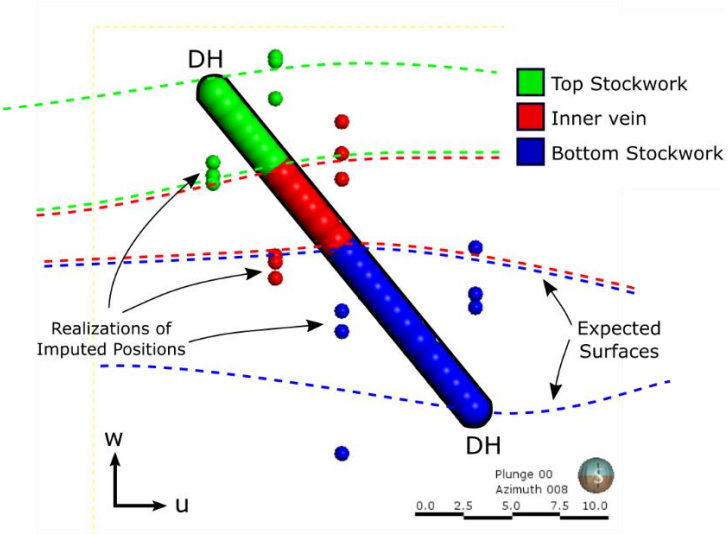

Figure 7.5: Section in one drill hole (central outlined) showing three imputed positions for each stratum. The small colored circles are different position realizations.

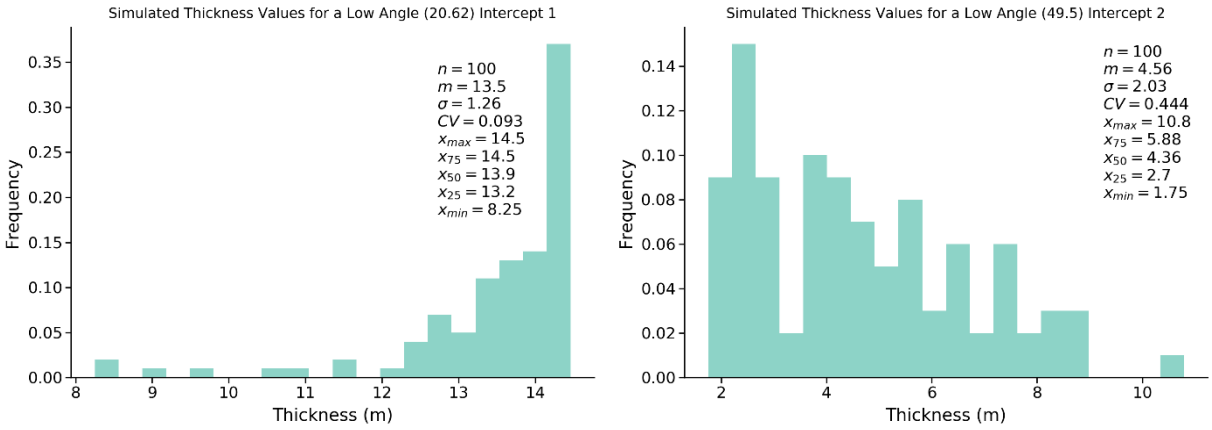

Figure 7.6: Histograms of imputed thickness data, for two intercepts. The first column shows the lower uncertainty on a low-angle intercept, while second column shows higher variability.

7.3.2. Surface Simulation

Surfaces are simulated using drill hole data and imputed positions data. Position and thickness are kept as pairs to prevent crossing between footwall and hangingwall of each stratum. An equilateral triangular grid of 15m of triangle side is created. An extrapolation border of 200m is expanded around external drill holes. Data is normal score transformed for simulation. Bottom stockwork footwall, the reference surface, is simulated first using position. Upper surfaces are simulated sequentially using thickness. Both results are back transformed to the original units. Simulated thickness values are then added to reference surface. Surfaces are triangulated using 2D Delaunay triangulation. A cross section of a surface realization can be seen on Figure 7.7.

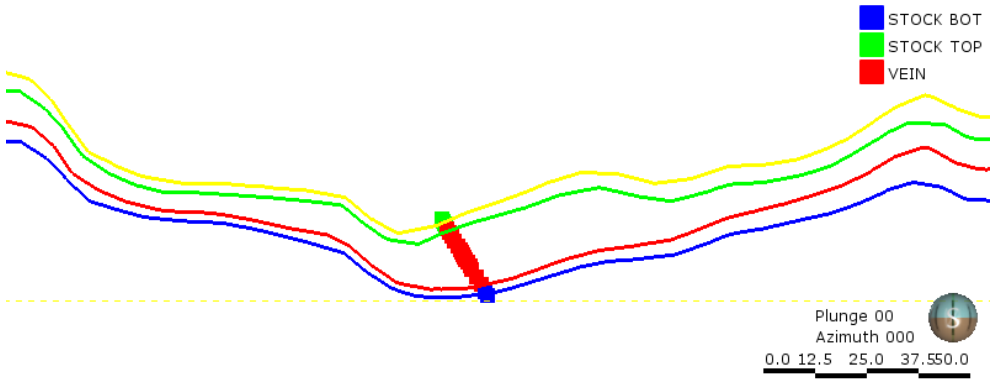

Figure 7.7: Cross section of a footwall and hangingwall surface realization. Drill hole traces are in black.

7.4. Other Uncertainties

7.4.1. Boundary Modeling

Different boundaries are modeled as areal limits for each surface realization using distance function methodology. All strata are clipped using the same boundary for that realization. For this case study, there are no drill holes and samples bounding the external limits of the vein. Therefore, control points to bound the external limits are used. The control points are based on the project inferred resources limits, which is around 100m distant from drill hole samples. A plan view with samples and control points can be seen on Figure 7.8. Global kriging is used to interpolate distance function values (Figure 7.9).

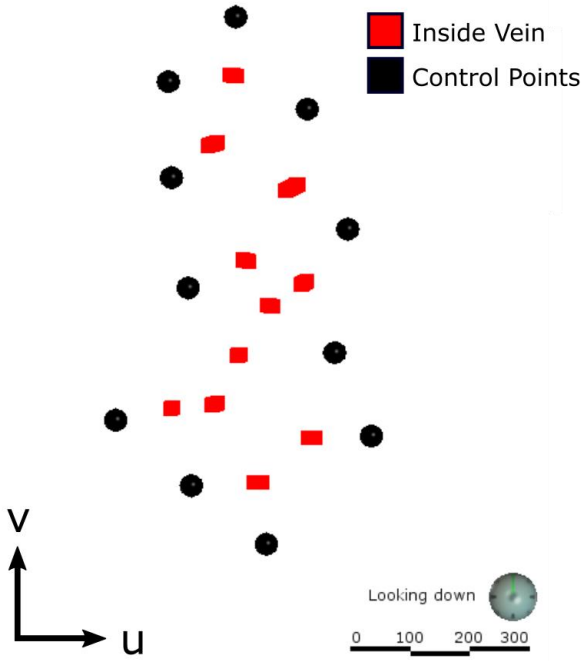

Figure 7.8: Plan view of drill holes intercepts (red) and control points (black).

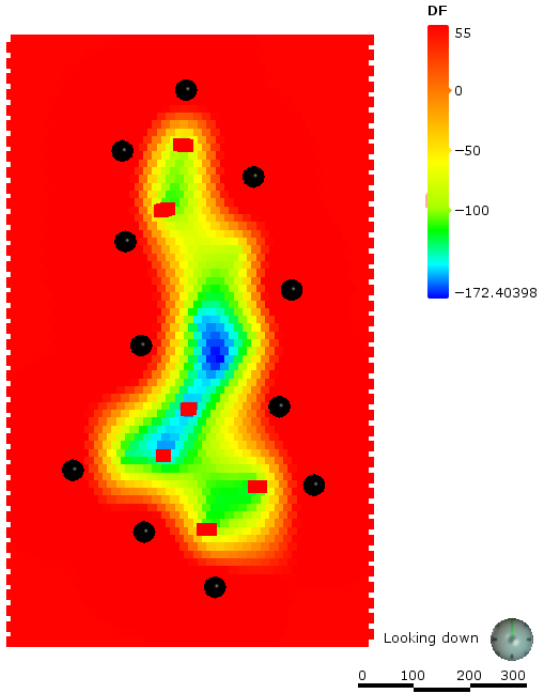

Figure 7.9: Interpolation of distance function values on the triagular grid. Inside samples are in red, control points are in black.

The C parameter should be calibrated before boundary modeling. The graph generated for the calibration can be seen on (Figure 7.10). The lack of data makes the selection the C parameter arbitrary. The chosen value for C parameter is 50 as the distance between drill holes and control points are 100m.

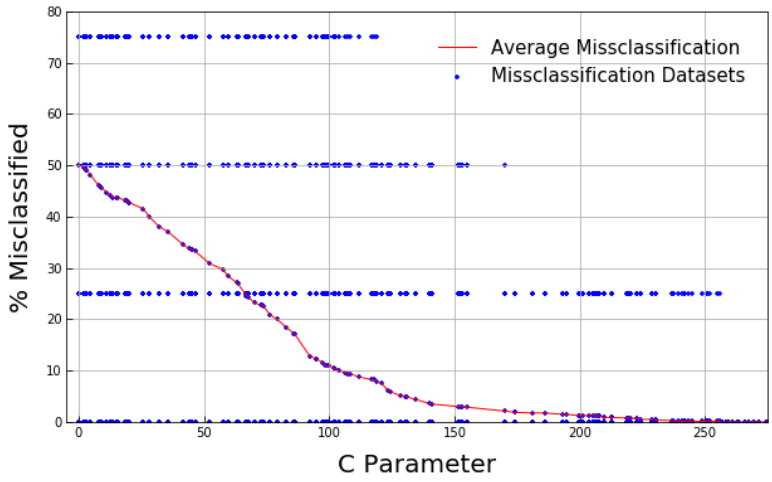

Figure 7.10: Misclassification and C parameter.

For each surface realization a different boundary is assigned. A random value is selected between $-C$ to $+C$, sampled from a uniform distribution.

7.4.2. Surfaces and Vein Solid Processing

Vein PLCs are generated by clipping surfaces realizations with distance function boundaries. Border nodes are recognized for each realization and surfaces linked. An example of a final watertight solid realization can be seen on Figure 7.11. Two files are generated: a file containing all nodes and its u, v, and w coordinates; another containing all facets from the triangulation with the nodes that form each facet. These files are enough for TetGen to generate the tetrahedralization.

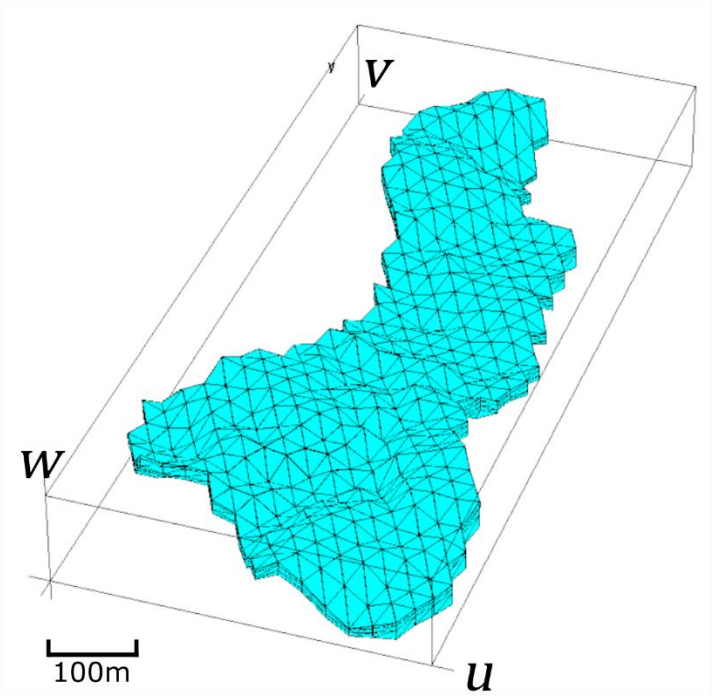

Figure 7.11: Watertight solid generated from a surface realization, boundary clipping, and border linking.

7.4.3. Grade Simulation

Silver grades are modeled for metal content uncertainty evaluation. Data histograms of the entire mineralization (all stratum together) can be seen on Figure 7.12, and each stratum on Figure 7.13. An arbitrary capping of 150 g/t is applied to the data, which represents p95

of the distribution. Tetrahedralization is executed for each watertight solid realization, respecting stratum boundaries (Figure 7.14). For global uncertainty, spatial bootstrap is applied for each stratum. Results from spatial bootstrap can be seen on Figure 7.15. Proportional modeling will be carried out. Each tetrahedron barycenter and nodes position is calculated relatively to the thickness in that section. Tetrahedrons are then discretized using the 27-point design. Silver grades variograms presented poor structuration and continuity due to lack of samples. Variogram model is based on geological information and visual inspection. The following normal score variogram is assumed for silver grade simulation:

$$\gamma(\mathbf{h}) = 0.12 + 0.88 \cdot Sph_{\substack{ahmax=120 \\ ahmin=70 \\ ahvert=3}}(\mathbf{h})$$

The anisotropy is selected arbitrary by visual inspection of the data. Silver grades look more continuous on strike (azimuth 0), followed by the dip (azimuth 90°), and thickness (vertical). Sequential Gaussian simulation is executed for each vein geometry realization, within separated stratum. A realization CDF of the silver grades within each stratum can be seen on Figure 7.16. Some results on uncertainty can be seen in the next section.

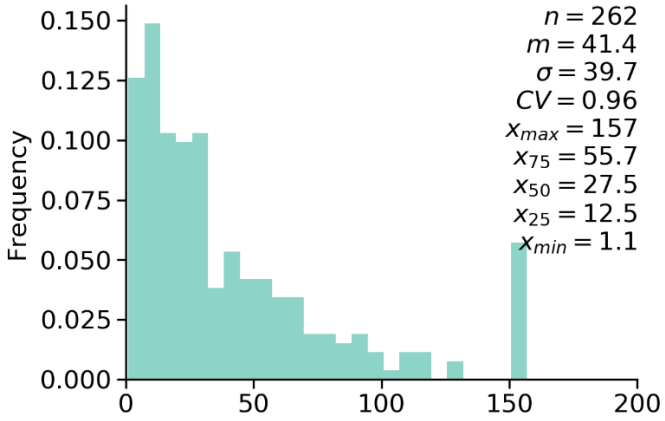

Figure 7.12: Ag grade histogram for the entire mineralization (all stratum together).

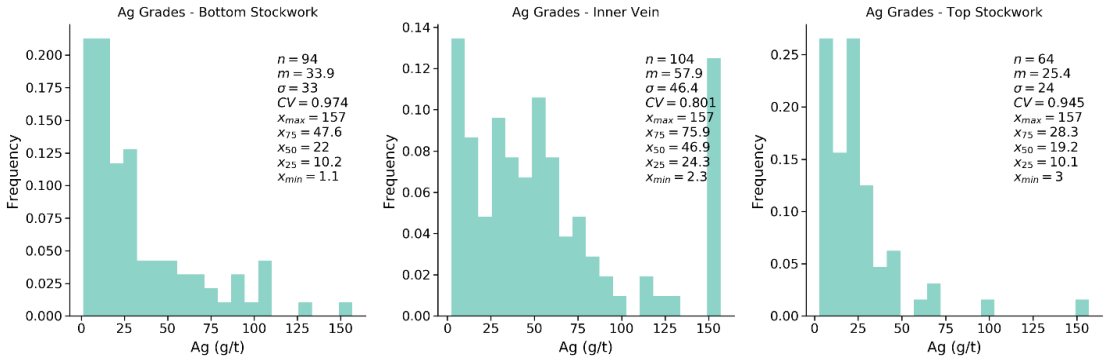

Figure 7.13: Ag grade histograms for each stratum.

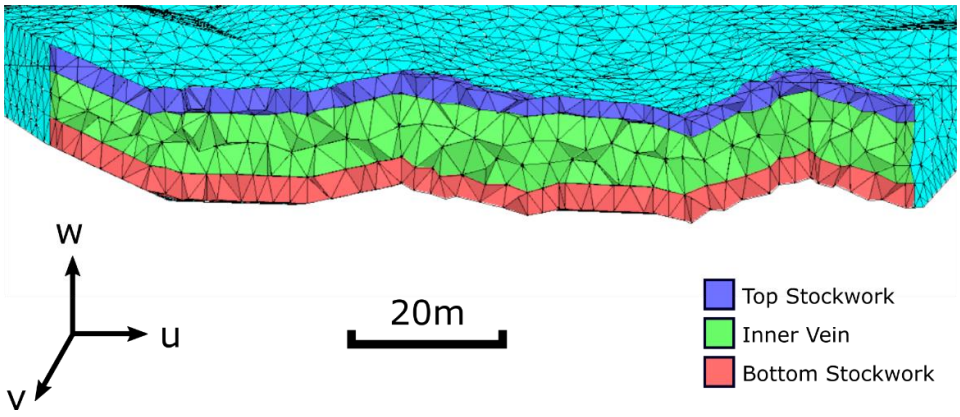

Figure 7.14: Cross-section showing the tetrahedralization honoring stratum surfaces.

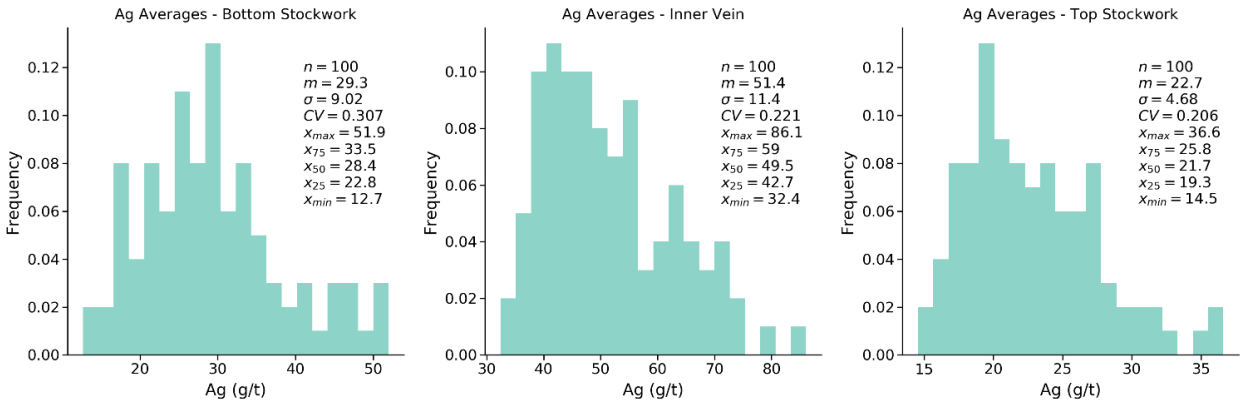

Figure 7.15: Spatial bootstrap averages for silver grade, separated by stratum.

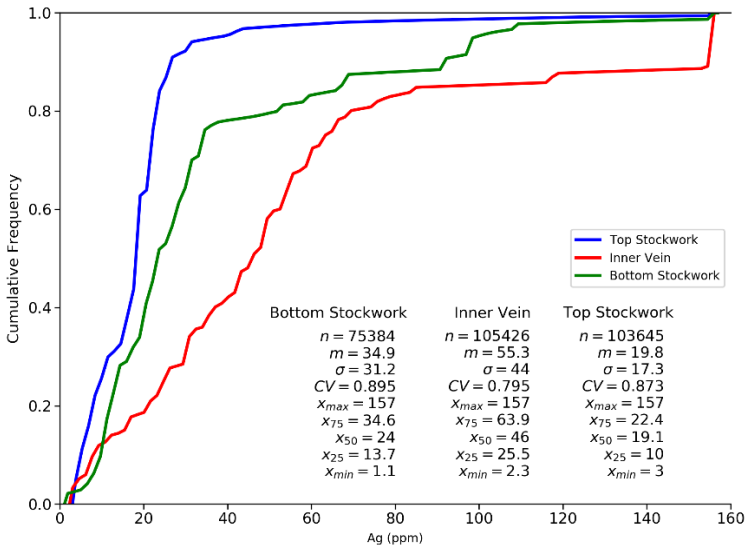

Figure 7.16: A realization CDF of Ag grades histograms for each stratum.

7.5. Results and Considerations

Data from a silver epithermal deposit is used. The Total Least Squares (TLS) method is used to fit the plane on data. Calculated strike azimuth and dip angle are 253.46° and 74.28°, respectively, which match the structural data and visual inspection of the ore body wireframe model. Imputation of intercepts position is executed. As expected, highly inclined drill holes (comparing to fitted plane) present higher variability than low-angle intercepts. Surfaces are then simulated using different imputation files. Each realization is clipped by a different boundary C parameter. There are 100 realizations of the vein geometry. Anisotropy is considered to be proportional. Samples and tetrahedrons are flattened accordingly and respecting each stratum position. Silver grade simulation is executed for the unstructured grid, within each stratum. Global tonnage and metal are calculated for each realization and a response table is created for comparing input variable and response variables. Distributions are shown on Figure 7.17.

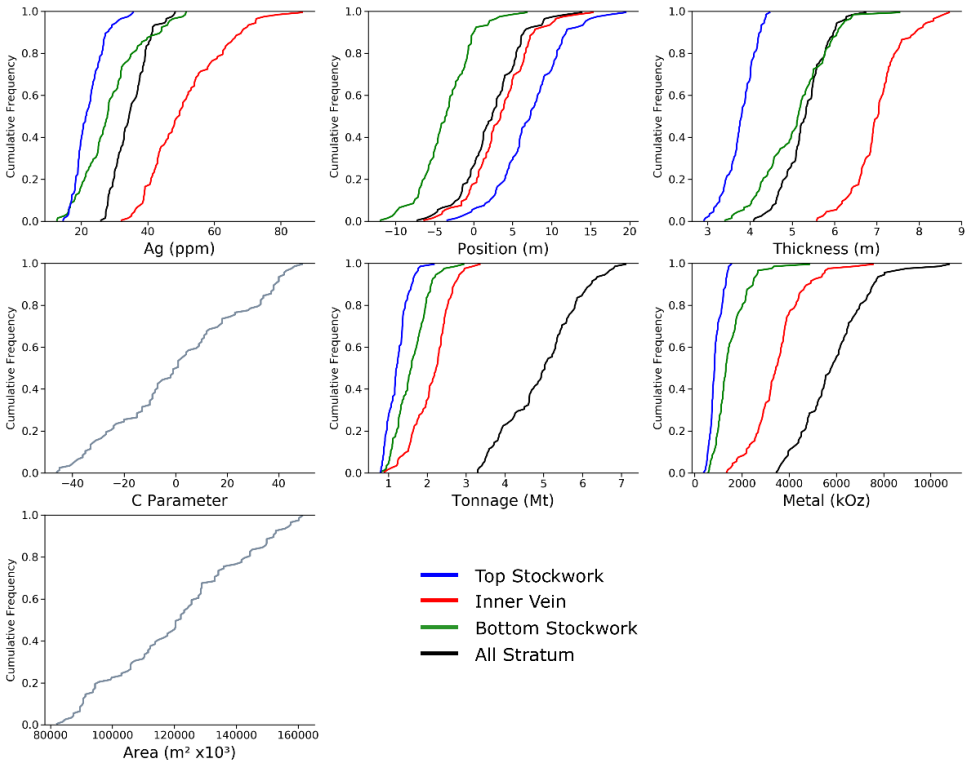

Figure 7.17: Distribution of input parameters (Ag, position, thickness, and C parameter) and response variables (area, Mt, and kOz). Each color represent a stratum. The black lines are the entire mineralization (all strata).

The total silver content (kOz) distribution can be seen on (Figure 7.18). By comparing p90 with 7556 kOz, and p10 with 3966 kOz, the absolute difference is 3590 kOz. Consequentially, there is 62% of metal uncertainty on the silver vein resources. As there are only 11 drill holes intercepting the vein, this high uncertainty on the metal is explained.

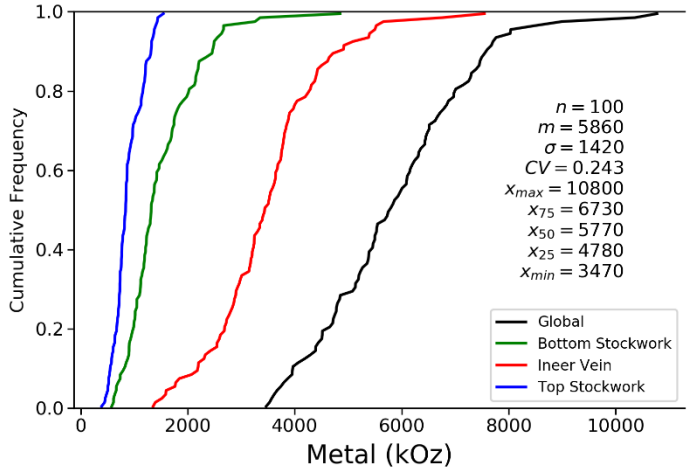

Figure 7.18: Distribution of silver content for each stratum and global. Statistics are for the global mineralization.

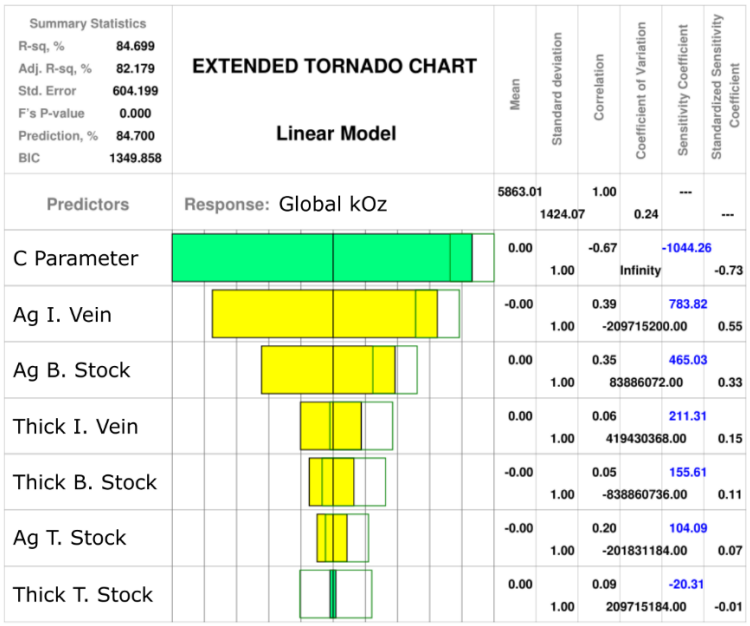

Figure 7.19: Tornado chart showing the impact of each input variable to the metal content (kOz).

For this case study, it is possible to state that C parameter and silver grades of the inner vein have the highest impact on global silver content (Figure 7.19). This is also expected, as the inner vein presents higher grades, followed by the bottom stockwork. The bottom stockwork has the less impact on metal resources. Even though the bottom stockwork is thicker, its grades are lower. The opposite happens with the top stockwork, where the thickness values are lower, but grades are higher. Probability maps can be seen on Figure 7.20. Boundaries are arbitrary because the drilling has not identified the extents of the vein.

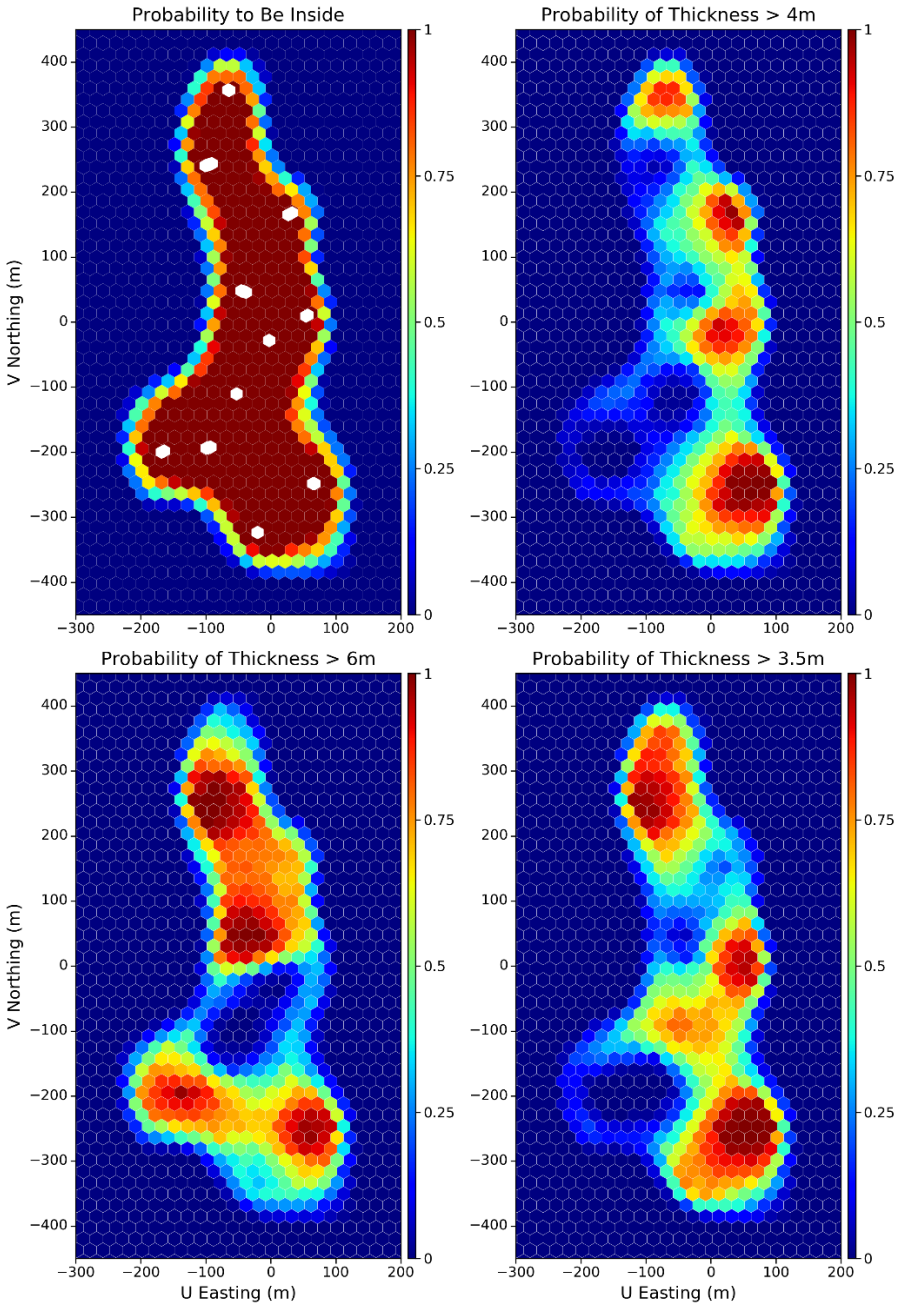

Figure 7.20: Probability map to be inside the vein and minimum thickness for each stratum. Samples inside are in white.

Chapter 8. Conclusion and Future Work

A comprehensive probabilistic workflow is presented. Steps and results are demonstrated. This chapter reviews problems identified in tabular vein deposits modeling. It also reviews the contributions of the thesis for geometric uncertainty evaluation. There are many challenging topics when it comes vein resources uncertainty quantification. Some limitations and proposals for future research and work are presented.

8.1. Review and Contributions

Tabular vein deposits represent important mining operations worldwide. Uncertainty in the geometry and resources of veins and other tabular deposits is addressed. Uncertainty can impact mine planning and operation. Accurate resources and reserves will mitigate these impacts. Drilling, exploration, and mine planning can be supported by a probabilistic estimation of vein resources. Current techniques do not provide an assessment of the uncertainty in these deposits. A new workflow is proposed and demonstrated.

For this thesis, simple tabular vein deposits are addressed. These are simple vein structures with single or multiple stacked layers with gentle folds and disturbances. Complex veins with tight folding, bifurcations, interlacing, and faults are not the focus. There are many types of deposit that can be incorporated to this definition of tabular vein deposits, including: hydrothermal vein deposits (Au, Ag, Zn, Pb, W, U, Co, Sn, and PGE); magmatic deposits (PGE, Ni, Cu, Cr, V, Ti); Sedimentary-exhalative deposits (Pb, Zn); and weathered deposits (Al, Ni, Mn, kaolin, sulphides).

Traditional modeling and resource estimation techniques are reviewed. Methods and workflows for mineral resource evaluation can be divided in two steps. The first step is the definition of the estimation domains, that are defined as volumes of rock with similar and consistent geological and statistical characteristics. The second step is the estimation and simulation grades and properties within a block model contained by the interpreted stationary domain. The definition is of the estimation domain for tabular vein deposits is usually executed by explicit modeling, implicit modeling, or surface interpolation. The first is a deterministic methodology that consists in manual digitization, sectional interpretation, and linking polylines together to generate the volumetric solid. It involves complex

manipulation and is time consuming, generating a single vein solid as a result. The second is a much faster deterministic methodology. The idea is to automatically model wireframes using distance or volume functions based on data configuration, categories, and anisotropy. Downsides are the control of 2D anisotropy of veins and also the generation of a single solid model as a result. The third methodology is also deterministic and based on the interpolation of hangingwall and footwall surfaces using RBF or global kriging. The strong 2D anisotropy is accounted for with this technique but the result is equally a single solid model. The use of kriging is a common practice for vein resources estimation, but there is no joint uncertainty quantification. Simulation methods could be applied to grade within the fixed ore body geometry. Fixing a single geometry will result in unrealistic uncertainty quantification.

The proposed framework consists in evaluating the geometric and other uncertainties, implement post-processing and sensitivity analysis to quantify uncertainty. Geometric uncertainty accounts for the creation of a local coordinates system, position and thickness uncertainty, and surface simulation. The local coordinates system is necessary as the original system is not related to the vein geometry and grade anisotropy. Quantification of final resources can be inefficient. A plane is fitted with vein samples and a local coordinates system is created using Total Least Squares (TLS). In this new system, thickness and grade modeling are convenient and anisotropy is modeled accordingly. Position and thickness uncertainty on surface intersections from drill holes with shallow angle intersections are dealt with data imputation. Distributions of the position and thickness of each intercept are calculated, merged, and sampled. A different input data file is considered for each surface simulation. A reference surface is selected, and its geometry simulated using position values. The opposite surface is simulated using thickness values. Position and thickness are kept as pairs to avoid crossing. Other uncertainties are external boundaries and holes, grades, and parameter uncertainty. Fixing a single boundary for the vein is not realistic, and so, multiple boundaries should be modeled. Boundaries are modeled using the distance function methodology. A different boundary is selected for each realization. If there are no negative intercepts, manual control points should be placed to manage extrapolation. Grades are usually modeled in regular grids that do not relate to the vein geometry. An unstructured tetrahedron grid is used for the task. The tetrahedron grid fits exactly the

geometry of the vein. Since unstructured grids are being simulated, an appropriate algorithm should be used. Grade anisotropy is carried by calculating w' coordinate according to proportional or surface conforming anisotropies. A discretization design is proposed with regular refinement of the tetrahedron. This regular refinement generates sub-tetrahedra of equal volume. Before simulation, parameter uncertainty is recommended. Simulating with fixed input histogram can substantially underestimate the global uncertainty in the deposit. The Spatial Bootstrap methodology is used for the task. Each geostatistical realization is executed using the many different distributions are generated from Spatial Bootstrap.

Results from vein geometry and grade simulation can be summarized with post-processing and sensitivity analysis. Some post-processing includes the average of all simulations (e-type), probabilities and mean above thresholds, probability to be ore and global uncertainty. For vein resources management, the probability to be in the vein and the thickness uncertainty are highly recommended. Probability surfaces can be generated for specified quantiles. Many aspects and steps of mining planning and operation can be supported by these calculations. Mining can be also supported by sensitivity analysis of the input and response variables. Sensitivity analysis supports the understanding of the relationships between input and responsible variables. Input variables can be ranked, and most important variables can be investigated. The multiple simulated vein surfaces can be used for reserves assessment. Stope optimization can be executed based on surfaces positioning in each realization. Results could be used to support mineral resource classification and reporting. Resource classification criteria selection could take advantage of all probability maps generated. Reporting could be generated using important quantiles, and so, uncertainty on expected values can be declared.

The main contribution of the thesis is the development of a flexible workflow for uncertainty quantification on tabular vein deposits. The sequence of the workflow starts with creation of local coordinates system, position and thickness imputation, surface simulation, boundary modeling, parameter uncertainty, grade simulation within an unstructured grid that fits vein geometry, post-processing, and sensitivity analysis. Within this workflow, the core development is on geometric data imputation, surface simulation, and boundary modeling. Most of current techniques does not account for these factors

while modeling. Results shown in the case studies reinforces the importance of considering all these factors for vein resources estimation. There is high uncertainty on position and thickness of inclined drill holes. The more inclined, the drill holes, the higher the uncertainty on the positioning of surfaces. The variability in the vein geometry is demonstrated by surface simulation and boundary modeling. Expected surfaces and solids can be used for general mine planning and operation. Scenarios and probabilities may be used for further mine planning optimization and reporting.

8.2. Future Work

The proposed framework exposes some limitations that may be interesting topics for future work and research on vein resources modeling. Geometric data imputation is executed by calculating and sampling merged thickness and position distributions. Each imputed data is not added as data for the next drill hole imputation. The conditioning from nearby drill holes may be important. For future research, imputation of geometric data could be executed sequentially. The conditioning and influence of imputed data could be measured and evaluated.

Position and thickness imputation are based on nearby samples. Thickness values are based on nearly vertical drill holes. There is a chance there are no perpendicular drill holes nearby or in the domain. Thickness values should be calculated by other methods. A possible method is to generate a deterministic model of the vein by interpolating footwall and hangingwall with all geological input available. Thickness could be sampled on a selected resolution, or at drill hole location, by subtracting hangingwall from footwall elevation. These sampled values could be used for geometric imputation process.

The workflow accounts for grade anisotropy inside the vein considering w' coordinates transformation accordingly to proportion to thickness or surface conforming; however, it does not account for trends. The existence of non-stationary trends inside veins could be a source of unrealistic prediction of resources. Therefore, trends should be modeled properly. A comprehensive framework for trend modeling is presented by Qu (2018); this could be adapted to vein grade modeling.

High-quality data is valuable as a foundation for all modeling. This quality depends on the number, distribution and orientation of samples, sampling procedures, crushing and milling

methods, and continuity of the grade (Sinclair & Blackwell, 2002). An implicit assumption is that the location of the data is exactly known. Drill holes can deviate or deflect depending on the rock type or geological structures. Small deviations can lead to significant discrepancies between the planned and executed drill hole location. The program of quality assurance and quality control (QA/QC) evaluate the error on sample assays and survey measurements. Errors from QA/QC reports could be incorporated to the uncertainty evaluation.

For the proposed workflow, external boundaries and holes are clipped with the distance function methodology. This clipping results in vertical cuts on the boundaries of the veins. There are many ways of modeling boundaries. An interesting topic for future research is to generate these boundaries as pinch-outs instead of clipping. The closing point of the vein could be at the expected boundary.

A natural extension of this thesis is to consider complex vein structures. More complex mineralization may present tight folds, faulting, interlacing and bifurcating surfaces. For intense folding of a single vein structure, defined by footwall and hangingwall, the construction of a local coordinates system with unfolding techniques may solve the problem. With a parameterized fold, all subsequent steps from this workflow could be executed and uncertainty quantified. For faulted veins, each fault block should be defined previously. Vein coordinates may be transformed to an unfaulted local coordinates system. With the vein put back to its original genesis geometry, all subsequent steps of this workflow could be applied. An additional feature for investigation is the probabilistic modeling of the fault surface. Instead of fixing a single geometry for the fault surface, many realizations could be generated, resulting in a more complete modeling of the uncertainty. Interlacing and bifurcating veins modeling is complex. There might be the necessity of mapping all bifurcating points. Regions towards the single structures could be modeled with this workflow. Regions towards bifurcation should be modeled as different vein structures. Some processing should be executed at bifurcation regions to smoothly connect distinct regions.

References

Alabert, F. G. (1987). The practice of fast conditional simulations through the LU decomposition of the covariance matrix. *Math Geol* 19(5):369--386

Barnett, R. M., Manchuk, J. G., & Deutsch, C. V. (2014). Projection pursuit multivariate transform. *Mathematical Geosciences*, 46(3):337--359.

Bertossi, L. G. et al. Implicit Geological Modelling Versus Traditional Modelling.: A Case Study Applied to a Lateritic Nickel Deposit. In: *APCOM* 36, Porto Alegre. p. 1 - 8.

Bey, J. (1995). Tetrahedral grid refinement. *Computing,* 55: 355

Carvalho, D., & Deutsch, C. V. (2017). Developments on Tabular Vein Geometry Modeling. *CCG Annual Report 19, Paper 309*

Caumon, G., Grosse, O., Mallet, J. L. (2005) High resolution geostatistics on coarse unstructured flow grids. *Geostatistics Banff 2004*, 1:703--712

Ceyhan, M. (2009). World distribution of uranium deposits (UDEPO) with uranium deposit classification. *International Atomic Energy Agency, IAEA TECDOC-1629*, 1, 117.

Chilès, J. P., Aug, C., Guillen, A., & Lees, T. (2004). Modelling the geometry of geological units and its uncertainty in 3D from structural data: the potential-field method. In *Proceedings of international symposium on orebody modelling and strategic mine planning*, *Perth, Australia* (pp. 313-320).

Chilès, J. P., Delfiner P., (2011). *Geostatistics: Modeling spatial uncertainty*, 2nd ed. Wiley Series in Probability and Statistics, New York

Cowan, E. J., Beatson, R. K., Ross, H. J., Fright, W. R., McLennan, T. J., Evans, T. R., ... & Oshust, P. A. (2003). Practical implicit geological modelling. In *Fifth*

International Mining Geology Conference (pp. 17-19). Australian Institute of Mining and Metallurgy Bendigo, Victoria.

de Groen, P. P. (1998). An introduction to total least squares. *arXiv preprint math/9805076*.

Deutsch, C. V. (2004). A Statistical Resampling Program for Correlated Data: Spatial Bootstrap. *CCG Annual Report 6, Paper 401*

Deutsch, C. V. (2005). A Short Note on Prediction of Uncertainty in Tonnage and Grade of Vein Type Deposits. *CCG Annual Report 7, Paper 305*

Deutsch, C. V. (2015). All Realizations all the Time. *CCG Annual Report 17, Paper 101*

Deutsch, C. V. (2017). Setup of Simulation for Large Scale Resource Uncertainty. *CCG Annual Report 19, Paper 101*

Deutsch, C. V., & Journel, A. G. (1998). *GSLIB: Geostatistical software library and user's guide*. Oxford University Press New York.

Deutsch, C. V., Monteiro, M., Zanon, S., & Leuangthong, O., (2002). Procedures and Guidelines for Assessing and Reporting Uncertainty in Geostatistical Reservoir Modeling. *CCG Annual Report 4, Paper 107*

Edwards, R., & Atkinson, K. (1986). *Ore deposit geology and its influence on mineral exploration*. - 466 pp, London, New York (Chapman and Hall).

Efron, B. (1982). *The jackknife, the bootstrap, and other resampling plans* (Vol. 38). Siam.

Hartmann, E. (1998). A marching method for the triangulation of surfaces. *The Visual Computer, 14(3)*, 95-108.

Hosseini, A. H., & Deutsch, C. V. (2007). A Distance Function Based Algorithm to Quantify Uncertainty in Areal Limits. *CCG Annual Report 9, Paper 128*

Isaaks, E. H. (1990). *The Application of Monte Carlo Methods to the Analysis of Spatially Correlated Data*. PhD Thesis, Stanford University, Stanford, United States.

Isaaks, E. H., & Srivastava, R. M. (1989). *Applied geostatistics*, volume 2. Oxford University Press New York.

Journel, A. G. (1974). Geostatistics for conditional simulation of ore bodies. *Economic Geology*, 69(5), 673-687.

Journel, A., & Huijbregts, C. (1978). *Mining Geostatistics*. Blackburn Press.

Lillehagen, N. B. (1979). The estimation and mining of Gove bauxite reserves. In *Symp. Ser.-Australas. Inst. Min. Metall*. (pp. 19-32).

Lindgren, W. (1922). A suggestion for the terminology of certain mineral deposits. *Economic Geology*, 17(4), 292-294.

Luster, G. R. (1985). *Raw materials for Portland cement: applications of conditional simulation of coregionalization.* PhD Thesis. Stanford University, p 531.

Mallet, J. L. (2002). *Geomodeling*. Oxford University Press.

Manchuk, J. (2007). S*tope Design and Sequencing.* MSc. Thesis, University of Alberta, Edmonton, Canada.

Manchuk, J. (2010a). *Geostatistical Modeling of Unstructured Grids for Flow Simulation.* PhD Thesis, University of Alberta, Edmonton, Canada.

Manchuk, J. (2010b) Geostatistics on Unstructured Grids: Application to Teapot Dome. *CCG Annual Report 12, Paper 106*

Manchuk, J., & Deutsch, C. V. (2015). Latest SGSIM Program. *CCG Annual Report 17, Paper 401*

Marsh, E.E., & Anderson, E.D. (2011) Ni-Co laterite deposits: U.S. Geological Survey Open-File Report 2011–1259, 9 p.

Martin, R., & Boisvert, J. (2016). Programs for Modeling Domains with Radial Basis Functions. *CCG Annual Report 18, Paper 413*

Martin, R., & Boisvert, J. (2017). Examining the Shape Properties of Iteratively Refined Implicit Models. *CCG Annual Report 19, Paper 110*

Matheron, G. (1973). The intrinsic random functions and their applications. *Advances in applied probability*, 5(3), 439-468.

Munroe, M. J., & Deutsch, C. V. (2008). A Methodology for Modeling Vein-Type Deposit Tonnage Uncertainty. *CCG Annual Report 10, Paper 301*

Neufeld, C., & Wilde, B. (2005). A Global Kriging Program for Artifact-Free Maps. *CCG Annual Report 7, Paper 403*

Ostenberg, B. C., & Deutsch, C. V. (2017). Transforming Vein Deposit Coordinates for Improved Resource Estimation. *CCG Annual Report 19, Paper 312*

Pyrcz, M. J., & Deutsch, C. V. (2014). *Geostatistical reservoir modeling*. Oxford University Press.

Qu, J. (2018). *A Practical Framework to Characterize Non-Stationary Regionalized Variables*. PhD Thesis, University of Alberta, Edmonton, Canada.

Rezvandehy, M., & Deutsch, C. V. (2014). Combining Multivariate Gaussian Distributions from Different Sources. *CCG Annual Report 16, Paper 127*

Rezvandehy, M., & Deutsch, C. V. (2018). Declustering experimental variograms by global estimation with fourth order moments. *Stochastic Environmental Research and Risk Assessment*, 32(1), 261-277.

Rossi, M. E., & Deutsch, C. V. (2014). *Mineral resource estimation*. Berlin, Germany: Springer.

Saltelli, A., Ratto, M., Andres, T., Campolongo, F., Cariboni, J., Gatelli, D., ... & Tarantola, S. (2008). *Global sensitivity analysis: the primer*. John Wiley & Sons.

Si, H. (2015). TetGen, a Delaunay-based quality tetrahedral mesh generator. *ACM Transactions on Mathematical Software (TOMS)*, 41(2), 11.

Silva, D. A., & Deutsch, C. V. (2012). Modeling Multiple Rock Types with Distance Functions: Methodology and Software. *CCG Annual Report 14, Paper 307*

Silva, D. S. F., & Boisvert, J. (2014). Two New Tools: Directional Survey to GSLIB XYZ Format and Drill Hole Spacing. *CCG Annual Report 16, Paper 404*

Sinclair, A. J., & Blackwell, G. H. (2006). *Applied mineral inventory estimation*. Cambridge University Press.

Wilde, B. J., & Deutsch, C. V. (2011). A New Way to Calibrate Distance Function Uncertainty. *CCG Annual Report 13, Paper 105*

Xu, W., & Journel, A.G. (1994). DSSIM: A general sequential simulation algorithm, *Stanford Center for Reservoir Forecasting Report 7*

Zagayevskiy, Y. V., & Deutsch, C. V. (2011). Updated code for sensitivity analysis based on regression. *CCG Annual Report 13, Paper 401*.

Zienkiewicz, O. C., & Taylor, R. L. (2005). *The finite element method for solid and structural mechanics*. Elsevier.